

# PHASE TRANSITIONS IN POLYELECTROLYTE SYSTEMS

by

Anoop Varghese

Enrolment No. PHYS10200604015

The Institute of Mathematical Sciences  
Chennai 600113

*A thesis submitted to the  
Board of Studies in Physical Sciences*

*In partial fulfilment of requirements  
For the Degree of*

**DOCTOR OF PHILOSOPHY**  
*of*  
**HOMI BHABHA NATIONAL INSTITUTE**



October, 2012

# Homi Bhabha National Institute

## Recommendations of the Viva Voce Board

As members of the Viva Voce Board, we recommend that the dissertation prepared by **Anoop Varghese** titled “Phase Transitions in Polyelectrolyte Systems” may be accepted as fulfilling the dissertation requirement for the Degree of Doctor of Philosophy.

\_\_\_\_\_  
External Examiner – P. B. Sunil Kumar      **Date :**

\_\_\_\_\_  
Chairman – Purusattam Ray      **Date :**

\_\_\_\_\_  
Guide – Rajesh Ravindran      **Date :**

\_\_\_\_\_  
Co-Guide – Satyavani Vemparala      **Date :**

\_\_\_\_\_  
Member – Ronojoy Adhikari      **Date :**

\_\_\_\_\_  
Dean – Ghanashyam Date      **Date :**

Final approval and acceptance of this dissertation is contingent upon the candidate's submission of the final copies of the dissertation to HBNI.

We hereby certify that we have read this dissertation prepared under our direction and recommend that it may be accepted as fulfilling the dissertation requirement.

\_\_\_\_\_  
Rajesh Ravindran      **Date :**

\_\_\_\_\_  
Satyavani Vemparala      **Date :**

## STATEMENT BY AUTHOR

This dissertation has been submitted in partial fulfillment of requirements for an advanced degree at Homi Bhabha National Institute (HBNI) and is deposited in the Library to be made available to borrowers under rules of HBNI.

Brief quotations from this dissertation are allowable without special permission, provided that accurate acknowledgement of source is made. Request for permission for extended quotation from or reproduction of this manuscript in whole or in part may be granted by the Competent Authority of HBNI when in his or her judgment the proposed use of the material is in the interests of scholarship. In all other instances, however, permission must be obtained from the author.

Anoop Varghese

# DECLARATION

I, hereby declare that the investigation presented in the thesis has been carried out by me. The work is original and has not been submitted earlier as a whole or in part for a degree/diploma at this or any other Institute/University.

Anoop Varghese

## ACKNOWLEDGEMENTS

First of all, I would like to thank my Ph.D. supervisors Dr. R. Rajesh and Dr. Satyavani Vemparala for their wonderful guidance, and to them, I dedicate this thesis. I joined Dr. Rajesh first for a reading course in advanced statistical mechanics, and I believe I did not show any convincing signs for hope during the course, primarily because of my lack of right motivation. In spite of being aware of my state of mind, Dr. Rajesh accepted me as his Ph.D. student, and I thank him for taking that brave step. Dr. Vani was always helpful to me whenever I approached her with any academic or non-academic problems. Indeed, she always goes one step further than what I ask for. I thank her for her helps and encouragement.

My parents and my other family members, especially my mother and sister, have always been a support and encouragement to me. I thank them for their understanding, patience and love.

Like many others who pursue research as a career, I too was motivated by inspiring teachers. I would like to express my gratitude to my college teachers Robin Francis and Jose Mathews for the wonderful discussions we had, which have helped me in many ways in my pursuit of Physics. My thanks are also due to my native neighbour Jaison Mathew, who had been a mentor in my academics since my school days.

My stay in IMSc has been a memorable one because of the friendships I have enjoyed over here. I thank Mubeena, Yadu, Sreejith and my batch mates Rajeev, Krishnakumar, Somdeb and Sandipan for their friendship, encouragement and helps; special thanks to Rajeev for his helps in computation related issues. The retrospection of attending schools and conferences with Rajeev and Somdeb, going for concerts and discussing Physics and music with Krishnakumar, frequent visitations to Kerala restaurants and fun time with Sreejith, Mubeena and Yadu will always be evoking. Thanks are also due to many other friends, especially my sports friends, whom I have not named here.

God does not often find a place in the acknowledgment page of scientific writings. As for me, this acknowledgment would be incomplete without thanking him. I thank the

Almighty for what he has been to me, and for his promises on what he would be to me.

I believe what I have achieved, at the end of six years of stay in IMSc, more than anything else if there are any, is a passion for research. I hope it will remain in me, and I thank once again all those who have contributed to that, directly or indirectly.

## SYNOPSIS

Polyelectrolytes (PEs) are polymers whose monomers contain ionizable groups that dissociate in polar solvents, releasing charged counterions into the solvent, thereby making the polymer backbone charged. Many biological molecules such as DNA, proteins, F-actin filaments are examples of PEs. The thermodynamic properties of a PE is different from that of a neutral polymer because of the interplay between the long-range Coulomb interactions and short-range excluded volume interactions. For low linear charge densities of the polymer backbone, thermal fluctuations dominate over electrostatic interactions, and the counterions will be uniformly distributed in the solution. For high linear charge densities, electrostatic interactions dominate thermal fluctuations, and the counterions condense on the PE chain. As the linear charge density is increased from low values to high values, the system undergoes a series of phase transitions. In this thesis titled “Phase transitions in polyelectrolyte systems” we study different phases of three different PE systems, and the transitions between them. The first system is a single flexible PE chain in a solvent containing explicit counterions. In this system, we identify the counterion condensation and the condensed counterion mediated collapse of the PE chain as phase transitions. In addition, we argue against the existence of intermediate phases between the extended and collapsed phases. The second system is a collection of similarly charged rod-like PE chains in the presence of neutralizing counterions. In this system, we study the aggregation of PE chains induced by condensed counterions, and relate this transition to the extended-collapsed transition of a single flexible PE chain. The third system that we consider is a two-dimensional charged disc surrounded by freely moving oppositely charged counterions, and we study it in both the canonical and microcanonical ensembles. The Coulomb interactions in PE systems are long-ranged, i.e., they decay slower than  $r^{-d}$  for  $r \gg 1$ , where  $r$  is the inter-particle separation and  $d$  is the dimension of the system. A possible consequence is the inequivalence of different statistical ensembles. By comparing the thermodynamics obtained from the analytical solutions in the

canonical and microcanonical ensembles, we show that the ensembles are identical for the counterion condensation on a two-dimensional charged disc. Below, we discuss each of the problems in more detail.

## Phase transitions of a single polyelectrolyte chain

The counterion condensation in PE system is a well studied problem. It was theoretically predicted that the counterions of a rigid PE chain condenses on the chain when the dimensionless parameter

$$A = \frac{q^2}{4\pi\epsilon b k_B T}$$

exceeds a critical value. Here,  $q$  is the charge per monomer,  $\epsilon$  is the permittivity of the medium,  $k_B$  is the Boltzmann constant,  $b$  is the bond length and  $T$  is the temperature.  $A > 1$  corresponds to the situation where the electrostatic interaction dominates the thermal fluctuations. The prediction of counterion condensation was later confirmed by experiments and computer simulations. It has been shown recently, using Monte Carlo simulations, that the counterion condensation on model geometries like charged cylinders and two dimensional charged discs is a second-order phase transition. Another interesting phenomena in PE systems is the extended-collapsed transition of a flexible PE chain. It has been observed in experiments and simulations that a flexible PE chain collapses from the extended phase when  $A$  exceeds a critical value. This transition is induced by the condensed counterions on the PE chain, and the physical origin of the transition is still a subject of debate. Despite the difference in the opinion about the mechanism of the collapse, many theoretical studies predict that the collapse of the chain from the extended phase is a first-order transition.

We studied, using MD simulations, the counterion condensation transition and extended-collapsed transition of a single flexible PE. We used the bead-spring model for the polyelectrolyte chains. The short-range excluded volume interactions among monomers and counterions are modelled using Lennard-Jones potential. We summarize below our main

results.

- The counterion condensation transition on a flexible PE chain is a second-order phase transition. To study this transition, we have used the number of non-bonded neighbors per monomer as the order parameter. For a given monomer, a non-bonded neighbor is defined as any monomer or counterion that is not connected to it by a bond and within a distance  $b$ . The relative fluctuation in the number of non-bonded neighbors per monomer has a peak at a critical value of  $A$ , and the peak height increase with the number of monomers. The scaling of the peak height with the number of monomers strongly suggests that the counterion condensation is a second-order phase transition.
- The extended-collapsed transition of the PE chain is a first order phase transition. To study this transition, we track the variation of the asphericity of the chain and the electrostatic energy per monomer as a function of  $A$ . Both these quantities show a jump at a critical value of  $A$  indicating the transition. Also, the relative fluctuation in the electrostatic energy per monomer shows a peak at the critical value. We also observe that the probability distribution of both asphericity and electrostatic energy per monomer are double peaked near the critical point. The discontinuity in electrostatic energy per monomer, and the two peaks in the probability distributions strongly suggest that the transition is first-order.
- The “Sausage phase”, which was recently proposed as a possible phase with non-zero value of asphericity, between the extended phase and condensed-collapsed phase, does not exist in the thermodynamic limit. We demonstrate this by showing that the asphericity of a PE chain decreases with the number of monomers as a power law, for values of  $A$  above the critical value of the extended-collapsed transition.
- The critical value of the counterion condensation transition and the extended-collapsed transition decreases with increase in valency of the counterions.

## Aggregation of rod-like polyelectrolyte chains mediated by condensed counterions

Similarly charged objects in general repel each other. A counterintuitive phenomena in PE systems is the attraction of similarly charged PE chains. The attraction is induced by the condensed counterions on the PE chains, and results in the aggregation of the chains. Although it has been unambiguously shown, using theoretical, experimental and computational methods, that divalent and trivalent counterions can mediate attraction between similarly charged PE chains, it still remains unclear whether monovalent counterions can mediate such attraction. While some theoretical and experimental studies argue for the attraction, other theoretical, experimental and computational studies argue the opposite.

Using MD simulations, we studied the aggregation of rod-like PE chains in the presence of monovalent, divalent and trivalent counterions. Our main results are briefly listed below.

- Monovalent counterions can induce aggregation of similarly charged PE chains if  $A$  is higher than a critical value.
- The kinetics of the aggregation is independent of  $A$  and the valency of the counterions. The number of aggregates decay with time as a power law and the exponent is independent of  $A$  and valency of the counterions.
- The critical value of  $A$  for the aggregation of rod-like PE chains is very close to the critical value the extended-collapsed transition of a single flexible PE chain for all the valencies that we have studied.
- We measured the effective mean potential  $W(d)$  of a system of two parallel rod-like PE chains in the presence of monovalent counterions as a function of the separation and  $A$ .  $W(d)$  develops a well of attraction for  $A$  greater than the critical value. The value of  $A$  for which the depth of the potential becomes of the order of  $k_B T$  roughly coincides with the critical value of aggregation.

- The nature of the angular distribution of the condensed counterions around two parallel rod-like PEs changes with the separation between them. At high enough values of  $A$ , at which there is an attraction between the PEs, the condensed counterions are found to be organized around the two PEs in a correlated fashion.

## **Ensemble equivalence for counterion condensation on a charged disc**

Statistical mechanics provides a framework to derive the thermodynamic properties of a system with macroscopic number of degrees of freedom. Depending on the nature of the system, different statistical ensembles such as microcanonical, canonical and grand canonical ensembles can be used to derive the relation between various thermodynamic quantities. If the interaction in the system is short-ranged (decay faster than  $r^{-d}$  for large  $r$ ), different statistical ensembles are equivalent, i.e., they yield the same thermodynamic behavior. This result is a consequence of the energy of a short-range system being the sum of the energies of the subsystems. This additivity property does not hold for systems for which the interactions are long-ranged. As a result, for long-range systems, different statistical ensembles can be inequivalent. PE systems are clearly long-ranged, and as result, the thermodynamics derived from different statistical ensembles could be different. However, most studies on PE systems have been restricted to the canonical ensemble. Also, the number of exactly solvable models of PE systems where one can study the issue of ensemble inequivalence is very much limited. In a recent work, the problem of counterion condensation on two-dimensional charged disc was studied in the canonical ensemble, by the exact evaluation of the canonical partition function. We solved this model in the microcanonical ensemble by calculating the microcanonical entropy exactly. Our main results are

- The microcanonical entropy is piecewise linear and concave in energy.
- The linear portions of the entropy correspond to the first-order poles in the canonical

partition function.

- The energy–temperature relation in the microcanonical ensemble is identical to that of the canonical ensemble.
- It is known that the canonical and microcanonical ensembles are equivalent if the microcanonical entropy is concave in energy, even if the interactions are long-ranged. Since the microcanonical entropy is concave for the system that we have considered, the canonical and microcanonical ensembles are equivalent for this system.

# Contents

<b>1</b>	<b>Introduction</b>	<b>1</b>
1.1	Neutral polymers . . . . .	2
1.1.1	Random flight model . . . . .	3
1.1.2	Excluded volume interactions . . . . .	4
1.1.3	Semi-flexible polymers . . . . .	6
1.2	Polyelectrolytes . . . . .	7
1.2.1	Flory theory for polyelectrolytes . . . . .	7
1.2.2	Counterion condensation . . . . .	8
1.2.3	Effect of counterion condensation on the confirmation of a polyelectrolyte chain . . . . .	10
1.2.4	Effect of counterion condensation in multiple chain systems . . . .	11
1.3	The choice of the statistical ensemble for studying polyelectrolyte systems	11
<b>2</b>	<b>Introduction to Molecular Dynamics Simulations</b>	<b>15</b>
2.1	Introduction . . . . .	15
2.1.1	Ensemble average and time average . . . . .	17
2.1.2	Force fields . . . . .	18
2.1.3	Periodic boundary conditions . . . . .	20
2.2	Algorithms for integrating the equation of motion . . . . .	21
2.3	Constant temperature molecular dynamics simulations . . . . .	23
2.3.1	Andersen thermostat . . . . .	23

2.3.2	Nosé-Hoover thermostat . . . . .	24
2.3.3	Langevin Dynamics . . . . .	25
2.4	Long-range interactions . . . . .	26
2.4.1	Ewald summation method . . . . .	26
2.4.2	Particle-particle/particle-mesh method . . . . .	28
2.5	Coarse-grained molecular dynamics simulations of polymers . . . . .	29
<b>3</b>	<b>Phase Transitions of a Single Polyelectrolyte in a Poor Solvent</b>	<b>31</b>
3.1	Introduction . . . . .	31
3.1.1	Counterion condensation transition . . . . .	33
3.1.2	Extended-collapsed transition . . . . .	35
3.2	Model and simulation method . . . . .	37
3.3	Results and Discussion . . . . .	40
3.3.1	Configurations of the polyelectrolyte chain . . . . .	40
3.3.2	Distribution of counterions . . . . .	40
3.3.3	Number of non-bonded neighbours and the condensation transition	43
3.3.4	Transition from extended phase to collapsed phase . . . . .	45
3.3.5	Existence of Sausage phase . . . . .	46
3.3.6	The effect of valency of counterions on counterion condensation transition and extended-collapsed transition . . . . .	48
3.4	Conclusions . . . . .	50
<b>4</b>	<b>Aggregation of Similarly Charged Rod-Like Polyelectrolytes</b>	<b>52</b>
4.1	Introduction . . . . .	52
4.2	Model and simulation method . . . . .	55
4.3	Results and Discussion . . . . .	57
4.3.1	Aggregation of rod-like polyelectrolyte chains . . . . .	57
4.3.2	Extended-Collapsed transition of a single flexible polyelectrolyte chain . . . . .	62

4.3.3	The effective interaction potential between two rod-like PE chains with monovalent counterions . . . . .	64
4.3.4	The angular distribution of the condensed counterions . . . . .	65
4.4	Conclusions . . . . .	67
<b>5</b>	<b>Ensemble Equivalence for Counterion Condensation on a Two-Dimensional Charged Disc</b>	<b>68</b>
5.1	Introduction . . . . .	68
5.1.1	Concavity of a function and the Legendre transformation . . . . .	69
5.1.2	The equivalence between canonical and microcanonical ensemble .	74
5.2	Ensemble equivalence for counterion condensation transition on a charged disk . . . . .	78
5.2.1	Model and canonical partition function . . . . .	78
5.2.2	The microcanonical ensemble . . . . .	82
5.2.3	The ensemble equivalence . . . . .	84
5.3	Summary . . . . .	86
5.A	The leading term in $g(E)$ . . . . .	87
<b>6</b>	<b>Conclusion and Future Directions</b>	<b>89</b>
6.1	Conclusions . . . . .	89
6.2	Future Directions . . . . .	91

# List of Figures

2.1	A plot of the Lenard-Jones potential. . . . .	20
3.1	Snapshots of the polyelectrolyte chain configurations for different values of $A$ . For the sake of clarity, counterions are not shown and figures are not in the same scale. (a) globular phase, (b) dumbbell phase, (c) pearl-necklace phase, (d) extended phase, (e) sausage phase and (f) globular phase. . .	41
3.2	Mean fraction of counterions $\langle N_c/N \rangle$ within a distance $2\ell_B$ from the polyelectrolyte chain as a function of $A$ . Inset: $\langle N_c/N \rangle$ as a function of the monomer-monomer attraction energy $\epsilon_{mm}$ for $N = 100$ and $A = 0.89$ . . .	42
3.3	Ratio of the radius of gyration $R_g$ to the number of monomers $N$ as a function of $A$ . Inset: The data for $R_g/N^{1/3}$ collapse for different $N$ for $A \gtrsim 6.25$ . . . . .	43
3.4	The number of non bonded neighbours per monomer $\langle n_b \rangle$ as a function of $A$ for different $N$ . . . . .	44
3.5	The relative fluctuation $\chi_b$ of the number of non bonded neighbours, as defined in Eq. (3.10), as a function of $A$ for different $N$ . Inset: Data collapse when $\chi_b$ and $A$ are scaled as in Eq. (3.11), where $A' = 1.08$ for $N = 50$ and $A' = 0.89$ otherwise. . . . .	45
3.6	Mean Coulomb energy per monomer $\langle E_c \rangle$ as a function of $A$ for different $N$ . Inset: $\langle E_c \rangle \sim N^{2/3}$ in the collapsed phase. . . . .	46

3.7	Fluctuation in the Coulomb energy per monomer $\chi_c$ as a function of $A$ . Inset: Time series of the electrostatic energy per monomer, for $N = 200$ , and $A = 6.50$ . . . . .	47
3.8	Asphericity $Y$ (as defined in Eq. (3.14)) as a function of $A$ . Inset: Variation of asphericity $Y$ with chain length $N$ for $A = 10.93$ . The slope of the straight line is $-0.33$ . . . . .	48
3.9	The relative fluctuation $\chi_b$ in the number of non bonded neighbours, as defined in Eq. (3.10), as a function of $A$ for different $Z$ for $N = 384$ . The y-scale has been rescaled for clarity. Inset: Variation of $\chi_b$ for $Z = 2$ , and for different chain lengths. . . . .	49
3.10	Asphericity $Y$ (as defined in Eq. (3.14)) as a function of $A$ . Inset: Proba- bility density of $Y$ for $Z = 2$ near the transition point. . . . .	50
4.1	The two dimensional projection of the RLPEs at time steps (A) 0, (B) $1.90 \times 10^6$ , (C) $8.90 \times 10^6$ and (D) $4.72 \times 10^7$ . The counterions are monova- lent and are not shown for clarity. The RLPEs aggregate, with the number of aggregates decreasing in time. The data are for $A = 9.43$ . . . . .	58
4.2	(A) The variation of the average aggregate size with $A$ . The data shown by crosses are obtained from simulations where 50 RLPEs, each consists of 30 monomers, are initially randomly distributed. For the data shown by circles we start at high value of $A$ where initially all RLPEs are pre- assembled to a single aggregate. The initial configuration for a lower value of $A$ is the final configuration of the previous value of $A$ . (B) The relative fluctuation $\chi_c$ in electrostatic energy of a single flexible PE as defined in Eq. (4.12). The number of monomers is chosen as 600. The height of the peaks have been rescaled for clarity. (C) The variation of asphericity $Y$ [see Eq. (4.13)] with $A$ of the single PE. . . . .	60

4.3	The variation of $\langle N_a \rangle$ , the average number of aggregates, with time $t$ for different values of $A$ and valency. The data is log-binned and averaged over five different initial configurations. The solid black lines are power laws $\sim t^{-2/3}$ . . . . .	61
4.4	The reversible work $W$ needed to bring two rod-like PEs from a separation of $5\sigma$ to $d$ , in the presence of monovalent counterions. The averages are taken over a production run of $10^7$ steps, after the system has been equilibrated over $10^7$ steps. . . . .	64
4.5	The angular distribution $P(\theta)$ of condensed monovalent counterions around a given PE for $A = 9.43$ . . . . .	66
5.1	(a) Plot of the function $f(x) = ax^2 - bx^4$ . The local concavity condition in Eq. (5.5) has been violated only in the segment $CD$ . The segment $BCDE$ lies below the chord $BE$ , and hence the global condition in Eq. (5.3) has been violated. In this case, we say that the segment $BCDE$ is not concave. (b) The derivative of $f(x)$ , $p = 2ax - 4bx^3$ . . . . .	71
5.2	Plot of the function $F(x, p) = px - f(x) = px - ax^2 + bx^4$ . For $p = 0$ , $x_1$ and $x_3$ are global minima. For $p > 0$ , $x_1$ becomes the global minima and for $p > 0$ $x_3$ is the global minimum. $x_2$ is always the local maximum. . .	72
5.3	(a) Solution of Eq. (5.12) at which $F(x, p)$ is globally minimum. The stable solution for $p < 0$ has been extended to the region $p > 0$ at which it become unstable. Similarly, the stable solution for $p > 0$ has been extended to the region $p < 0$ at which it become unstable. (b) The Legendre transformation $g(p)$ of the function $f(x) = ax^2 - bx^4$ . It has been plotted parametrically using Eq. (5.12) and (5.13). The extended lines correspond to the unstable solutions and the non-concave curve corresponds to the local maxima of $F(x, p)$ . . . . .	73

5.4	(a) Plot of non-concave microcanonical entropy $s(u)$ . The curve $ABCDE$ represents $s(u)$ , and $ABC'DE$ is the concave envelope $\tilde{s}(u)$ of $s(u)$ . (b) The energy-temperature relations. The curve thick curve is obtained from Eq. (5.22) and the curve $abcde$ corresponds to Eq. (5.20). The specific heat is negative in the green region which corresponds to the green region in (a).	77
5.5	A charged disc of charge $+q$ and radius $a$ is placed at the center of a circular container of radius $R$ . The counterions are distributed in the annular region between the disc and the circular boundary, and each counterion carries a charge $-q'$ .	79
5.6	The variation of microcanonical entropy $S$ with energy $E$ is shown for different $L$ . The data are for $N = 3$ and $\chi = 3$ . The solid black lines correspond to the limiting curve obtained from Eq. (5.44). They have been shifted upwards and extended to the left and right for clarity since the unshifted lines are indistinguishable from the curve for $L = 200$ .	84
5.7	The energy-temperature relation for $N = 3$ , $\chi = 3$ for different $L$ in the (a) microcanonical ensemble and (b) canonical ensemble. For large values of $L$ , the transition points are given by $(\beta\chi)_c = \xi(k^*, k^* - 1)$ .	85

# Chapter 1

## Introduction

Polyelectrolytes (PEs) are charged polymers in a solution containing oppositely charged neutralising counterions [1, 2, 3]. The charges on the polymer backbone result from the dissociation of ionizable groups that are present in the polymer into the solution. This dissociation of a neutral polymer into charged polymer and oppositely charged counterions is similar to the dissociation of simple salts like NaCl, and therefore polyelectrolytes are also often called polysalts.

PEs are ubiquitous in biological systems, making the study of PEs important in understanding complex bimolecular phenomena. For instance, DNA molecules are negatively charged polymers that are few meters long and carry a total charge of the order of  $10^{10}$  electronic charges [4]. These DNA molecules are confined in cells of nuclei of radii few micrometers, wherein they undergo complex processes such as replication and transcription [4]. The charged nature of DNA plays an important role in the mechanism of these complex phenomena.

PEs also find many industrial and biomedical applications, primarily because of their solubility in water. The solubility of PEs is a consequence of the gain in entropy in releasing the counterions into the solution. As a result, polyelectrolytes like dry polyacrylic acid can absorb a mass of water many times more than their own mass. This feature of PEs is used in making industrial products like water absorbents or household products

like diapers.

Many properties of polyelectrolyte systems can be derived by using the tools and methods of thermodynamics and statistical mechanics. The thermodynamic behaviour of PEs is determined by the balance between energy and entropy arising from long-ranged Coulomb interactions, short-ranged attraction, excluded volume interactions, mobility of neutralising counterions, and conformational freedom of the polymer backbone. These different competing factors make the behaviour of PEs complex, and the theoretical study of PEs quite challenging.

When the electrostatic effects are negligible, the behaviour of PEs is similar to that of neutral polymers. For high linear charge densities, or low temperatures, the electrostatic effects become important and the behaviour of PEs will be qualitatively different from that of neutral polymers. Despite the greater complexity of PEs, many of the tools and methods that are used to study the behaviour of neutral polymers can be used or extended for the study of PEs as well. In the next two sections, we briefly discuss the basic concepts of neutral and charged polymers.

## 1.1 Neutral polymers

The thermodynamic properties of a polymer can in principle be studied by taking in to account all the microscopic details of the polymer. However, many of the large scale behaviour of a polymer do not depend on the microscopic details, and can be studied using simpler coarse grained models which preserve the macroscopic behaviour [5, 6]. The simplest coarse grained model for neutral polymers is the random walk or random flight model, for which the basic concepts of probability theory and stochastic processes can be used to derive the static and dynamic properties of a polymer [6, 5].

### 1.1.1 Random flight model

In the random flight model, the monomers are modelled as point particles connected through bonds or links, and the interaction between the monomers are neglected. Let  $\mathbf{R}_i$  be the position vectors of the monomers. Then the end to end vector of the chain is given by

$$\mathbf{R} = \mathbf{R}_{N+1} - \mathbf{R}_1 = \sum_{i=1}^N \mathbf{r}_i . \quad (1.1)$$

Here,  $N+1$  is the number of monomers and  $\mathbf{r}_i = \mathbf{R}_{i+1} - \mathbf{R}_i$ , the bond vectors. The mean and mean square end to end distance are given by

$$\langle \mathbf{R} \rangle = \sum_i \langle \mathbf{r}_i \rangle , \quad \text{and} \quad \langle \mathbf{R}^2 \rangle = \sum_{i,j} \langle \mathbf{r}_i \mathbf{r}_j \rangle , \quad (1.2)$$

where the expectation values are taken with respect to the distribution  $\psi(\{\mathbf{r}_i\})$  of the bond vectors. If the direction and magnitude of the bond vectors are independent, the distribution  $\psi$  can be written as the product of the distributions  $\phi(\mathbf{r}_i)$  of individual bond vectors. In such cases, the polymer chain is called *freely joint* or *ideal* chain. Let  $\int d\mathbf{r}_i \phi(\mathbf{r}_i) \mathbf{r}_i = 0$  and  $\int d\mathbf{r}_i \phi(\mathbf{r}_i) \mathbf{r}_i^2 = b^2$ . We then obtain

$$\langle \mathbf{R} \rangle = 0 , \quad \text{and} \quad \langle \mathbf{R}^2 \rangle = Nb^2 . \quad (1.3)$$

Also, from the central limit theorem [7], it follows that the distribution of the end to end vector  $\mathbf{R}$  for large  $N$  is Gaussian, irrespective of the distribution  $\phi(\mathbf{r}_i)$ , as long as  $b$  is finite. For large  $N$  and finite  $b$ , the distribution of  $\mathbf{R}$  in three dimensions is given by

$$\Phi(\mathbf{R}) = \frac{3}{2\pi Nb^2} \exp\left(-\frac{3\mathbf{R}^2}{2Nb^2}\right) . \quad (1.4)$$

The free energy of a ideal chain chain is given by

$$F(R) = E(R) - TS(R) , \quad (1.5)$$

where the energy  $E$  is zero because of the absence of interactions and the entropy  $S(R)$  is given by  $k_B \log \Omega(\mathbf{R})$ , where  $\Omega(\mathbf{R})$  is the number of configurations for which the end to end vector is  $\mathbf{R}$ . It is clear that  $\Omega(\mathbf{R})$  is proportional to  $\Phi(\mathbf{R})$ . Therefore the free energy is given by

$$F(R) = \frac{3\mathbf{R}^2}{2Nb^2\beta} , \quad (1.6)$$

where we have dropped terms that are independent of  $R$  and  $\beta$  is the inverse temperature. Since any distribution  $\phi(\mathbf{r}_i)$  with finite variance  $b^2$  gives the same distribution function for the end to end vector, the choice of the form of  $\phi(\mathbf{r}_i)$  can be made on the grounds of analytical simplicity. One of the most commonly used distribution function is the Gaussian distribution, which is given by

$$\phi(\mathbf{r}) = \frac{3}{2\pi b^2} \exp\left(-\frac{3\mathbf{r}^2}{2b^2}\right) . \quad (1.7)$$

A polymer chain modelled using this distribution is named as Gaussian chain.

### 1.1.2 Excluded volume interactions

For the random flight models described in the previous sections, it was assumed that the monomers are point particles and the interactions between the particles were ignored. The monomers of real polymers occupy non-zero volume and therefore steric repulsion will be present among the monomers. Apart from the steric repulsion, there can be other direct interactions, and also solvent mediated interactions. The nature of the interaction between monomer pairs of polymer chain in a solvent can be described [5, 8] in terms of the second virial coefficient [9]. The second-virial coefficient is a measure of the strength of two-body interactions, and is given by

$$B(T) = \int d\mathbf{r} [1 - \exp(-\beta u(r))] , \quad (1.8)$$

where  $u(r)$  is the effective interaction potential for the monomer pair, and includes both the direct interactions among the monomers and also the interactions mediated by the solvent molecules. If  $B(T)$  is positive, the effective interaction between the pair is attractive, and this regime is called *poor solvent* regime. In the poor solvent regime, as a result of attraction between the monomers, the polymer will be in a collapsed form. If  $B(T)$  is negative, the effective interaction is repulsive and the polymer is said to be in *good solvent* regime. In this regime, the polymer minimises monomer-monomer interactions and maximises monomer-solvent interactions and exists in an extended form. If  $B(T) = 0$ , the two-body interactions among the monomers vanish, and the polymer in such condition is said to be in *theta solvent* regime.

Flory theory [10, 8, 5] is an approximate, yet powerful, method to incorporate excluded volume interactions into the random flight models. The Flory theory is based on the virial expansion [9] of the interaction free energy in terms of the monomer density  $\rho_m = N/R^d$ , where  $d$  is the dimension of the system. The Flory free energy for a neutral polymer can be written as

$$\beta F = \frac{dR^2}{2Nb^2} + B(T) \left( \frac{N}{R^d} \right)^2 R^d + C(T) \left( \frac{N}{R^d} \right)^3 R^d, \quad (1.9)$$

where  $C(T)$  is the third virial coefficient arising from three body interactions. The higher order interaction terms have been dropped. The first term in the free energy is the contribution from the entropic term, given by Eq. (1.6) (replacing dimensionality 3 by  $d$ ). When  $B > 0$ , the third term in the free energy can be neglected compared to the first two terms. In that case, the minimisation of  $F$  with respect to  $R$  gives the scaling  $R \sim N^{3/(d+2)}$ . This corresponds to a regime where the polymer behaves like a self-avoiding walk corresponding to a good solvent. For a poor solvent ( $B < 0$ ), the stability of the polymer chain is determined by the balance between the second and third term in the free energy. Minimising the resulting free energy with respect to  $R$  yields the scaling  $R \sim N^{1/d}$ . This corresponds to the collapsed regime. For a theta solvent ( $B = 0$ ), the stability of the chain is determined by the balance between the entropic term and the

three-body term, and in that case, the minimisation of the free energy gives the scaling  $R \sim N^{2/(d+1)}$ . Therefore, as the second virial coefficient is varied from negative value to positive value, the chain undergoes a transition from a collapsed regime ( $R \sim N^{1/d}$ ) to an extended regime ( $R \sim N^{3/(d+2)}$ ). This transition of a neutral polymer chain with the change in solvent quality is often called Globule-Coil transition [11].

### 1.1.3 Semi-flexible polymers

So far, we have been considering polymers with out any bending rigidity, i.e., there is no restriction on the angles between bonds. Such polymer chains are called *flexible* polymers. In practice, polymers can be stiff, for which there is an energy penalty for conformations which are different from rod-like structures. Such polymers are called semi-flexible polymers. Semi-flexible polymers are better described in the continuum limit ( $b \rightarrow 0$ ). In the continuum limit, a polymer chain is described by a curve  $\mathbf{r}(s)$ , where  $s$  is contour length of a given point on the chain. The Hamiltonian of a semi-flexible chain is defined as [6]

$$H = \frac{E_0}{2} \int_0^L ds \left( \frac{\partial^2 \mathbf{r}}{\partial s^2} \right)^2 . \quad (1.10)$$

Here,  $\frac{\partial^2 \mathbf{r}}{\partial s^2}$  is the local curvature of the chain,  $L$  contour length between the two end points, and  $E_0$  is a constant. It can be shown that the end to end distance of a semi-flexible chain with this Hamiltonian is given by [6]

$$R^2 = 2\ell_p L + 2\ell_p^2 (e^{-L/\ell_p} - 1) , \quad (1.11)$$

where  $\ell_p = E_0/k_B T$ , and is known as persistence length. There are two limiting cases for a semi-flexible chain depending on the value of  $\ell_p$ . If  $L \gg \ell_p$ , we get  $R^2 = 2\ell_p L$ , and therefore, in this limit the chain behaves as a an ideal chain. For  $L \ll \ell_p$ , we get  $R^2 = L^2$ , and therefore the chain is rod-like. In computer simulations of semi-flexible

polymers, discrete models of the polymer are used, and the elasticity of the chain is taken in to account by introducing a potential energy for every pair of neighbouring bonds as a function the angle between them.

## 1.2 Polyelectrolytes

PEs are charged polymers in a solution containing neutralising counterions. The static and dynamic properties of PEs are very rich and they depend on a number of parameters like the linear charge density of the PE backbone, temperature, solvent quality and valency of counterions. As a result of the presence of long-ranged Coulomb interactions and the mobility of counterions, the study of PEs is quite challenging, and a unified theory for all the ranges of parameters of the system has not been achieved yet. Similar to neutral polymers, Flory theory has been successful in deriving different scaling relations in PE systems.

### 1.2.1 Flory theory for polyelectrolytes

The Flory theory for PEs is similar to that for neutral polymers. For very low linear charge density of the PE backbone, the effects of counterions on the conformational properties of the PE can be neglected. For a charged polymer in a theta or good solvent, the contribution to the interaction free energy from the short-ranged interactions can be neglected compared to the contribution from electrostatic interactions. The Flory free energy can then be written as the sum of contributions due the conformational entropy of the PE chain and the electrostatic interactions. The contribution from the conformational entropy of the PE backbone is same as that of a neutral polymer. Assuming that the PE backbone occupies a spherical region of radius  $R$ , the electrostatic contribution to the Flory free energy can be taken as that of a uniformly charged sphere. In that case,

avoiding the prefactors of each contribution, the Flory free energy can be written as

$$F = \frac{k_B T R^2}{N b^2} + \frac{(N q)^2 \ell_B k_B T}{R} . \quad (1.12)$$

Here,  $\ell_B$  is the Bjerrum length [12]  $e^2/4\pi\epsilon k_B T$ , and  $q$  is the charge of a monomer. Bjerrum length is the separation between two electronic charges below which electrostatic interactions dominate over thermal fluctuations. For water at room temperature,  $\ell_B$  is approximately 7.2 nm. Minimisation of the free energy in Eq. (1.12) with respect to  $R$  gives the scaling  $R \sim N$ , and a PE chain with this regime is said to be extended. If  $q = 0$ , then the polymer is neutral, and the theta and good solvent conditions give the scaling  $R \sim N^{1/2}$  and  $R \sim N^{3/5}$  respectively. Therefore, as the charge per monomer is increased from zero, or effectively the dielectric constant is decreased from a high value, the PE chain in a theta solvent undergoes a transition from the scaling regime  $R \sim N^{1/2}$  to an extended configuration. Similarly, if the polymer is in a good solvent, it will make a transition from a self-avoiding configuration ( $R \sim N^{3/5}$ ) to an extended configuration. For PE chain in poor solvent, the contribution to the interaction free energy from short-ranged interactions becomes important, and the free energy in Eq. (1.12) has to be modified. It can be shown that, as the linear charge density is increased, a PE chain in a poor solvent undergoes a transition from a collapsed configuration ( $R \sim N^{1/3}$ ) to the extended configuration through intermediate configurations called pearl-necklace configurations [13, 14].

### 1.2.2 Counterion condensation

So far we have been considering polymers at low linear charge densities where the motion of the counterions are dominated by thermal fluctuations. For high linear charge densities, the electrostatic effects on the motion of counterions has to be taken in to account. Separate existence of a charged polymer and its counterions is not energetically favourable. The energy of the system will be reduced if the counterions condense on

polymer so as to neutralise the bare charges on the polymer. At the same time, the counterions will lose entropy as a result of condensation. Therefore, equilibrium fraction of condensed counterions will be determined by the balance between the energy reduction and the loss of entropy due to the condensation.

There are two main streams of the study of counterion condensation, one is based on the theory of G. S. Manning [15, 16] and the other on the Poisson-Boltzmann approach, initiated by Fuoss et. al. [17]. Both the theories predict that monovalent counterions start condensing on a rod-like charged polymer when the parameter

$$A = \frac{q^2 e^2}{4\pi\epsilon b k_B T}, \quad (1.13)$$

exceeds a critical value of 1.  $A$  is often called the Manning parameter. For  $A < 1$ , the counterions are completely decondensed. For  $A > 1$ , a fraction  $1 - 1/A$  of the counterions are condensed on the PE chain, even if the boundaries of the container are at infinity. This property is a consequence of the long range interaction between the rod and the counterions.

The prediction of counterion condensation has been verified in experiments [16]. One of the quantities that monitors the counterion condensation is the osmotic pressure. In polyelectrolyte system, the osmotic pressure is dominated by the contribution from the free counterions. As a result of the condensation, the number of available free counterions in the system decreases, and as result, the osmotic pressure changes.

Even though the Manning theory and Poisson-Boltzmann approach derive many identical results, there are many quantitative and qualitative differences between the two approaches. For instance, Manning theory treats the condensed counterions as bound ions and the counterions that are not condensed as completely free. In the Poisson-Boltzmann approach, the distribution of counterions is described in terms of the density profile which is peaked at the surface of the polymer for  $A > 1$ . A comparison of Manning theory and Poisson-Boltzmann approach, and the similarities and differences between the two can

be found in Ref. [18]

Although the Manning theory and the Poisson-Boltzmann approach for the counterions are strictly valid only for rod-like and infinitely long charged polymers, these theories are to a good approximation applicable to most of the flexible PEs. The reason is that the PEs are approximately rod-like ( $R \sim N$ ) at values of  $A$  ( $A \approx 1$ ) at which the counterions start experiencing the presence of the charged PE backbone. In extreme poor solvent conditions, the polymer chain may not be completely extended even at  $A \approx 1$  [19], and therefore, more generalised theories are needed to study the counterion condensation in such systems.

### **1.2.3 Effect of counterion condensation on the confirmation of a polyelectrolyte chain**

The condensation of counterions on an extended PE chain alters the stability of the extended configuration of the chain. The condensation of counterions causes the collapse of an extended PE chain into highly compact configurations depending on the rigidity of the PE backbone. For instance, a flexible PE chain collapses into compact globular configurations and semi-flexible PE chain into toroid-like configurations. Such collapse was first observed in experiments, where it was found that DNA molecules collapse in to highly compact configurations upon the addition of multivalent cations [20]. The collapse of PE chain induced by the counterion condensation is purely of electrostatic origin, since such collapse has been observed in good solvent condition also. There are various theoretical proposal for the mechanism of the collapse, and it still a subject of debate.

The pathway of the collapse from an extended configuration to the collapse configuration, as the linear charge density is varied, depends on the nature of the PE chain. If a flexible PE chain is weakly charged, i.e., if only a fraction of the monomers is charged, the chain undergoes the transition from the extended configuration to the globular configu-

ration through an intermediate pearl-necklace configuration. For a strongly charged PE, such intermediate pearl necklace structures do not exist.

#### **1.2.4 Effect of counterion condensation in multiple chain systems**

Similarly charged objects in general repel each other. One of the striking features of multiple chain PE system is the attraction between similarly charged PE chains. The attraction is mediated by the condensed counterions, and the attraction is purely of electrostatic origin. The attraction between similarly charged PE chain was first observed in experiments [21]. It was observed that charged DNA molecules attract each other to form aggregates when multivalent counterions are added to the solution containing DNA molecules. Similar aggregation was later found for many other rod-like PEs like F-actin, microtubules and mosaic viruses [22]. The aggregation of similarly charged PEs were further studied using theoretical methods and computer simulations. Despite these studies, it remains unclear whether monovalent counterions can mediate aggregation of similarly charged PEs. Although experimental evidence exists [23, 24, 25, 26, 27] for aggregation mediated by monovalent counterions, almost all the computer simulations failed to observe the monovalent counterion mediated attraction [28, 29, 30, 31, 32, 33]. Also, while a few theoretical studies [34, 35] argue for the monovalent counterions mediated aggregation, other theoretical studies argue the opposite [36, 37, 38].

### **1.3 The choice of the statistical ensemble for studying polyelectrolyte systems**

The aim of statistical mechanics is to derive the thermodynamics of a system with macroscopic number of degrees of freedom. Depending on the nature of the system, different statistical ensembles such as microcanonical, canonical and grand canonical ensembles

can be used to derive the thermodynamics. For short range systems, these ensembles are equivalent, i.e., they all yield the same thermodynamics in the thermodynamic limit. For long-range system, it has been shown, using exactly solvable models, that different statistical ensembles can be inequivalent [39, 40]. This inequivalence may be manifested as negative specific heat and magnetic susceptibility in the microcanonical ensemble, difference in the order of phase transitions etc. The crucial ingredient that makes the thermodynamics of long-range systems different from short-range system is the non-additivity of total energy. For a short-range system, the total energy of the system will be sum of energies of the subsystems. For long-range systems the additivity of energy does not hold, and it may lead to the inequivalence of different statistical ensembles. It is not necessary that all systems with non-additive long-range interactions will show ensemble inequivalence. The non-additivity of energy along with the non-concavity of the microcanonical entropy results in ensemble inequivalence.

Coulomb interactions are non-additive long-range interactions, and hence different statistical ensembles may not be equivalent for PE systems. It is therefore important to study a given thermodynamic property of PE system in different statistical ensemble and compare the results with experimental observations. However, almost all the theoretical and computational studies on PEs have been restricted to the canonical ensemble. Unfortunately, the number of exactly solvable models of PE systems, where one can pinpoint ensemble equivalence, are very much limited.

## Contribution of this thesis

In this thesis, we study the thermodynamic properties of three different PE systems. The first system that we study is a single flexible PE chain in the presence of monovalent counterions. Using molecular dynamics simulations, we show that counterion condensation in this system is a second-order phase transition, and the condensed counterion induced collapse of the PE chain is a first-order phase transition. We argue that, for a

strongly charged PE, no intermediate phase exists between the extended phase and the condensed-collapsed phase with spherical symmetry. By condensed-collapsed phase we mean the phase which results from the condensation of counterions on the PE backbone. We find that the critical value of the Manning parameters for both the counterion condensation transition and extended-collapse transition decreases with increase in valency of the counterions. We also show that the variation of the fraction of condensed counterions with the number of monomers can be explained in terms of the effective size of the PE chain. These results are described in detail in chapter 3.

The second system that we consider is a collection of similarly charged rod-like PE chains in the presence of neutralising counterions. Using molecular dynamics simulations, we show that monovalent counterions can induce aggregation of similarly charged PE chains above a critical value of Manning parameter. We argue that the absence of such aggregation in the previous simulations [28, 29, 30, 31, 32, 33] can be attributed to the low values of Manning parameter used in those simulations. The critical value of Manning parameter for the aggregation of similarly charged PE chain is found to be very close to the critical value for the extended-collapse transition of a single flexible PE chain for all the valency of counterions that we have considered. The kinetics of aggregation is found to be independent of the valency of counterion and Manning parameter. We also find that the angular distribution of the condensed counterions on the PE chains plays an important role in generation of an attractive interaction between similarly charged PE chains. These results are discussed in detail in chapter 4.

The third system that we study is a two-dimensional charge disc surrounded by freely moving oppositely charged counterions. We study this system both in canonical and microcanonical ensembles, and comparing the analytical solutions in both the ensembles, we show that the ensembles are equivalent for this system, even though the interactions are long-ranged. The microcanonical entropy is piecewise linear and concave in energy, and the concavity of the microcanonical entropy ensures the equivalence of the ensemble. The derivation of the canonical partition function and microcanonical entropy and the

demonstration of the equivalence of the ensembles are given in detail in chapter 5.

## **Publications**

1. *Phase Transitions of a Single Polyelectrolyte in a Poor Solvent with Explicit Counterions*, A. Varghese, S. Vemparala and R. Rajesh, J. Chem. Phys. **135**, 154902 (2011)
2. *Ensemble Equivalence for Counterion Condensation on a Two Dimensional Charged Disc*, A. Varghese, S. Vemparala and R. Rajesh, Phys. Rev. E **85**, 011119 (2012)
3. *Phase Transitions of a Single Polyelectrolyte Chain in a Poor Solvent with Multivalent Counterions*, A. Varghese, S. Vemparala and R. Rajesh, AIP Conf. Proc. **1447**, 129 (2012)
4. *Aggregation of Rod-like Polyelectrolyte Chains in the Presence of Monovalent Counterions*, A. Varghese, R. Rajesh and S. Vemparala, J. Chem. Phys. **137**, 234901 (2012)

# Chapter 2

## Introduction to Molecular Dynamics Simulations

In this chapter, we briefly discuss the principles and methods of molecular dynamics simulations, that will be used in the later chapters. We first discuss the Born-Oppenheimer approximation, which is the basis for using classical equations of motions to study the large-scale behaviour of molecular systems whose small-scale behaviour is determined by Quantum Mechanics. We then discuss about the ensemble- and time-averaging, commonly used force-fields for molecular systems, algorithms for integrating the equations of motion, and periodic boundary conditions. Constant temperature molecular dynamics simulations, and long-range nature of polyelectrolyte systems demand special techniques, and we discuss these issues in Section 3 and 4. And finally, in Section 5 we discuss about the coarse-graining of polymers.

### 2.1 Introduction

The static and dynamical properties of a multi-particle system can in principle be obtained by solving the Schroedinger equation  $H\psi = E\psi$  of the system, where  $H$  is the Hamiltonian and  $\psi$  is the state of the system with energy  $E$ . In general, the number

of constituent particles of a thermodynamic system is of the order of  $10^{23}$  and the interactions among the constituents are nontrivial. Solving the Schroedinger equation for such systems is practically impossible. Progress can be made by coarse graining the system, reducing the number of degrees of freedom. One of such coarse graining methods is the Born-Oppenheimer approximation. To understand the basic idea behind the Born-Oppenheimer approximation, consider a molecule consisting of  $N$  atoms. The nuclei of the atoms are much heavier than the electrons, and as a result, there are two time scales of motion present in the system. One corresponds to the fast motion of the electrons and the other to the slower motion of the nuclei, and these time scales are different by orders of magnitude. The Born-Oppenheimer approximation says that, due to the fast motion of the electrons, the motion of the nuclei and the electrons can be treated separately in a self-consistent manner. Let  $\{\mathbf{r}_i\}$  be the position vectors of the nuclei of the constituent atoms, and  $E_0(\{\mathbf{r}_i\})$  be the energy of the ground state of the electronic state. By Born-Oppenheimer approximation, when the positions of the nuclei change, the electronic configuration changes instantaneously to the new ground state corresponding to the new positions of the nuclei. Or, one can say that the nuclei of the atoms in the molecule move in an effective potential  $E_0(\{\mathbf{r}_i\})$  created by the electrons. The total potential  $U(\{\mathbf{r}_i\})$  of the system will then be the sum of the effective potential  $E_0(\{\mathbf{r}_i\})$  and the Coulomb potential  $\sum_{i \neq j} q_i q_j / 4\pi\epsilon |\mathbf{r}_i - \mathbf{r}_j|$ , where  $q_i$  is the charge of the  $i^{\text{th}}$  nuclei. It can also be shown that, under the Born-Oppenheimer approximation, the motion of the nuclei can be treated classically. The equations of motion of the nuclei are then given by the Newton's equation

$$m_i \ddot{\mathbf{r}}_i = -\frac{\partial U}{\partial \mathbf{r}_i} , \quad (2.1)$$

where  $m_i$  is the mass of the  $i^{\text{th}}$  nuclei. For a system consisting of  $N$  particles, the equations of motion are  $3N$  coupled differential equations. For a general potential  $U(\{\mathbf{r}_i\})$ , these equation can not be solved exactly and numerical methods have to be used. A systematic

way of integrating the equations of motion numerically as a function of time is called Molecular Dynamics (MD) simulation.

### 2.1.1 Ensemble average and time average

There are two ways by which the average thermodynamic properties of a macroscopic system can be calculated. One may start with a given initial condition of the system and then evolve it using Newton's equations of motion. Let  $O(\{\mathbf{r}_i, \mathbf{p}_i\})$  be any physical quantity pertaining to the system corresponding to the microscopic state  $\{\mathbf{r}_i, \mathbf{p}_i\}$ . Then the time average of  $O$  is defined as

$$\langle O \rangle_{time} = \lim_{T \rightarrow \infty} \int_0^T dt O(\{\mathbf{r}_i(t), \mathbf{p}_i(t)\}). \quad (2.2)$$

In the second method, one may consider a large number of replicas of the same system distributed in different microscopic states. Let  $\rho(\{\mathbf{r}_i, \mathbf{p}_i\}) d\mathbf{r} d\mathbf{p}$  be the number of systems in the phase space element  $d\mathbf{r} d\mathbf{p} = d\mathbf{r}_1 \dots d\mathbf{r}_N d\mathbf{p}_1 \dots d\mathbf{p}_N$  around the point  $(\{\mathbf{r}, \mathbf{p}\})$ . Then the ensemble average of the physical quantity  $O$  is defined as

$$\langle O \rangle_{ens} = \frac{\int d\mathbf{r} d\mathbf{p} \rho(\{\mathbf{r}_i, \mathbf{p}_i\}) O(\{\mathbf{r}_i, \mathbf{p}_i\})}{\int d\mathbf{r} d\mathbf{p} \rho(\{\mathbf{r}_i, \mathbf{p}_i\})}. \quad (2.3)$$

One of the basic assumptions of statistical mechanics is that the ensemble average and time average are equivalent in the long time limit, i.e.,  $\langle O \rangle_{time} = \langle O \rangle_{ens}$ . This assumption is also known as the ergodic hypothesis [9]. This assumption refers to the fact that the system during its time evolution visits the phase space volume elements in accordance with the phase space distribution  $\rho$ . If the system is isolated then the positions and momenta evolve according to the Newton's equations and the corresponding phase space distribution  $\rho$  is proportional to  $\delta(E - H(\{\mathbf{r}_i, \mathbf{p}_i\}))$ , where  $H$  is the Hamiltonian of the system. If the system is not isolated, depending on the specification of the system, the equations of motion and the corresponding phase space distribution will be modified. For example, if the system is in contact with the heat bath, the distribution function is

the Boltzmann distribution;  $\rho(\{\mathbf{r}_i, \mathbf{p}_i\}) \propto \exp(-\beta H(\{\mathbf{r}_i, \mathbf{p}_i\}))$ , and it can be shown that the system that evolves according to the Nosé-Hoover equations samples the phase space points consistent with this distribution. More discussion on Nosé-Hoover equations of motion are given in Section 2.3.2

### 2.1.2 Force fields

The explicit functional form of the interaction potential  $U(\{\mathbf{r}_i\})$  for describing systems of interest can in principle be calculated by solving the Schroedinger equation. As mentioned earlier, solving the Schroedinger equation for realistic systems is practically intractable. One then relies on the empirical forms for the interaction potential which captures the essential features of the interactions. For a typical molecular system,  $U(\{\mathbf{r}_i\})$  has the following contributions.

#### 1. Bond stretching potential

The bond potential  $U_{bond}$  acts between two neighbouring atoms or units in a molecule.

The most commonly used form of  $U_{bond}$  is given by

$$U_{bond}(r) = \frac{1}{2}k_b(r - b)^2, \quad (2.4)$$

where  $r$  is the separation between the atoms,  $b$  is the equilibrium bond length and  $k_b$  is the strength of the bond.

#### 2. Bond bending potential

For linear or rigid molecules, there is an energy penalty for configurations for which neighbouring bond vectors do not point in the same direction. In simulations, this feature can be implemented by introducing a potential energy associated with the angle between two neighbouring bonds. One of the most commonly used bond bending potential has the following form:

$$U_\theta = k_\theta [\cos \theta - 1] , \quad (2.5)$$

where  $\theta$  is the angle between two neighbouring bonds and  $k_\theta$  is a measure of rigidity of the molecule. For  $k_\theta = 0$ , the bonds of the molecules are freely joint, and for large values of  $k_\theta$ , the molecule becomes rigid or rod-like.

### 3. Torsion potential

There are molecules for which there is a potential energy associated with the torsion of the molecule. Consider three consecutive bonds of a molecules and label the atoms as 1, 2, 3 and 4. Let  $\hat{n}_{12}$  and  $\hat{n}_{23}$  be the unit vectors in the direction of  $\mathbf{r}_{12} \times \mathbf{r}_{23}$  and  $\mathbf{r}_{23} \times \mathbf{r}_{34}$  respectively, where  $\mathbf{r}_{ij}$  is the bond vector connecting atoms  $i$  and  $j$ . The torsion angle  $\phi$  associated with the three bond vectors is defined as  $\cos \phi = \hat{n}_{12} \cdot \hat{n}_{23}$ . The most commonly used torsion potential corresponding to the torsion angle  $\phi$  is given by

$$U_\phi = k_\phi [\cos \phi - 1]. \quad (2.6)$$

Apart from these bonded interactions, there can be short-range excluded volume interactions and Coulomb interactions, among the constituent particles of the system. The excluded volume interactions arise from the finite size of the particles, and are usually modelled by the Lennard-Jones potential, which is given by

$$U_{LJ}(r) = 4\epsilon \left[ \left( \frac{\sigma}{r} \right)^{12} - \left( \frac{\sigma}{r} \right)^6 \right] , \quad (2.7)$$

where  $\sigma$  is the inter-particle separation at which the potential becomes zero and  $\epsilon$  is the depth of the potential (See Fig. (2.1)).  $U_{LJ}(r)$  is repulsive for  $r < 2^{1/6}\sigma$ , and attractive for  $r > 2^{1/6}\sigma$ .  $U_{LJ}$  is a rapidly decaying function and for computational efficiency, it is convenient to introduce a cut-off distance  $r_c$  above which  $U_{LJ}(r)$  is set to zero. Then obviously the potential will be discontinuous at  $r = r_c$ . To avoid this discontinuity, shifted potential of the form  $U_{LJ}(r) - U_{LJ}(r_c)$  is often considered, which makes the potential

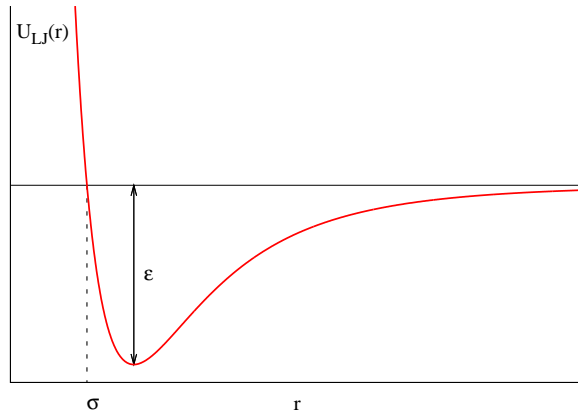


Figure 2.1: A plot of the Lennard-Jones potential.

vanish smoothly at  $r = r_c$ .

### 2.1.3 Periodic boundary conditions

In MD simulations, finite number of particles are often used to study the thermodynamic properties of a system with macroscopic number of degrees of freedom. For systems with small number of particles, the fraction of the number of particles at the boundary of the simulation box is comparable with that in the bulk. The environment felt by the particles at the boundary of the simulation box is different from that in the bulk. This will cause surface effects, which are not negligible for small systems, and therefore the thermodynamic properties obtained from the simulation will be considerably different from that of the system under consideration. These surface effects can be overcome by implementing periodic boundary conditions. With periodic boundary conditions, the original simulation box is periodically replicated in all three directions in the space. For a particle at  $\mathbf{r}$  in the original simulation box, one also consider its periodic images at positions  $\mathbf{r} + \mathbf{n}L$ , where  $\mathbf{n} \equiv \{n_x, n_y, n_z\}$  and  $L$  the length of the simulation box.  $n_x, n_y$  and  $n_z$  are integers, and  $\mathbf{n} = 0$  corresponds to the original simulation box. Under periodic boundary conditions, a particle interacts not only with the other particles in the original simulation box, but also with all the periodic images of these particles and

also the self-image. For short-range interactions, since the inter-particle potential decays rapidly, a cut-off distance above which the potential is set to zero is often used. If the cut-off distance is smaller than the length of the simulation box, then for the evaluation of potential and forces, it is necessary to consider only the first periodic images ( $\mathbf{n} = 1$ ) of the infinite periodic images. This is called minimum image convention. For long-range interactions, the contribution from all the infinite periodic images have to be considered and special techniques are required for the evaluation of potential and forces. Some of those techniques are described in Section 2.4.

## 2.2 Algorithms for integrating the equation of motion

The equation of motion in Eq. (2.1), a second-order differential equation, can be written as two coupled first-order differential equations of the form

$$\dot{\mathbf{r}}_i = \frac{\mathbf{p}_i}{m_i} , \quad (2.8)$$

and

$$\dot{\mathbf{p}}_i = \mathbf{f}_i , \quad (2.9)$$

where  $\mathbf{f}_i = -\frac{\partial U}{\partial \mathbf{r}_i}$  is the total force acting on the  $i^{\text{th}}$  particle, and  $\mathbf{p}_i = m_i \mathbf{v}_i$ . One of the most commonly used algorithms for solving these equations is the Verlet algorithm [41]. The Verlet equations for updating the positions and velocities can be derived as follows; using the Taylor expansion of  $\mathbf{r}(t)$  one gets

$$\mathbf{r}(t + \Delta t) = \mathbf{r}(t) + \mathbf{v}(t)\Delta t + \frac{\mathbf{f}(t)}{2m} (\Delta t)^2 + \mathcal{O}(\Delta t^3) , \quad (2.10)$$

and

$$\mathbf{r}(t - \Delta t) = \mathbf{r}(t) - \mathbf{v}(t)\Delta t + \frac{\mathbf{f}(t)}{2m} (\Delta t)^2 + \mathcal{O}(\Delta t^3) . \quad (2.11)$$

Adding the above two equation one get the Verlet equation for the position coordinates

$$\mathbf{r}(t + \Delta t) = 2\mathbf{r}(t) - \mathbf{r}(t - \Delta t) + \frac{\mathbf{f}(t)}{m}(\Delta t)^2 + \mathcal{O}(\Delta t^4) . \quad (2.12)$$

The advantage of this equation is that the velocities do not appear in this equation and hence the knowledge of the velocity is not required to update the positions. However, the velocities are required for the calculation of the kinetic energy. Subtracting Eq. (2.11) from Eq. (2.10) we get

$$\mathbf{v}(t) = \frac{\mathbf{r}(t + \Delta t) - \mathbf{r}(t - \Delta t)}{2\Delta t} + \mathcal{O}(\Delta t^2) . \quad (2.13)$$

This equation has the disadvantage that the velocity at  $t$  can be determined only after computing the position at  $t + \Delta t$ . This disadvantage can be overcome by a modified Verlet algorithm, namely the velocity Verlet algorithm [42]. In this algorithm, the positions and velocities are updated using the expressions

$$\mathbf{r}(t + \Delta t) = \mathbf{r}(t) + \mathbf{v}(t)\Delta t + \frac{\mathbf{f}(t)}{2m} (\Delta t)^2 , \quad (2.14)$$

and

$$\mathbf{v}(t + \Delta t) = \mathbf{v}(t) + \frac{\mathbf{f}(t + \Delta t) + \mathbf{f}(t)}{2m} \Delta t . \quad (2.15)$$

It can be shown [43] that this algorithm is equivalent to the position Verlet algorithm, and therefore the accuracy of velocity Verlet algorithm is same as that of the original Verlet algorithm. The velocity Verlet algorithm is implemented in three steps. In the first step, the position is updated using Eq. (2.14). In the second step, force at  $t + \Delta t$  is calculated using the updated position  $\mathbf{r}(t + \Delta t)$ . In the third step, the velocity is updated using Eq. (2.15).

## 2.3 Constant temperature molecular dynamics simulations

The solution of the equations of motion in Eq. (2.8) and (2.9) are phase space trajectories along which the total energy of the system is a constant. The kinetic energy, which is a measure of the temperature, and the potential energy fluctuate along these trajectories. In practice, we often come across systems which are in contact with heat reservoirs. These heat reservoirs are associated with a constant temperature, and exchange energy with the system. For such case, the distribution of energy of the system is given the Maxwell-Boltzmann distribution (canonical distribution). In order to maintain a constant temperature and to achieve canonical distribution for the energy of the system, the equations of motion in Eq. (2.8) and Eq. (2.9) have to be modified, incorporating the effect of the heat reservoir. These modified equations of motions or schemes to realize the canonical distribution of energy are called constant temperature MD or canonical MD. The most commonly used methods to implement constant temperature MD are Andersen thermostat, Nosé-Hoover thermostat and Langevin dynamics.

### 2.3.1 Andersen thermostat

In Andersen thermostat [44], a number of particles of the system are randomly chosen at regular intervals and then the velocities of the chosen particles are replaced with the velocities drawn from the Maxwell-Boltzmann distribution corresponding to the desired temperature. It can be shown that this procedure generate the canonical distribution [44]. The velocity replacement of the particles can be thought of as collisions of the particles with an imaginary heat bath. Between collisions, the system evolves according to the equations of motion in Eq. (2.8) and Eq. (2.9). The role of the collisions is to drive the system from one constant energy shell to the other such that the system samples all the possible energy levels. The strength of the coupling between the system and the heat bath is determined by the frequency of collisions  $\nu$ . If  $\nu$  is very small, the different energy

levels will be sampled slowly and the canonical distribution will be realised only over a long time. If  $\nu$  is very high, the system will make transition among the the energy levels very often and hence the configurations with the same energy will be sampled at a low rate. The optimum collision frequency depends on the nature of the system under consideration.

Though the Andersen thermostat generates the canonical distribution, it is not advisable to use this thermostat for determining the dynamic properties of the system. When the velocities of the particles are independently replaced with the velocities drawn from Boltzmann distribution, the correlations in the velocities of the system will be destroyed, which are important in the evaluation of dynamic properties such as diffusion constant.

### 2.3.2 Nosé-Hoover thermostat

The Nosé-Hoover thermostat [45, 46] is a deterministic thermostat that generates the canonical distribution for the energy. In a Nosé-Hoover thermostat, the equations of motion in Eq. (2.8) and Eq. (2.9) are modified in order to incorporate the effect of a heat bath. The equations of motion in the Nosé-Hoover thermostat are

$$\dot{\mathbf{r}} = \frac{\mathbf{p}_i}{m_i} , \quad (2.16)$$

$$\dot{\mathbf{p}}_i = -\frac{\partial U}{\partial \mathbf{r}_i} - \xi \mathbf{p}_i , \quad (2.17)$$

and

$$\dot{\xi} = \left( \sum_i \frac{p_i^2}{m_i} - \frac{3N}{\beta} \right) / Q , \quad (2.18)$$

where  $\beta$  is the inverse temperature and  $N$  is the number of particles in the system. The parameter  $\xi$  can be thought of as the degree of freedom representing the heat bath. The value of  $Q$  determines the strength of the coupling between the system and the heat bath. When the kinetic energy of the system  $\sum_i p_i^2/2m_i$  falls below the desired thermal energy  $3N/2\beta$ , the parameter  $\xi$  decreases (See Eq. (2.18)) so as to increase the momentum of

the particles (See Eq. (2.17)). This is analogous to the flow of energy from the heat bath to the system. In the same way, when the kinetic energy of the system is more than the desired thermal energy, energy flows from the system to the heat bath. If the coupling constant  $Q$  is very low, the energy flow between the system and the heat bath will be oscillatory with very high amplitude, and the system takes very long time to equilibrate. If  $Q$  is very high, the energy flow will be very slow, and the sampling of configurations with different energy will be slow. In the limit  $Q \rightarrow \infty$ , the Nosé-Hoover equations of motion reduce to the energy conserving equations of motion in Eq. (2.8) and Eq. (2.9). The details about the implementation of the Nosé-Hoover equations of motion can be found in Ref. [43].

### 2.3.3 Langevin Dynamics

In MD simulations of macromolecules in a solvent, most of the computation time will be expended on simulating the solvent molecules which may be very large in number. When we are interested in the dynamics and equilibrium properties of the macromolecule alone, it is then desirable to take in to account the effect of the solvent molecules in an implicit way. Langevin dynamics is one of the methods which treats the solvent molecules implicitly. In Langevin dynamics simulation, the effect of solvent appears as two contributions to the force acting on the constituent atoms of the system. The first contribution is the viscous force  $-\gamma\mathbf{p}_i$  exerted by the solvent molecules and the second one is a random force  $\boldsymbol{\eta}_i$  which can be thought of as the result of random collisions of the solvent molecules with the constituent atoms of the system. The equation of motion of Langevin dynamics can be written as

$$m_i\ddot{\mathbf{r}}_i = -\frac{\partial U}{\partial \mathbf{r}_i} - \gamma\mathbf{p}_i + \boldsymbol{\eta}_i , \quad (2.19)$$

where the random force  $\boldsymbol{\eta}$  has the following statistical properties

$$\langle \eta_{i\alpha} \rangle = 0 , \quad (2.20)$$

and

$$\langle \eta_{i\alpha}(t) \eta_{j\beta}(t') \rangle = 2m_i \gamma k_B T \delta_{ij} \delta_{\alpha\beta} \delta(t - t') , \quad (2.21)$$

where  $k_B$  is the Boltzmann constant and  $T$  is the desired temperature of the system. In Langevin dynamics simulations, the implicit solvent molecules serve as the heat bath for the system under consideration. The details about the implementation of the Langevin equation can be found in Ref. [47].

## 2.4 Long-range interactions

As we mentioned earlier, for systems with long-range interactions and under periodic boundary conditions, a given particle interacts with all the infinite periodic images of all the particles in the original simulation box. Therefore, in order to evaluate the potential felt by a given particle, the contribution from all the infinite periodic images has to be considered. Coulomb interactions are long-ranged, and therefore special techniques are required for the evaluation of potential in charged systems. The most commonly used methods for the evaluation of potential in charged systems are the Ewald summation method and particle-particle/particle-mesh method.

### 2.4.1 Ewald summation method

To understand the basic idea behind the Ewald summation method [48], consider a point particle of charge  $q$  located at  $\mathbf{r}_i$ . Then the charge density can be written as  $\rho(\mathbf{r}) = q\delta(\mathbf{r} - \mathbf{r}_i)$ . The first step in the Ewald summation method is to rewrite the charge density as  $\rho(\mathbf{r}) - q\rho_g(\mathbf{r}) + q\rho_g(\mathbf{r})$ , where  $\rho_g(\mathbf{r})$  is given by

$$\rho_g(\mathbf{r}) = \left(\frac{\alpha}{\pi}\right)^{3/2} \exp(-\alpha|\mathbf{r} - \mathbf{r}_i|^2) , \quad (2.22)$$

where the parameter  $\alpha$  determines the width of the distribution  $\rho_g(\mathbf{r})$ . The potential generated by the charge density  $\rho(\mathbf{r}) - q\rho_g(\mathbf{r})$  is short-ranged because of the cancellation of the original charge  $q$  by the charge distribution  $-q\rho_g(\mathbf{r})$ . It can be shown that [43] the potential generated by the charge distribution  $\rho(\mathbf{r}) - q\rho_g(\mathbf{r})$  is given by

$$\phi_1(r) = \frac{q}{4\pi\epsilon|\mathbf{r} - \mathbf{r}_i|} \text{erfc}(\alpha^{1/2}|\mathbf{r} - \mathbf{r}_i|) , \quad (2.23)$$

where  $\text{erfc}(x)$  is the complimentary error function and is given by  $\text{erfc}(x) = 1 - \text{erf}(x)$ ;  $\text{erf}(x)$  is the error function  $(2/\pi^{1/2}) \int_0^x du \exp(-u^2)$ . Since  $\phi_1(r)$  is short-ranged, one may introduce a cut-off distance  $r_c$  above which the potential can be set to zero. The potential generated by the charge distribution  $q\rho_g(\mathbf{r})$  is given by

$$\phi_2(\mathbf{r}) = \frac{q}{4\pi\epsilon|\mathbf{r} - \mathbf{r}_i|} \text{erf}(\alpha^{1/2}|\mathbf{r} - \mathbf{r}_i|) . \quad (2.24)$$

Now consider all the periodic images of the point charge  $q$  at  $\mathbf{r}_i$ . Then the charge density is given by  $\rho(\mathbf{r}) = \sum_{\mathbf{n}} q\delta(\mathbf{r} - \mathbf{n}L)$ . As for the single point charge, we rewrite the charge density as  $\rho(\mathbf{r}) - \rho_G(\mathbf{r}) + \rho_G(\mathbf{r})$ , where  $\rho_G(\mathbf{r}) = \sum_{\mathbf{n}} q\rho_g(\mathbf{r} + \mathbf{n}L)$ . The potential due to the charge distribution  $\rho(\mathbf{r}) - \rho_G(\mathbf{r})$  is the sum of of the potentials given in Eq. (2.23), i.e.,

$$\Phi_1(r) = \sum_{\mathbf{n}} \phi_1(\mathbf{r} - \mathbf{n}L) \quad (2.25)$$

$$= \sum_{\mathbf{n}} \frac{q}{4\pi\epsilon|\mathbf{r} - \mathbf{r}_i - \mathbf{n}L|} \text{erfc}(\alpha^{1/2}|\mathbf{r} - \mathbf{r}_i - \mathbf{n}L|) . \quad (2.26)$$

The function  $\text{erfc}(x)$  is rapidly decaying, and hence one may set the summand to zero for large  $\mathbf{n}$  and  $|\mathbf{r} - \mathbf{r}_i - \mathbf{n}L|$ . The potential generated by the charge distribution  $\rho_G(\mathbf{r})$

is the sum of the potentials given in Eq. (2.24), and is given by

$$\Phi_2(r) = \sum_{\mathbf{n}} \phi_2(\mathbf{r} - \mathbf{n}L) \quad (2.27)$$

$$= \sum_{\mathbf{n}} \frac{q}{4\pi\epsilon|\mathbf{r} - \mathbf{r}_i - \mathbf{n}L|} \text{erf}(\alpha^{1/2}|\mathbf{r} - \mathbf{r}_i - \mathbf{n}L|) . \quad (2.28)$$

The function  $\text{erf}(x)$  is a slowly decaying function and hence one needs to evaluate all the infinite terms in the summation. A great simplification arises if one consider the problem in the reciprocal space. Let  $\rho_G(\mathbf{k})$  and  $\Phi_2(\mathbf{k})$  are the Fourier transforms of  $\rho_G(\mathbf{r})$  and  $\Phi_2(\mathbf{r})$ , where  $\mathbf{k}$  is the reciprocal lattice vector,  $\mathbf{k} = \frac{2\pi}{L}\mathbf{l}$ , with  $\mathbf{l} \equiv (l_x, l_y, l_z)$ .  $l_x, l_y$  and  $l_z$  are integers such that  $\exp(i\mathbf{k} \cdot \mathbf{n}L) = 1$ . Then the Poisson equation  $\nabla^2 \Phi_2(\mathbf{r}) = -\rho_G(\mathbf{r})/\epsilon$  in the real space takes the form  $k^2 \Phi_2(\mathbf{k}) = \rho_G(\mathbf{k})/\epsilon$  in the Fourier space.  $\rho_G(\mathbf{k})$  can easily be evaluated, and one can show that the inverse Fourier transform of  $\Phi_2(\mathbf{k})$  gives

$$\Phi_2(r) = \sum_{\mathbf{k}} \frac{q}{L^3 \epsilon k^2} \exp(-i\mathbf{k} \cdot (\mathbf{r} - \mathbf{r}_i)) \exp(-k^2/4\alpha) , \quad (2.29)$$

where  $k = |\mathbf{k}|$ . It can be seen that the summand decays very fast with  $k$ , and as result, one may introduce a cut-off  $\mathbf{k}_c$  above which the summand can be set to zero. In summary, the potential generated by a point charge and all its periodic images can be written as the sum of two contributions  $\Phi_1(\mathbf{r})$  and  $\Phi_2(\mathbf{r})$ .  $\Phi_1(\mathbf{r})$  is generated by an infinitely periodic array of point charges screened by smeared charges with opposite sign.  $\Phi_2(\mathbf{r})$  is the sum of potential generated by an infinitely periodic array of Gaussian charge distributions.  $\Phi_1(\mathbf{r})$  and  $\Phi_2(\mathbf{r})$  are evaluated in the real and reciprocal space respectively. This method can easily be generalised to a periodic system of many particles with non-identical charges.

### 2.4.2 Particle-particle/particle-mesh method

In this section, we briefly outline the particle-particle/particle-mesh (PPPM) method for the evaluation of forces and potential due to long-range interactions. The PPPM method mainly consists of three steps. In the first step, the continuous charge distribution in the

system is assigned to the finely spaced grid points in to which the simulation box has been divided. As the second step, the Poisson equation is solved for the potential at these grid points using fast Fourier transform methods. Also, the electric field at each grid point has been calculated by taking the discrete derivative of the potential at these grid points. In the third step, the potential or electric field on these grid points are assigned to the original charged particles in the system. The details about each step involved in the PPPM method and its implementation can be found Ref. [49]. The advantage of PPPM method over the Ewald method is that the computational time required for the latter scales with the number of particles as  $\mathcal{O}(N^{3/2})$ , whereas for in case of PPPM, it scales as  $\mathcal{O}(N \log N)$ .

## 2.5 Coarse-grained molecular dynamics simulations of polymers

The behaviour of macromolecules such as polymers can in principle be studied by taking in to account the atomistic details of the molecule. One of the practical difficulties in simulating in such detail is the presence of multiple time scales in the system. For instance, the time scale associated with the vibration of atoms in the monomers of a polymer is much smaller than the autocorrelation time of the end to end vector of the polymer. If one is interested in the properties associated with vibration of the atoms in the molecule, the time step used in the simulation must be much smaller than the time scale associated with such vibrations. In that case, in order to observe the large scale behaviour of the system, the system has to simulated for longer times, which are often practically difficult for real polymers. Apart from the temporal scales, another aspect of computational difficulties comes from spatial scale of the problem; typical polymers consist of  $10^4 - 10^5$  monomers, each of which is made of many atoms, and the computational time required often varies as the square of the number of constituents. Fortunately, many of the large scale properties of thermodynamic systems like polymers in general do not depend on the

microscopic details. Therefore, coarse-grained models, which retain the essential features of a polymer, can be used to study such large scale properties. One of the most commonly used and the simplest coarse-grained model for polymers is the *bead-spring* model. In this model, each monomer is represented by a single unit called *bead*, and the connectivity of the monomers is taken in to account by *springs* that connects the beads. There are mainly two advantages for such coarse graining. First, since the microscopic details have been coarse-grained, larger time steps can be used, allowing probing of long time-scale phenomena. Secondly, since the constituent atoms in a monomer has been represented by a single unit, a larger number of monomers (beads) closer to that in real polymers can be used for a given computational time. It is to be noted that the coarse-graining procedure is not unique; for instance, instead of single monomer, a set of monomers can be represented as a single unit. The level of course graining is often based on the specific large scale property under consideration. In this thesis, we follow a coarse-graining method where each monomer is represented as a single degree of freedom.

# Chapter 3

## Phase Transitions of a Single Polyelectrolyte in a Poor Solvent

### 3.1 Introduction

A flexible polyelectrolyte (PE) chain in a poor solvent undergoes a series of phase transitions as the linear charge density of the chain is varied keeping temperature fixed. The rich phase diagram resulting from a competition between the long range Coulomb interaction and the short range excluded volume interaction has been studied theoretically [50, 51, 52, 53, 54, 13, 14, 15, 55, 56], numerically [53, 54, 13, 14, 57, 58, 59, 60, 19] and experimentally [61, 62, 63, 64, 65, 66, 67]. At very low charge densities, the PE chain is in a collapsed phase, with the counterions uniformly distributed throughout the solution [19]. On increasing the charge density, the PE chain makes a transition into a pearl-necklace phase in which the chain has two (dumbbell) or more globules connected through a string of monomers [51, 52, 53, 54]. This transition is similar to the Rayleigh instability of a charged droplet [68, 69]. While the pearl-necklace phase has been observed in numerical simulations [60, 70, 19], the experimental status is unclear [61, 64, 66]. Further increase in charge density increases and decreases the number and size of the globules respectively, and the PE chain becomes extended. When the linear charge density exceeds

a threshold value, the electrostatic energy dominates over the thermal fluctuations and the counterions begin to condense onto the PE chain [15]. The condensed counterions form dipoles with the polymer monomers and the attraction among the dipoles leads to the collapse of the PE chain into a globule [58, 71]. Another proposed mechanism for the chain collapse is the onset of negative compressibility due to correlated thermal fluctuation [72]. Note that the collapse of the PE chain at high linear charge density differs from that at low linear charge density in that the former is induced by condensed counterions, while the later is driven by the solvent quality. We name the collapsed phase of the PE chain for which the counterions are condensed as condensed-collapsed phase. In between the extended and condensed-collapsed phases, for partially charged PE chains, the competition between the attraction due to condensed counterions and electrostatic repulsion due to uncompensated charges leads to the formation of a second pearl-necklace phase [13, 14, 57]. This pearl-necklace phase, in contrast to the one at low values of the linear charge density, exists even in good solvent conditions [14]. For fully charged PE chains, the strong electrostatic repulsion among the monomers prevents the formation of such pearl-necklace structure [13]. Recent simulations also show that, in extreme poor solvent conditions, where the short-range attraction between monomers is much larger than  $k_B T$ , the PE chain can make a direct transition from the initial collapsed phase to the final condensed collapsed phase without going through some or even all the intermediate phases [19].

Certain features of the phase diagram remain poorly understood. Recent simulations argue for the existence of an intermediate phase between the extended and the condensed collapsed phases [19, 60]. Referred to as the sausage phase, this phase is defined as a condensed-collapsed phase in which the shape of the collapsed PE becomes aspherical, having a non-zero mean asphericity. It is not clear whether this phase is just a finite size effect.

In addition, the nature of the counterion condensation transition is not well understood. By studying the condensation of counterions on a cylinder in three dimensions,

and on a disc in two dimensions, it was shown that condensation is a second-order phase transition [73, 74, 75]. However, to the best of our knowledge, the corresponding question has not been addressed for a three dimensional PE chain system.

In this chapter, we mainly focus on the following two aspects of the phase behaviour of a single PE: the counterion condensation transition and the transition of the PE chain from the extended phase to the condensed-collapsed phase (extended-collapsed transition). Below, we describe these two transitions in detail.

### 3.1.1 Counterion condensation transition

The counterion condensation transition in PE systems is of considerable importance, because many of the colligative and dielectric properties such as osmotic pressure and conductivity of the system depend on the fraction of counterions condensed on the PE chain. It has been studied extensively using experimental, computational and theoretical methods. One of the successful, and perhaps the simplest theory of counterion condensation is by Manning [15]. Manning modelled a PE chain as an infinite line of charges with uniform linear charge density and the counterions as point-like charged particles, and assumed that the system is infinitely dilute. Let  $\tau e$  be the linear charge density of the line of charge and  $-Ze$  the charge of the counterions. In the infinite dilution limit, the direct interaction among the counterions can be neglected, and in that case the potential energy of a counterion is given by

$$U(r) = \frac{2\tau Z \ell_B}{\beta} \log(r) , \quad (3.1)$$

where  $\ell_B$  is the Bjerrum length [12], the length scale below which electrostatic interactions dominate thermal fluctuations.

$$\ell_B = \frac{e^2}{4\pi\epsilon k_B T} . \quad (3.2)$$

Since the direct interactions among the counterions are neglected, the partition function of the system will be proportional to  $Z_1^N$ , where  $N$  is the number of counterions in the

system and  $Z_1$  is the one particle partition function

$$\begin{aligned}
Z_1 &= \int d^3r e^{-\beta U(r)} , \\
&\propto \int_0^R dr \, r \, e^{-2\tau Z \ell_B \log(r)} , \\
&= \int_0^R dr r^{1-2AZ} ,
\end{aligned} \tag{3.3}$$

where  $R$  is the lateral extension of the container, and  $A = \tau \ell_B$ .  $A$  is termed as the Manning parameter, and it is a measure of the relative strength of electrostatic interactions. From Eq. (3.3), it can be seen that the partition function diverges at small distance for  $AZ > 1$ . Manning argued that the system is not stable at these values of  $A$ , and that a fraction of the counterions will condense on the line of charges so as to meet the condition  $A_{eff}Z = \beta\tau'Z = 1$ , where  $\tau'$  is the reduced linear charge density due to condensation. If  $f$  is the fraction of condensed counterions, the charge neutrality condition implies  $\tau' = \tau - \tau fZ$ . Then solving the equation  $\beta\tau'Z = 1$ , we get the fraction of the condensed counterions as a function  $A$

$$f = 1 - \frac{1}{AZ} . \tag{3.4}$$

In summary, the condensed and decondensed regimes of the counterions is determined by the condition  $A = 1/Z$ . For  $AZ < 1$ , the counterions are decondensed and distributed in the solution, and when  $AZ > 1$ , a fraction  $1/AZ$  of the counterions will be condensed on the line of charges. Using these arguments, Manning estimated the colligative parameters such as the activity and osmotic coefficient of the idealised PE system. These estimates were in quantitative agreement with the experimental data for real PE systems [15]. Manning's proposal that a fraction of counterions will be condensed on the PE chain for  $A > 1/Z$  was later confirmed by a number of experiments. Most of these experiments were carried out either at  $A > 1/Z$  or  $A < 1/Z$ . In 1984, Klein et. al. [76] varied  $AZ$  from 0.82 to 1.85 through the theoretical threshold  $AZ = 1$ , by changing the dielectric

constant of the medium. They found that the electrophoretic mobility of the system changes abruptly near  $A = 1/Z$ . It was observed that the conformation of the PE chain does not change in this range of  $A$ , and hence the fall in mobility was argued to be due to the condensation of counterions. In a later experiment, Panafiel et. al. [77] found that the ionic conductivity of the PE system falls near  $A = 1/Z$ , again suggesting the charge renormalisation due to the counterion condensation. In summary, Manning theory, despite its simplicity and assumptions, explains the experimentally observed properties of a range of real PE systems. Another successful approach for the counterion condensation is based on the Poisson-Boltzmann equation, initiated by Fuoss et. al. [17]. This approach is more involved and will not be discussed in detail here. A comparison between Manning theory and the Poisson-Boltzmann approach can be found in Ref. [18].

The criticality of the counterion condensation transition was recently studied by Netz et. al. [73, 74]. Using Monte Carlo simulations, and finite-size and finite-particle analysis, they showed that the counterion condensation on an infinitely long charged cylinder is a second-order phase transition. They evaluated the critical exponents and found that the exponents are in accord with the mean field theory based on Poisson-Boltzmann equation [17]. A similar analysis, to our knowledge, has not been attempted for the counterion condensation in flexible PEs.

### 3.1.2 Extended-collapsed transition

The coil-globule transition in PE systems became an active area of research since the discovery of the coil-globule transition of DNA by Lerman [78] in 1971. Lerman observed that DNA molecules in aqueous solution collapse in to highly compact structures when suitable amount of neutral polymers such as polyethylene glycol (PEG) is added to the solution. The minimum concentration of PEG required for the collapse was found to be decreasing with increasing concentration of the added salts. The physical explanation for the collapse phenomena is that the PEG molecules make the solution poor for the DNA backbone, i.e., the effective interactions among the segments of the DNA molecules

become attractive. As a result, at a critical value of the concentration of the PEG molecules, the DNA molecules collapse in to a compact structure. The role of the added salt is to screen the repulsion among the charged phosphate groups in DNA, and thus the concentration of PEG required for the collapse of DNA molecules decreases with the increasing concentration of the salts. Later in 1976, Gousule et. al. [20] showed that a similar collapse of DNA molecules occur when multivalent cations are added to the solution containing no PEG molecules. It was argued that the collapse mechanism has a different physical origin, since the solvent quality of the solution was not considerably changed on the addition of the cations. In an another set of experiments, Wilson et. al. [79] showed that the collapse of DNA molecules is followed by the condensation of cations on the DNA molecules. They studied the collapse of DNA molecules in the presence of multivalent cations of various valencies. They found that the collapse of the DNA molecules is triggered by the neutralisation of 90% of the phosphate groups in the DNA molecules, irrespective of the valency of the cations.

A physical explanation for the collapse of DNA chain resulting from the counterion condensation was first given by Maquet et. al. [80]. They argued that the condensed counterions not only screen the repulsive interactions among the charged phosphate groups in the DNA, but also induce attraction among the segments of the molecule via the correlated density fluctuations of the condensed counterions. In 1998, Brilliantov et. al. [81] gave a similar argument for the collapse. They argued that correlations in the counterion density fluctuations give rise to the negative compressibility in the system, which result in a first-order like collapse of the PE chain. The role of the counterion density fluctuations on the collapse of PE was further studied by Kardar et. al. [71] and they also argued that the correlated density fluctuation give rise to the attraction among the segments of the PE chain. In a molecular dynamics simulation study, Winkler et. al. [58] analysed the structural arrangement of the condensed counterions on the PE chain. They found that the condensed counterions form dipoles with the oppositely charged monomers of the PE chain and the attraction among these dipoles lead to the collapse of the chain. In this

study also, the spacial correlations among the condensed counterions found to play an important role in the collapse of the PE chain. Solis et. al. [82] gave an alternate theoretical explanation for the collapse, which is opposite to the previously proposed theoretical explanations. They assumed that the condensed counterions and the monomers form a dense network, where the counterions do not fluctuate but are localised to the monomers. Using these assumptions they estimated the free energy for the extended and collapsed configuration of the PE and predicted a first-order like collapse of the PE chain. These theories, despite the difference in the opinion about the physical origin of the collapse, predict a first-order like collapse of a PE chain under similar conditions. To our knowledge, the nature, especially the order, of this transition has not been investigated using computational methods.

In the following sections, we present our results of molecular dynamics simulations of a single flexible PE chain in a poor solvent in the absence of added salts. The linear charge density of the PE backbone has been taken as the tuning parameter while all the other parameters have been kept constant. We primarily focus on the counterion condensation transition and the extended-collapsed transition of the PE chain.

## 3.2 Model and simulation method

The atomistic simulations of real polymer systems are computationally expensive because of the large number of degrees of freedom. Therefore, in general, suitably course-grained models which capture the essential features of the realistic systems are adopted for computational purposes. In our simulations, we use the most commonly used coarse-grained model of PEs, namely the bead-spring model. In a bead-spring model, the PE chain is modelled as  $N$  spherical beads (monomers) connected through springs where each monomer carries a charge  $qe$ . The counterions are modelled as spherical beads, each carrying a charge  $-Zqe$ , where  $Z = 1, 2$  and  $3$  correspond to monovalent, divalent and trivalent counterions. The number of counterions in the system is equal to  $N/Z$  so that

the system is overall charge neutral. We have set  $Z = 1$  for our simulations, except for the discussion in Sec. 3.3.6. The PE chain and the counterions are assumed to be in a medium of uniform dielectric constant  $\epsilon$ . The potential energy due to the pair of particles  $i$  and  $j$  consists of three interactions.

Coulomb interaction: The electrostatic energy is given by

$$U_c(r_{ij}) = \frac{q_i q_j}{4\pi\epsilon\epsilon_0 r_{ij}}, \quad (3.5)$$

where  $q_i$  is the charge of  $i^{th}$  particle, and  $r_{ij}$  is the distance between particles  $i$  and  $j$ .

Excluded volume interaction: The excluded volume interactions are modelled by the Lennard-Jones potential, which for two particles at a distance  $r_{ij}$ , is given by

$$U_{LJ}(r_{ij}) = 4\epsilon_{ij} \left[ \left( \frac{\sigma}{r_{ij}} \right)^{12} - \left( \frac{\sigma}{r_{ij}} \right)^6 \right], \quad (3.6)$$

where  $\epsilon_{ij}$  is the minimum of the potential and  $\sigma$  is the inter particle distance at which the potential becomes zero. We use reduced units, in which the energy and length scales are specified in units of  $\epsilon_{ij}$  (counterion-counterion) and  $\sigma$  respectively. The depth of the attractive potential  $\epsilon_{ij}$  is chosen as 1.0 for monomer-counterion and counterion-counterion pairs and 2.0 for monomer pairs, while  $\sigma$  is set to 1.0 for all pairs. We use the shifted Lennard-Jones potential in which  $U_{LJ}(r_{ij})$  is set to zero beyond a cut off distance  $r_c$ . The value of  $r_c$  equals 1.0 for monomer-counterion and counterion-counterion pairs and 2.5 for monomer-monomer pairs. With this choice of the parameters, the excluded volume interaction is purely repulsive for all the pairs other than the monomer-monomer pairs. The effective short-range attraction among the monomers mimics poor solvent conditions. An alternate way of realising poor solvent conditions by tuning the short-range interactions may be found in Ref. [70].

Bond stretching interaction: The bond stretching energy for pairs in the polymer that

are connected directly through springs is given by

$$U_{bond}(r_{ij}) = \frac{1}{2}k(r_{ij} - b)^2, \quad (3.7)$$

where  $k$  is the spring constant and  $b$  is the equilibrium bond length. The values of  $k$  and  $b$  are taken as 500 and 1.12 respectively. This value of  $b$  is close to the minimum of Lennard-Jones potential.

The relative strength of the electrostatic interaction is parametrised by a dimensionless quantity  $A$ :

$$A = \frac{q^2 \ell_B}{b}, \quad (3.8)$$

where  $\ell_B$  is the Bjerrum length of the medium, defined in Eq. (3.2). The thermal fluctuations dominate over the electrostatic interactions for very low values of  $A$ , and the counterions will be uniformly distributed in the solution. When  $A$  is of order one, the electrostatic interaction energy is comparable to the thermal energy and the counterions begin to undergo Manning condensation[15]. In our simulation, we vary  $A$  from 0.055 to 14.29.

The equations of motion are integrated in time using the molecular dynamics simulation package LAMMPS [83, 84]. The simulations are carried out at constant temperature ( $T=1.0$ ), maintained through a Nosé-Hoover thermostat (coupling constant = 0.1) [45, 46]. The system is placed in a cubic box with periodic boundary conditions. At the start of the simulations, the configuration of the chain is randomly chosen and the counterions are distributed uniformly throughout the volume such that the charge neutrality is achieved. In our simulations, the length  $N$  of the chain is varied from 50 to 400, keeping the overall particle density of the system fixed at a constant value,  $3.61 \times 10^{-6}$  monomers per  $\sigma^3$ . At this density, there is no direct contact between the PE chain and any of its periodic images. We use the particle-particle/particle-mesh (PPPM) technique [49] to evaluate the energy and forces due to the long range Coulomb interactions. The time step of the integration is chosen as 0.001. Our simulation runs are divided into

an equilibration run ( $5 \times 10^6$  steps), followed by a production run ( $6 \times 10^6$  steps). All the data shown in the plots are measurements over only the production run ( $1.2 \times 10^5$  configurations). The errors in the plots are estimated by dividing the production into five statistically independent blocks and measuring the standard deviation of the mean values of the observable in each block [85].

### 3.3 Results and Discussion

#### 3.3.1 Configurations of the polyelectrolyte chain

Snap shots of the PE configuration for different values of  $A$  are shown in Fig. 3.1. For very small values of  $A$ , the electrostatic interactions can be ignored, and the polymer exists in a collapsed phase [Fig. 3.1(a)]. As  $A$  is increased, the globule breaks up into two [Fig. 3.1(b)] or more smaller globules [Fig. 3.1(c)]. This pearl-necklace configuration becomes extended on further increasing  $A$  [Fig. 3.1(d)]. Counterion condensation is initiated and for sufficiently large  $A$ , the polymer undergoes a collapse transition to form a sausage phase [19] [Fig. 3.1(e)] or a spherical globule [Fig. 3.1(f)]. We do not see any pearl-necklace phase between the extended phase and the condensed collapsed phase. This is consistent with the earlier simulations [13] where, unlike partially charged chains, strong electrostatic repulsion precludes the formation of a pearl-necklace phase in a fully charged PE chain. For partially charged PE chains, the attraction induced by the condensed counterions may dominate the repulsion among the monomers, and the PE chain would collapse locally, maintaining an extended configuration at large length scales. See Ref. [13] for more details.

#### 3.3.2 Distribution of counterions

We consider a counterion to be condensed onto the PE chain if its distance from any monomer of the chain is less than  $2\ell_B$ , consistent with similar definitions used earlier [58].

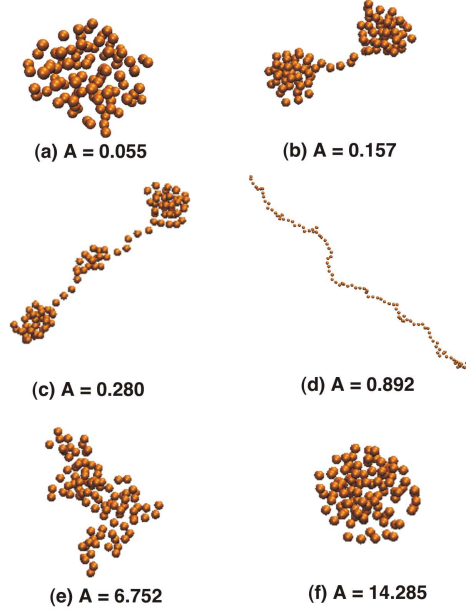


Figure 3.1: Snapshots of the polyelectrolyte chain configurations for different values of  $A$ . For the sake of clarity, counterions are not shown and figures are not in the same scale. (a) globular phase, (b) dumbbell phase, (c) pearl-necklace phase, (d) extended phase, (e) sausage phase and (f) globular phase.

Let  $N_c$  be the number of condensed counterions and  $N$  the number of monomers. The mean fraction of condensed counterions  $\langle N_c/N \rangle$  as a function of  $A$  is shown in Fig. 3.2 for different  $N$ . With the above definition of a condensed counterion, it is observed that the counterion condensation starts slightly below  $A = 1$ , consistent with the findings in Ref. [86]. Note that for the case of a infinitely long and uniformly charged cylinder or line of charges, the classic Manning condensation occurs at  $A = 1$ .

For a given value of  $A$ , the fraction of condensed counterions increases with increasing  $N$  and reaches a limiting value (see Fig. 3.2). A similar result was obtained for the good solvent case as well [58]. We find that the dependence of the fraction of condensed counterions on  $N$  is closely related to the dependence of the relative size  $R_g/N$  of the PE chain on  $N$  with fixed  $A$ . Here,  $R_g$  is the radius of gyration of the chain, given by

$$R_g = \sqrt{\frac{1}{N} \sum_{i=1}^N (\vec{r}_i - \vec{r}_{cm})^2}, \quad (3.9)$$

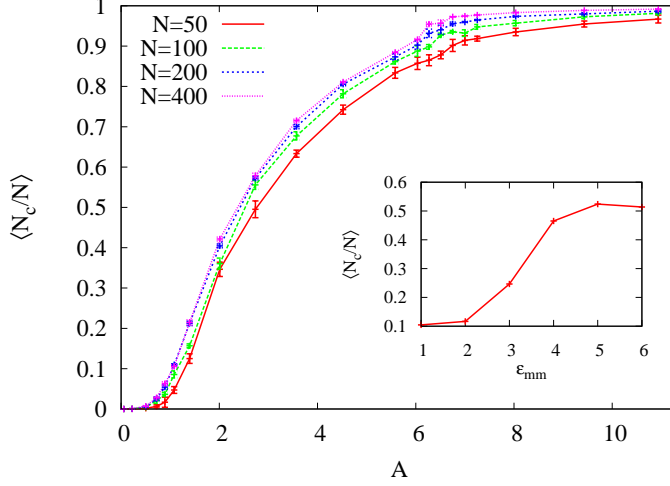


Figure 3.2: Mean fraction of counterions  $\langle N_c/N \rangle$  within a distance  $2\ell_B$  from the polyelectrolyte chain as a function of  $A$ . Inset:  $\langle N_c/N \rangle$  as a function of the monomer-monomer attraction energy  $\epsilon_{mm}$  for  $N = 100$  and  $A = 0.89$ .

where  $\vec{r}_i$  is the position of the  $i^{th}$  monomer and  $\vec{r}_{cm}$  is the centre of mass of the chain. For fixed  $A$ ,  $R_g/N$ , decreases with  $N$  in the region  $A \gtrsim 0.89$  where the condensation occurs (see Fig. 3.3). We now show that the decrease in  $R_g/N$  of a chain results in the condensation of more fraction of counterions.  $R_g/N$  of a PE chain with fixed  $A$  can be varied by changing the strength  $\epsilon_{mm}$  of the short-range attraction between the monomers. In the inset of Fig. 3.2, we show that increasing  $\epsilon_{mm}$ , keeping other parameters fixed, results in increased condensation. It is clear that increasing  $\epsilon_{mm}$  can only result in  $R_g/N$  of the PE chain becoming smaller. We therefore conclude that longer chains have smaller  $R_g/N$ , and thereby condense larger fraction of counterions than shorter chains. The increased condensation may be due to counterions experiencing lower electrostatic potential for a more compact chain.

We also observe that  $R_g/N$  shows a jump around  $A_c \approx 6.25$  (See Fig. 3.3). The jump is more pronounced for longer chains. For  $A > 6.25$ , radius of gyration  $R_g$  scales as  $N^{1/3}$  (see inset of Fig. 3.3), indicating that the chain is in a collapsed phase. We also observe a small kink in the fraction of condensed ions (see Fig. 3.2) around the same value of  $A$  where  $R_g/N$  shows a jump.

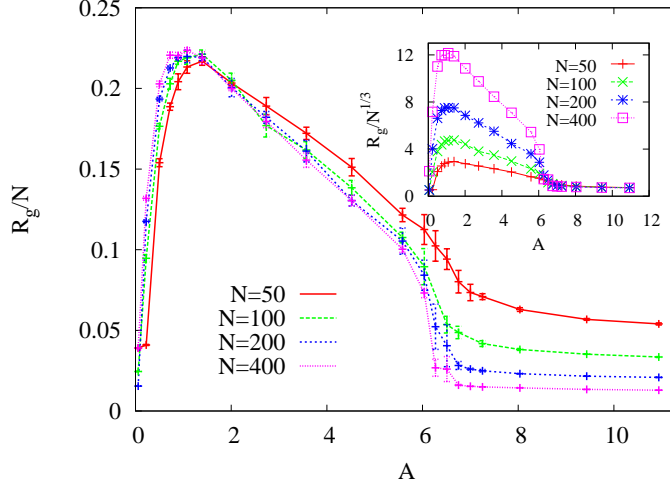


Figure 3.3: Ratio of the radius of gyration  $R_g$  to the number of monomers  $N$  as a function of  $A$ . Inset: The data for  $R_g/N^{1/3}$  collapse for different  $N$  for  $A \gtrsim 6.25$ .

### 3.3.3 Number of non-bonded neighbours and the condensation transition

The number of non-bonded nearest neighbours of a monomer has been used as an order parameter in studying the collapse transition of a neutral polymer [87]. We study its behaviour for the PE chain. For a given monomer, a non-bonded neighbour is defined as any monomer/counterion that is not connected to it by a bond and within a distance  $b$ . The variation of the mean number of non-bonded neighbours per monomer  $\langle n_b \rangle$  with  $A$  is shown in Fig. 3.4.  $\langle n_b \rangle$  decreases when the PE chain goes from the initial collapsed phase to the extended phase. It has the minimum around  $A' \approx 0.89$  where the chain is most extended. For  $A > A'$ ,  $\langle n_b \rangle$  increases monotonically, and close to  $A_c \approx 6.25$ , it has a jump with the jump size increasing with number of monomers  $N$ . This value of  $A$  corresponds to the counterion induced collapse of the PE chain from the extended phase (see inset of Fig. 3.3). We also study the relative fluctuations  $\chi_b$  of the number of non-bonded neighbours, where

$$\chi_b = \frac{N [\langle n_b^2 \rangle - \langle n_b \rangle^2]}{\langle n_b \rangle^2}. \quad (3.10)$$

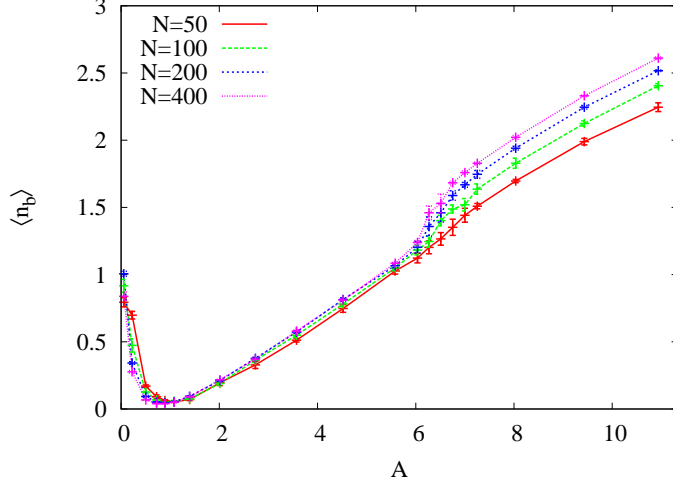


Figure 3.4: The number of non bonded neighbours per monomer  $\langle n_b \rangle$  as a function of  $A$  for different  $N$

It has a peak around  $A' \approx 0.89$  (see Fig. 3.5). The increasing peak height with the number of monomers  $N$ , indicates a divergence in the thermodynamic limit. This critical value  $A'$  corresponds to the onset of condensation of the counterions (see Fig. 3.2). At this value of  $A$ , the PE chain is fully extended and hence this condensation is reminiscent of Manning condensation on a cylinder or line of charges. The data for different values of  $N$  can be collapsed using the finite size scaling form

$$\chi_b \approx N^{\phi_1} f[(A - A')N^{\phi_2}], \quad N \gg 1, \quad (3.11)$$

where  $f$  is a scaling function, and  $\phi_1$  and  $\phi_2$  are exponents. Data collapse is seen for  $\phi_1 \approx 0.20$  and  $\phi_2 \approx 0.15$  (see inset of Fig. 3.5). Divergence of  $\chi_b$  with data collapse is a strong indication of condensation being a continuous phase transition. Earlier discussion of the order of the Manning like condensation has been restricted only to model systems of cylinder in three dimensions and disc in two dimensions, and a similar continuous transition has been reported in such systems [74, 73, 75].

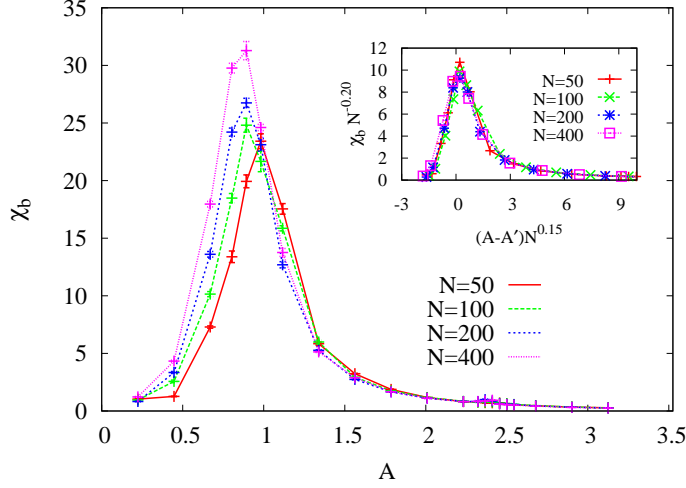


Figure 3.5: The relative fluctuation  $\chi_b$  of the number of non bonded neighbours, as defined in Eq. (3.10), as a function of  $A$  for different  $N$ . Inset: Data collapse when  $\chi_b$  and  $A$  are scaled as in Eq. (3.11), where  $A' = 1.08$  for  $N = 50$  and  $A' = 0.89$  otherwise.

### 3.3.4 Transition from extended phase to collapsed phase

To quantify the transition from the extended phase to the collapsed phase, the electrostatic energy per monomer  $E_c$  and its fluctuations are calculated. Only monomer-monomer pairs are used for calculating these quantities since we are interested in the configuration of the PE chain. The relative fluctuation  $\chi_c$  in the electrostatic energy is defined as

$$\chi_c = \frac{N [\langle E_c^2 \rangle - \langle E_c \rangle^2]}{\langle E_c \rangle^2}. \quad (3.12)$$

The mean electrostatic energy per monomer  $\langle E_c \rangle$  increases with  $A$  and has an abrupt jump at  $A_c \approx 6.25$  (see Fig. 3.6). The jump is more pronounced for higher values of  $N$ .

If the shape of the collapsed PE chain is roughly spherical, the volume  $\frac{4}{3}\pi R^3$  occupied by the chain should vary as the number of monomers, or  $R \sim N^{1/3}$ . The electrostatic energy of a uniformly charged sphere of total charge  $Q$  and radius  $R$  is given by

$$E = \frac{3}{5} \frac{Q^2}{4\pi\epsilon R} \quad (3.13)$$

Substituting  $Q = Nq$ , and taking  $R \sim N^{1/3}$ , one can easily see that the energy per

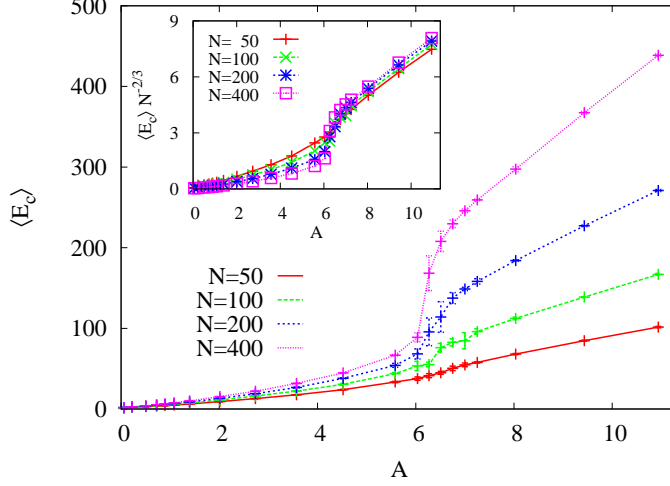


Figure 3.6: Mean Coulomb energy per monomer  $\langle E_c \rangle$  as a function of  $A$  for different  $N$ . Inset:  $\langle E_c \rangle \sim N^{2/3}$  in the collapsed phase.

monomer  $E/N$  scales as  $N^{2/3}$ . For  $A > A_c$ , we confirm that  $\langle E_c \rangle$  indeed scales as  $N^{2/3}$  (see inset of Fig. 3.6). The scaling of  $\langle E_c \rangle$  as  $N^{2/3}$  along with the scaling of  $R_g$  as  $N^{1/3}$  (see inset of Fig. 3.3) in this regime confirm that the polymer is indeed in a collapsed configuration.

The variation of the relative fluctuation  $\chi_c$  with  $A$  is shown in Fig. 3.7.  $\chi_c$  has a peak at  $A_c$ , close to the value of  $A$  at which  $\langle E_c \rangle$  has a discontinuity. The peaks are not resolved well. This is because, close to the transition point, the PE chain fluctuates between the extended and the collapsed phases during the time evolution. The inset of Fig. 3.7 shows a sample time series of  $E_c$ , near the transition point, for  $N = 200$ , where  $E_c$  fluctuates roughly between two values. This behaviour of  $\chi_c$  coupled with the sharp rise in  $\langle E_c \rangle$  (see Fig. 3.6) suggests a first order phase transition. Our findings are consistent with the previous theoretical results [72] that the extended to collapse transition of a PE chain is first order.

### 3.3.5 Existence of Sausage phase

The sausage phase was defined in Ref. [19] as an intermediate phase with non-zero asphericity, between the extended phase and condensed-collapsed phase. We show below

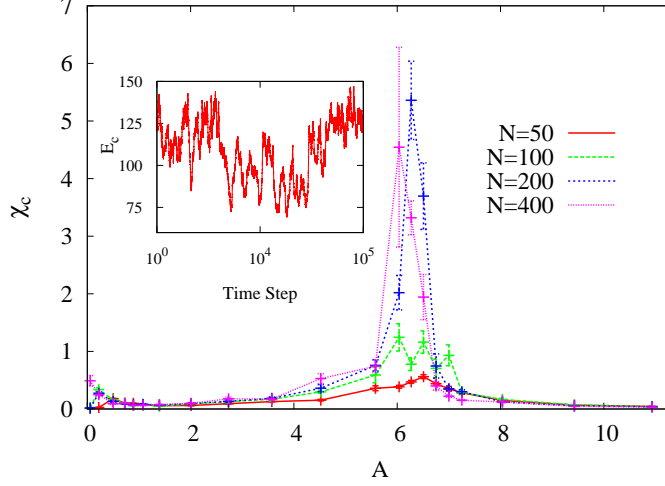


Figure 3.7: Fluctuation in the Coulomb energy per monomer  $\chi_c$  as a function of  $A$ . Inset: Time series of the electrostatic energy per monomer, for  $N = 200$ , and  $A = 6.50$ .

that such a phase with non-zero asphericity does not exist in the thermodynamic limit.

We define asphericity  $Y$  as

$$Y = \left\langle \frac{\lambda_1 - \frac{\lambda_2 + \lambda_3}{2}}{\lambda_1 + \lambda_2 + \lambda_3} \right\rangle, \quad (3.14)$$

where  $\lambda_{1,2,3}$  are the eigenvalues of the moment of inertia tensor with  $\lambda_1$  being the largest eigenvalue. The moment of inertia tensor  $G$  is

$$G_{\alpha\beta} = \frac{1}{N} \sum_{i=1}^N r_{i\alpha} r_{i\beta}, \quad (3.15)$$

where  $r_{i\alpha}$  is the  $\alpha^{th}$  component of the position vector  $\vec{r}_i$ . Asphericity  $Y$  is zero for a sphere (collapsed globule) and one for a linear rod (extended configuration). For all other configurations, it has a value between zero and one.

The variation of asphericity with  $A$  for different  $N$  is shown in Fig. 3.8. For very small values of  $A$ , asphericity increases corresponding to the extension of the initial collapsed phase. In the extended region  $0.89 \lesssim A \lesssim 6.25$ , asphericity increases with  $N$  and tends to one for large  $N$ . For  $A \gtrsim 6.25$ , asphericity decreases to zero with  $N$  as a power law (see inset of Fig. 3.8). Thus, for large  $N$ , asphericity jumps from one to zero as  $A$  crosses  $A_c \approx 6.25$ . The value of the transition point coincides with the extended to collapsed

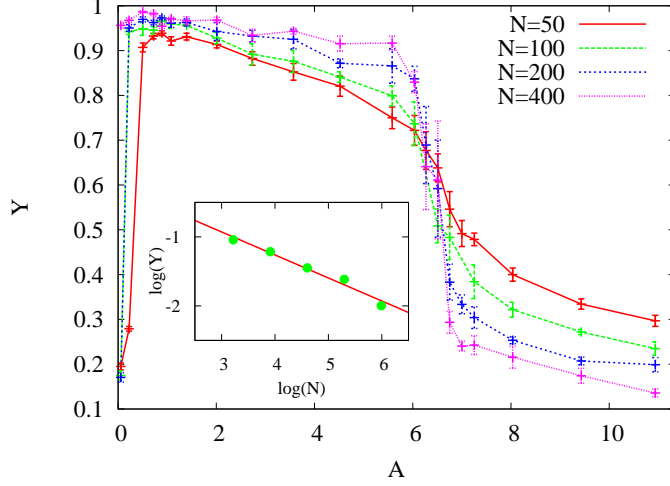


Figure 3.8: Asphericity  $Y$  (as defined in Eq. (3.14)) as a function of  $A$ . Inset: Variation of asphericity  $Y$  with chain length  $N$  for  $A = 10.93$ . The slope of the straight line is  $-0.33$ .

transition discussed in Sec. 3.3.4. As there is no second transition in asphericity or in  $\langle E_c \rangle$ , we conclude that the sausage phase suggested in Ref. [19] is identical with the collapsed phase and is not a different phase. The appearance of sausage-like phase for short chains could be a finite size effect.

### 3.3.6 The effect of valency of counterions on counterion condensation transition and extended-collapsed transition

In this section we present our preliminary results of the effect of valency of the counterions on the counterion condensation transition and the extended-collapsed transition. When the counterions are multivalent with valency  $Z$ , the system is charge neutralised by  $N/Z$  counterions, where  $N$  is the number monomers in the PE chain.  $Z = 2$  and  $3$  correspond to divalent and trivalent counterions. Fig. 3.9 shows the variation of the fluctuation  $\chi_b$  in the number of non-bonded neighbours (See Eq. (3.10)) with valency  $Z$ . It is clear that the effect of valency in the counterion condensation transition is to decrease the critical value of  $A$  at which the transition occurs.  $\chi_b$  has the peak around 0.89, 0.43 and 0.28 for monovalent, divalent and trivalent counterions. These values are close to the theoretically predicted values by Manning [15]. The theoretical values of the transition

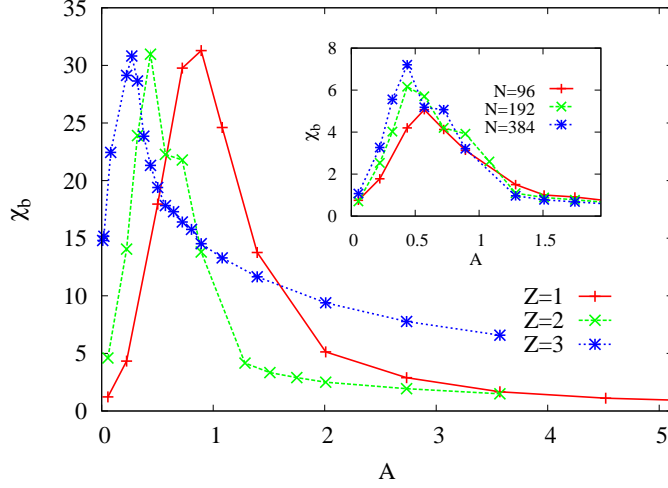


Figure 3.9: The relative fluctuation  $\chi_b$  in the number of non bonded neighbours, as defined in Eq. (3.10), as a function of  $A$  for different  $Z$  for  $N = 384$ . The y-scale has been rescaled for clarity. Inset: Variation of  $\chi_b$  for  $Z = 2$ , and for different chain lengths.

are given by  $A = 1/Z$ , i.e.,  $A = 1.0, 0.5$  and  $0.3$ . We note that the observed values are lower than the theoretical values for all the valencies.

The variation of the asphericity with  $A$  for different valencies has been shown in Fig. 3.10. The critical value of  $A$  at which asphericity  $Y$  makes the transition from  $Y \approx 1$  to  $Y \approx 0$  decreases with increasing valency. The transition occurs at  $A \approx 1.20$  and  $A \approx 0.37$  for divalent and trivalent counterions. Close to the transition point, the probability density of  $Y$  is double peaked (See Inset of Fig. 3.10), suggesting the first-order transition. For very short chains ( $N \approx 98$ ), the counterion condensation transition occurs before the chain gets fully extended.

For the case of multivalent counterions, the difference between the critical values of  $A$  for the counterion condensation transition and the extended-collapsed transition is very small. As a result, because of the numerical inaccuracies, we could not obtain a good data collapse for the fluctuation  $\chi_b$  in the number of non-bonded neighbours.

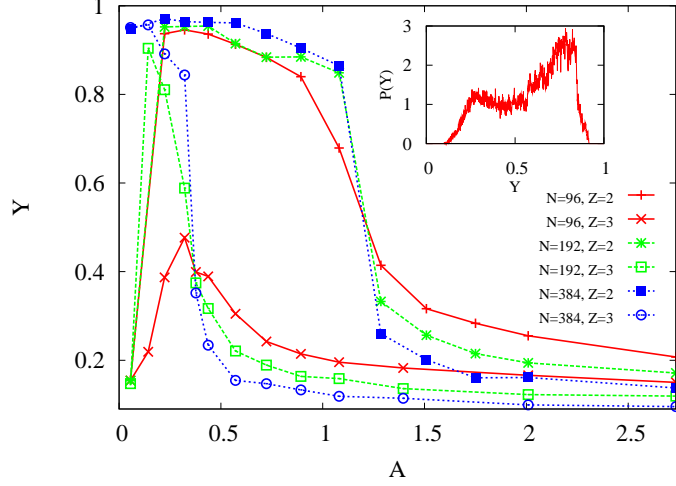


Figure 3.10: Asphericity  $Y$  (as defined in Eq. (3.14)) as a function of  $A$ . Inset: Probability density of  $Y$  for  $Z = 2$  near the transition point.

### 3.4 Conclusions

Using molecular dynamics simulations, we studied the phase diagram and transitions between the phases of a single PE chain in a poor solvent. The counterions were taken care of explicitly while the solvent was implicit. The dependence of various physical quantities on  $A$ , a dimensionless number that parametrised the strength of the electrostatic interaction, were calculated for different chain lengths  $N$ . Our main results are summarised below.

We quantified the transition associated with the condensation of counterions on the extended chain. The fluctuations of the non-bonded neighbours  $\chi_b$  diverges at a critical value of  $A$  with exponents that indicate a continuous transition. While the value of the exponents we obtain are not accurate, they indicate that data for different system sizes can be explained by one scaling function. We also find that the critical value of  $A$  for the counterion condensation transition decreases with increase in valency of the counterions. It would be interesting to study the number of non-bonded neighbours and its fluctuations for the good solvent problem as well as in the presence of salt.

We also analysed the sausage phase introduced in Ref. [19] as a new intermediate phase between the extended and collapsed phases. We show that the transition associated

with the discontinuity in asphericity and that associated with the extended to collapsed transition occur, within numerical error, at the same value of  $A$ . This, in conjunction with the fact that there is no second transition for either quantity, strongly suggests that the sausage phase does not exist independent of the collapsed phase, and was probably an artefact of earlier simulations [19] of chains of small size.

The counterion induced collapse of a PE chain was also quantified. The abrupt jump in  $R_g/N^{1/3}$ , in the mean electrostatic energy  $\langle E_c \rangle$ , and mean number of non-bonded nearest neighbours  $\langle n_b \rangle$ , transition of the chain between extended phase and collapsed phase near the transition point, combined with the peaks in the fluctuations of the electrostatic energy  $\chi_c$ , are evidences for a first order transition. This is consistent with the theoretical prediction in Ref. [72]. We also find that the critical value of  $A$  for the transition decreases with increase in valency of the counterions.

In addition, we find that the fraction of condensed counterions increases with  $N$  for fixed  $A$  in the extended phase. By studying its dependence on  $\epsilon_{mm}$  and the dependence of  $R_g/N$  on  $N$ , we argued that the increase in the fraction is related to longer chains having a smaller relative extension.

# Chapter 4

## Aggregation of Similarly Charged Rod-Like Polyelectrolytes

### 4.1 Introduction

Rod-like polyelectrolytes (RLPEs) are an important class of polyelectrolytes for which the persistence lengths of the polymer backbone are larger than their contour lengths. They are common in biological systems; examples include DNA [21], F-actin and microtubules [22]. RLPEs are also of interest theoretically because their thermodynamics is similar to the theoretically well studied idealized system of a charged cylinder with neutralizing counterions. RLPEs, even if similarly charged, may have attractive interactions mediated by the counterions. The aggregation of similarly charged PEs has been extensively studied experimentally [21, 22, 23, 24, 25, 26, 27, 88, 66, 89], theoretically [90, 91, 92, 38, 34, 93, 94, 95, 96, 97, 35] and numerically [28, 29, 31, 30, 32, 33, 98, 99, 100, 101]. Despite these studies, the role of counterion valency in aggregation remains unclear. Though it has been shown unambiguously that multivalent counterions can mediate aggregation [21, 22, 88, 23, 24, 25, 26, 66, 89, 90, 91, 92, 38, 34, 93, 94, 95, 96, 97, 35, 28, 29, 31, 30, 32, 98, 99, 100, 101], it is still being debated whether monovalent counterions can cause aggregation in the absence of multivalent salts. There are some

experimental [23, 24, 25, 26, 27] and theoretical [34, 35] results that argue for monovalent counterion induced aggregation of PEs. At the same time, other experimental [88, 89], theoretical [36, 37, 38] and numerical [28, 29, 30, 31, 32, 33] studies argue or report the absence of aggregation in the presence of monovalent counterions.

There are different proposals for the mechanism of the attraction between two similarly charged PEs. One of them suggests that the attraction is induced by the correlated longitudinal fluctuations of the condensed counterion density [92]. This theory predicts attraction in the presence of multivalent counterions, in agreement with early numerical simulations [28], for a range of system parameters. The validity of the Gaussian approximation made in the theory was questioned [102, 36], and more realistic, but simple models were considered [36, 38]. These models assume localization of the condensed counterions on a finite number of allowed sites around the PEs, and were able to explain multivalent counterion induced attraction in terms of spatial distribution of the condensed counterions around the PEs. However, these models predict the absence of attraction [102] or only a very weak attraction [38] for the case of monovalent counterions.

An alternate approach that explains the attraction of PEs is by Manning et. al. [34], and is based on the classical condensation theory [16]. Though this approach does not explicitly take into account counterion correlations, it reproduces attraction between similarly charged PEs. In fact, the theory predicts stronger attraction in the presence of monovalent counterions than divalent or trivalent counterions. This theory was later extended [97, 35], using extended condensation theory [103], to calculate the interaction free energy as a function of the separation between the PEs, linear charge density of the PEs and valency of the counterions. The analysis of the free energy shows that the attraction is a consequence of the increase in the number of condensed counterions and the counterion condensation volume with decrease in the separation between the PEs. Although these theories predict the formation of stable aggregates, mediated by monovalent counterions, a clear experimental or computational confirmation is still lacking. Most numerical simulations [28, 29, 30, 31, 32, 33] argue for the absence of aggregation

or report a weak attraction which is not strong enough to form stable aggregates [100].

A different phenomena in PE systems, mediated by counterions, is the extended–collapsed transition of a single flexible [58, 72, 104, 19] or semi-flexible PE [71]. As the linear charge density exceeds a critical value, an extended flexible PE chain makes a first-order transition [72, 104] to a globular phase, while an extended semi-flexible PE goes into a toroid-like phase [71]. As for aggregation of PEs, there are various proposals for the underlying mechanism of extended–collapsed transition, such as the negative compressibility of a neutral system of oppositely charged particles [72], the attraction among monomer-counterion dipoles [58], and the effective attraction induced by the counterion density fluctuations [71].

In this chapter, we present our results of molecular dynamics simulations on the aggregation of RLPEs induced by counterions of different valencies. We also try to establish a possible relation between the mechanisms of the aggregation of RLPEs and the extended–collapsed transition of a single flexible PE. The content of the chapter have been organised as follows. In Sec. 4.2, we discuss the model and the simulations methods used. In Sec. 4.3.1, we discuss the aggregation of RLPEs mediated by counterions of different valencies. We show that monovalent counterions induce aggregation of similarly charged RLPEs when the linear charge density of the polymer backbone is larger than a critical value. We also show that the critical linear charge density for aggregation decreases with increasing valency of the counterions. In Sec. 4.3.2, we show that the critical value of the linear charge density required for the aggregation is nearly equal to that of the extended–collapsed transition of a single flexible PE chain for monovalent, divalent and trivalent counterions. We thereby suggest that the mechanisms of the two seemingly different phenomena are closely related. In Sec. 4.3.3 and Sec.4.3.4, we discuss about the interaction between two parallel similarly charged RLPEs, neutralised by monovalent counterions, which held fixed at a separation  $d$ . In Sec. 4.3.3, we show that the effective interaction potential  $W(d)$  for the pair of RLPEs develops a well of attraction at high enough values of the linear charge density. The linear charge density at which the depth

of the potential well becomes of the order of thermal energy roughly coincides with the linear charge density at which the aggregation of RLPEs begins. In Sec. 4.3.4, we show that the angular distribution of condensed counterions around the two RLPEs changes with the separation between them, and also that the nature of the angular distribution determines whether the interaction between the RLPEs is attractive or repulsive.

## 4.2 Model and simulation method

We model a PE chain as  $N$  spheres (monomers), each with charge  $+qe$ , connected through springs. The counterions are modelled as spheres with charge  $-Zqe$ , where  $Z = 1, 2$  and  $3$  for monovalent, divalent and trivalent counterions respectively. All counterions have same valency, and the number of counterions is such that the system is overall charge neutral. The PE chain and the counterions are assumed to be in a medium of uniform dielectric constant  $\epsilon$ .

The interactions between particles  $i$  and  $j$  are of four types:

Coulomb interaction: The electrostatic energy is given by

$$U_c(r_{ij}) = \frac{q_i q_j}{4\pi\epsilon\epsilon_0 r_{ij}}, \quad (4.1)$$

where  $r_{ij}$  is the distance between particle  $i$  and  $j$ , and  $q_i$  is the charge of the  $i^{\text{th}}$  particle, and  $\epsilon_0$  is the permittivity of free space.

Excluded volume interaction: The excluded volume interactions are modelled by the Lennard-Jones potential, which for two particles at a distance  $r_{ij}$ , is given by

$$U_{LJ}(r_{ij}) = 4\epsilon_{ij} \left[ \left( \frac{\sigma}{r_{ij}} \right)^{12} - \left( \frac{\sigma}{r_{ij}} \right)^6 \right], \quad (4.2)$$

where  $\epsilon_{ij}$  is the minimum of the potential and  $\sigma$  is the inter particle distance at which the potential becomes zero. We use reduced units, in which the energy and length scales are specified in units of  $\epsilon_{ij}$  and  $\sigma$  respectively. The depth of the attractive potential  $\epsilon_{ij}$

and its range  $\sigma$  are set to 1.0 for all particle pairs. We use the shifted Lennard-Jones potential in which  $U_{LJ}(r_{ij})$  is set to zero beyond a cut off distance  $r_c$ . The value of  $r_c$  is chosen to be 1.0 such that the excluded volume interaction is purely repulsive for all the pairs.

Bond stretching interaction: The bond stretching energy for pairs that are connected through springs is given by

$$U_b(r_{ij}) = \frac{1}{2}k_b(r_{ij} - b)^2, \quad (4.3)$$

where  $k$  is the spring constant and  $b$  is the equilibrium bond length. The values of  $k_b$  and  $b$  are taken as 500 and 1.12 respectively. This value of  $b$  is close to the minimum of Lennard-Jones potential, and the spring constant  $k_b$  is large enough so that the bond length does not change appreciably from  $b$ .

Bond bending interaction: The rigidity of the polymer backbone is controlled by a three-body interaction given by

$$U_\theta(\theta) = k_\theta[1 + \cos \theta], \quad (4.4)$$

where  $\theta$  is the angle between the bonds. For RLPEs,  $k_\theta = 10^3$ , and for the chain lengths that we study, it is high enough to keep the chain linear and rigid. For flexible PEs,  $k_\theta = 0$ .

The relative strength of the electrostatic interaction is parameterized by a dimensionless quantity  $A$ :

$$A = \frac{q^2 \ell_B}{b}, \quad (4.5)$$

where  $\ell_B$  is the Bjerrum length [12],

$$\ell_B = \frac{e^2}{4\pi\epsilon\epsilon_0 k_B T}, \quad (4.6)$$

where  $k_B$  is the Boltzmann constant and  $T$  is temperature. In our simulations, we vary  $A$  from 0.22 to 10.93.

The equations of motion are integrated in time using the molecular dynamics simulation package LAMMPS [83, 84]. The simulations are carried out at constant temperature ( $T=1.0$ ), maintained through a Nosé-Hoover thermostat (coupling constant = 0.1) [45, 46]. The system is placed in a cubic box with periodic boundary conditions. We use the particle-particle/particle-mesh (PPPM) technique [49] to evaluate the energy and forces due to the long range Coulomb interactions. The time step of the integration is chosen as 0.001.

We have performed molecular dynamics simulations of PE systems of three different kinds. The first consists of 50 similarly charged RLPEs neutralized by either monovalent, divalent or trivalent counterions. This system is used to study aggregation. The second consists of a single flexible PE chain neutralized by monovalent, divalent or trivalent counterions. This system is used to locate the extended–collapsed transition of the PE chain. The third consists of two RLPEs fixed in space, parallel to each other and neutralized by monovalent counterions. This system is used to determine the effective attraction between the two RLPEs and the spatial distribution of the counterions as the linear charge density of the PE backbone is varied.

## 4.3 Results and Discussion

### 4.3.1 Aggregation of rod-like polyelectrolyte chains

To study aggregation, we consider a collection of 50 RLPE chains of 30 monomers each. The system is charge neutralized with monovalent, divalent or trivalent counterions. The density of the system is chosen as  $4.4 \times 10^{-4}$  monomers/ $\sigma^3$ . At this density, the mean separation between the chains is much larger than the length of the chains.

We first show that monovalent counterions can mediate aggregation of similarly charged RLPEs, in contrast to the previous experimental [88, 89], theoretical [36, 37, 38] and numerical [28, 29, 30, 31, 32, 33] studies. In Fig. 4.1(A)–(D), we show snap shots of the system with only monovalent counterions at increasing times for  $A = 9.43$ . For these val-

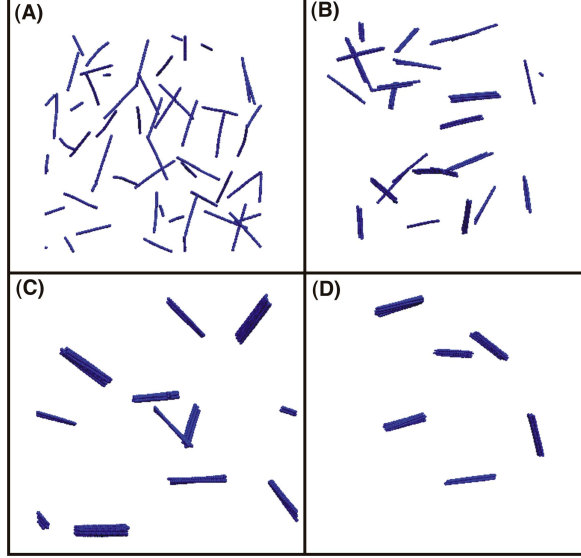


Figure 4.1: The two dimensional projection of the RLPEs at time steps (A) 0, (B)  $1.90 \times 10^6$ , (C)  $8.90 \times 10^6$  and (D)  $4.72 \times 10^7$ . The counterions are monovalent and are not shown for clarity. The RLPEs aggregate, with the number of aggregates decreasing in time. The data are for  $A = 9.43$ .

ues of  $A$ , electrostatic interactions are much larger than thermal energies. Aggregation can clearly be seen. We quantify aggregation by calculating the dependence of average aggregate size on  $A$ . Two PE chains are defined to form an aggregate if the distance between any monomer of the first chain and any monomer of the second chain is less than  $2\sigma$ . Similarly, a PE chain is defined to be part of an aggregate of size  $m$  ( $m > 2$ ) if the distance between the any monomers of the chain and any monomer of the  $m - 1$  chains in the aggregate is less than  $2\sigma$ . Other similar definitions for what constitutes an aggregate can be found in the literature [29, 98, 101], but we find that the results do not change noticeably with different choices of the definition.

Let  $N_m$  be the number of aggregates of size  $m$ . Then, the average aggregate size is given by  $\sum_{m=1}^{50} mN_m / \sum_{m=1}^{50} N_m$ . Measuring the equilibrium value of  $N_m$  turns out to be difficult in the aggregate regime because of large equilibration times and limited computational time. We, therefore, measure  $N_m$  after starting from two different types of initial conditions and discarding a fixed number of initial simulation steps. In the first type, we start from an initial random configuration of RLPEs and discard the first  $3 \times 10^7$

time steps. We then average the aggregate size over the next  $10^7$  time steps. The average aggregate size, thus computed, is shown by crosses in Fig. 4.2(A) as a function of  $A$  for counterions of different valency. The aggregation begins at  $A = 6.57, 2.50$  and  $1.45$  for monovalent, divalent and trivalent counterions respectively. These critical values of  $A$  correspond to an average aggregate size of 2.0. At high enough values of  $A$ , all the 50 chains aggregate to form a single aggregate for both divalent and trivalent counterions. For monovalent counterions, for the highest value of  $A$  (10.93) that we have studied, the final configuration of the system consists three aggregates of approximately 16 PEs each. We could not observe single aggregate formation within the maximum duration of our simulations ( $5 \times 10^7$ ). In the second type of simulations, we start with a high value of  $A$  and an initial condition where all the chains are in an aggregate. We then discard the first  $10^7$  time steps, and measure the aggregate size over the next  $10^6$  time steps.  $A$  is then decreased and the initial condition is chosen to be final state of the previous  $A$  value. The data thus obtained are shown by circles in Fig. 4.2(A). The values for  $A$  for which the two kinds of runs give the same value for average aggregate size can be taken to be the correct equilibrium value. The formation of a hysteresis loop is clearly seen.

The difficulty in equilibration in the aggregation regime is due to large diffusion time scales. As small aggregates form, they take longer and longer to diffuse and come close to each other before the next aggregation event can occur. We find that for values of  $A$  that are larger than the critical values, the aggregation kinetics is independent of  $A$  and the valency of the counterions. In Fig. 4.3, we show the time evolution of the history averaged number of aggregates  $\langle N_a \rangle$ . At the start of the simulations, the PEs are randomly distributed ( $\langle N_a \rangle = 50$ ). After initial transients, corresponding to counterion condensation,  $\langle N_a \rangle$  decays as a power law  $t^{-2/3}$  independent of valency.

From the decay law of the average number of aggregates, we can predict the dependence of the diffusion constant of an aggregate on its size  $m$ . In three dimensions, irreversible aggregation of particles is well described by the mean field Smoluchowski

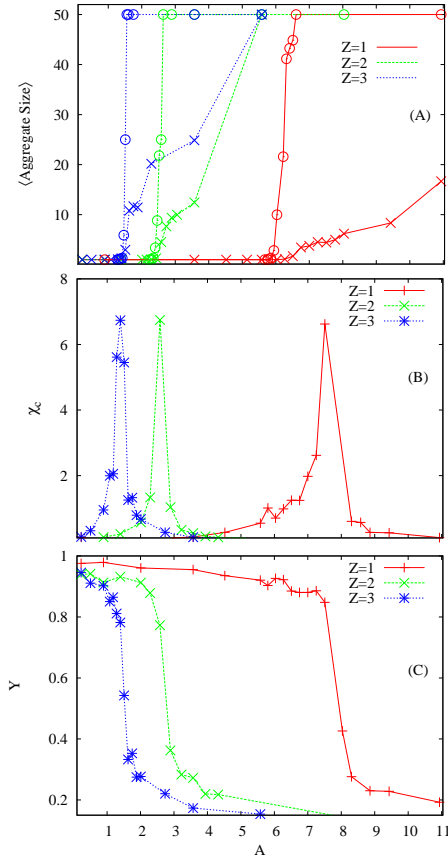


Figure 4.2: (A) The variation of the average aggregate size with  $A$ . The data shown by crosses are obtained from simulations where 50 RLPEs, each consists of 30 monomers, are initially randomly distributed. For the data shown by circles we start at high value of  $A$  where initially all RLPEs are pre-assembled to a single aggregate. The initial configuration for a lower value of  $A$  is the final configuration of the previous value of  $A$ . (B) The relative fluctuation  $\chi_c$  in electrostatic energy of a single flexible PE as defined in Eq. (4.12). The number of monomers is chosen as 600. The height of the peaks have been rescaled for clarity. (C) The variation of asphericity  $Y$  [see Eq. (4.13)] with  $A$  of the single PE.

equation (see [105, 106] for a review),

$$\begin{aligned} \frac{dN(m, t)}{dt} = & \frac{1}{2} \sum_{m_1=1}^{m-1} N(m_1, t) N(m-m_1, t) K(m_1, m-m_1) \\ & - \sum_{m_1=1}^{\infty} N(m_1, t) N(m, t) K(m_1, m), \quad m = 1, 2, 3, \dots, \end{aligned} \quad (4.7)$$

where  $N(m, t)$  is the number of aggregates of size  $m$  at time  $t$  and  $K(m_1, m_2)$  is the rate of collision of two aggregates of sizes  $m_1$  and  $m_2$ . In Eq. (4.7), the first term on the right hand side enumerates the number of ways an aggregate of size  $m$  may be created by collision, while the second term enumerates the number of ways  $N(m, t)$  can decrease due to collisions. The collision kernel  $K(m_1, m_2)$  is proportional to the sum of the diffusion constant and the sum of the surface areas of the aggregates of size  $m_1$  and  $m_2$ . If the aggregates are roughly spherical, then surface area of an aggregate of size  $m$  scales as  $m^{2/3}$ . On the other hand, if they are cylindrical, then surface area of an aggregate of size

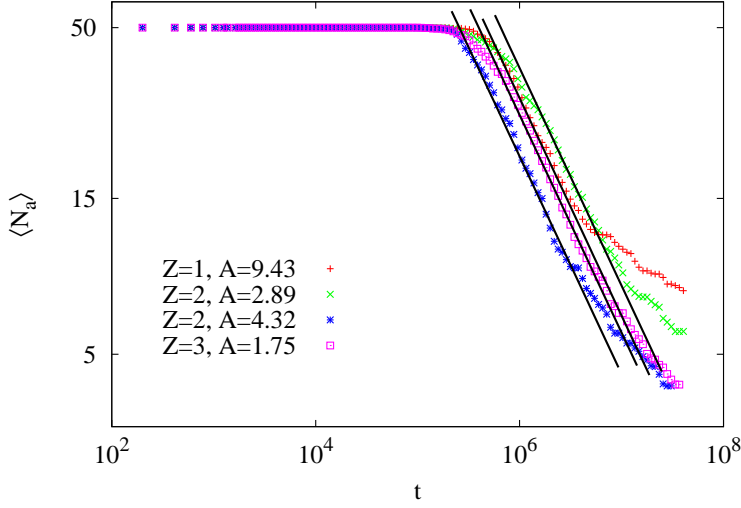


Figure 4.3: The variation of  $\langle N_a \rangle$ , the average number of aggregates, with time  $t$  for different values of  $A$  and valency. The data is log-binned and averaged over five different initial configurations. The solid black lines are power laws  $\sim t^{-2/3}$

$m$  scales as  $m^{1/2}$ . Thus, we write

$$K(m_1, m_2) \propto \left( \frac{1}{m_1^\alpha} + \frac{1}{m_2^\alpha} \right) (m_1^\tau + m_2^\tau), \quad (4.8)$$

where we have assumed that the diffusion constant  $D(m) \propto m^{-\alpha}$  and  $\tau$  takes on value  $2/3$ ,  $1/2$  or  $0$  depending on whether aggregates are spherical, cylindrical or point size particles. The homogeneity exponent  $\beta$  of the above kernel, defined through

$$K(\Lambda m_1, \Lambda m_2) = \Lambda^\beta K(m_1, m_2), \quad (4.9)$$

is

$$\beta = \tau - \alpha. \quad (4.10)$$

For irreversible aggregation governed by Eq. (4.7) with a kernel as in Eq. (4.8), the number of aggregates decrease with time as [105, 106]

$$N_a(t) \sim \frac{1}{t^{1/(1-\beta)}} \sim \frac{1}{t^{1/(1+\alpha-\tau)}} \quad (4.11)$$

Numerically, we find that  $N_a(t) \sim t^{-2/3}$ . This implies that  $\alpha = 1/2$  for point particles ( $\tau = 0$ ),  $\alpha = 1$  for cylindrical particles ( $\tau = 1/2$ ) and  $\alpha = 7/6$  for spherical particles ( $\tau = 2/3$ ). From our simulations, we find that aggregates are cylindrical in shape. Hence, we expect that  $D(m) \propto m^{-1}$ .

If the polyelectrolyte chains are flexible instead of rigid rods, then the aggregates will be spherical in shape. This will modify the collision kernel and we would expect a change in either the decay law exponent or the dependence of diffusion constant on mass.

In the earlier simulations [28, 29, 30, 31, 32, 33], the interaction between similarly charged RLPEs in the presence of monovalent counterions was found to be repulsive. Typical values of  $A$  used in these simulations are 2.10 [28], 2.90 [29, 30] and 4.17 [31], which are much smaller than the critical value ( $\approx 6.57$ ) above which we observe the aggregate formation. We suggest that the absence of attractive interactions required for aggregation in these simulations can be attributed to the inappropriate values of  $A$ .

### 4.3.2 Extended-Collapsed transition of a single flexible polyelectrolyte chain

In our earlier simulations [104], we had demonstrated that a single flexible PE chain undergoes a first-order transition from the extended configuration to the collapsed configuration, mediated by the counterions, when the parameter  $A$  exceeds a critical value. To establish a possible relation between the aggregation phenomena of RLPE chains and the extended–collapsed transition of a single flexible PE chain, we study the extended–collapsed transition of a single flexible PE chain of 600 monomers in the presence of monovalent and multivalent counterions. The density of the system is chosen as  $2.7 \times 10^{-6}$  monomers/ $\sigma^3$  such that the direct contact between the PE chain and its periodic images is avoided. The initial configuration of the PE chain is randomly chosen and the counterions are uniformly distributed inside the simulation box. The system is allowed to equilibrate for  $10^7$  steps and the averages are taken over a production run of  $10^7$  steps.

A useful quantity to study the extended–collapsed transition is the electrostatic energy per monomer  $E_c$ .  $E_c$  shows different scaling with the number of monomers in the extended and collapsed phases [104]. The relative fluctuation  $\chi_c$  in  $E_c$  is defined as

$$\chi_c = \frac{N [\langle E_c^2 \rangle - \langle E_c \rangle^2]}{\langle E_c \rangle^2}. \quad (4.12)$$

Fig. 4.2(B) shows the variation of  $\chi_c$  with  $A$ .  $\chi_c$  has a peak around 7.5, 2.57 and 1.40 for monovalent, divalent and trivalent counterions respectively. These peaks correspond to the extended–collapsed transition of the single PE chain.

The extended–collapsed transition can be further quantified by studying the variation of asphericity of the PE chain as a function of  $A$ . We define asphericity as

$$Y = \left\langle \frac{\lambda_1 - \frac{\lambda_2 + \lambda_3}{2}}{\lambda_1 + \lambda_2 + \lambda_3} \right\rangle, \quad (4.13)$$

where  $\lambda_{1,2,3}$  are the eigenvalues of the moment of inertia tensor with  $\lambda_1$  being the largest eigenvalue. The moment of inertia tensor  $G$  is

$$G_{\alpha\beta} = \frac{1}{N} \sum_{i=1}^N r_{i\alpha} r_{i\beta}, \quad (4.14)$$

where  $r_{i\alpha}$  is the  $\alpha^{th}$  component of the position vector  $\vec{r}_i$ . Asphericity  $Y$  is zero for a sphere (collapsed globule) and one for a linear rod (extended configuration). For all other configurations, it has a value between zero and one.

The variation of  $Y$  with  $A$  is shown in Fig. 4.2(C). For all the three valencies,  $Y$  makes a transition from a value close to one (extended configuration) to zero (collapsed configuration) at a critical value of  $A$ . The transition in  $Y$  occurs at the critical value of  $A$  where  $\chi_c$  has a peak, and corresponds to the extended–collapsed transition of the PE chain. We note that these critical values roughly coincide with the critical values for the aggregation of rod-like PE chains in the presence counterions of the corresponding valency. This suggests that the underlying mechanisms of the collapse of a single PE

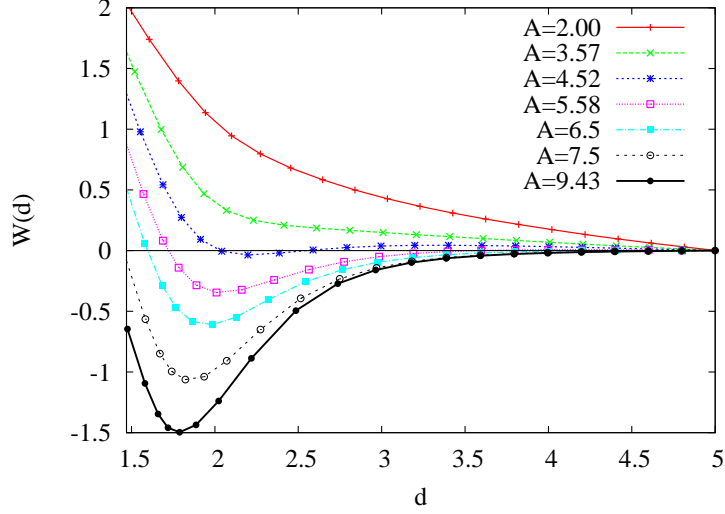


Figure 4.4: The reversible work  $W$  needed to bring two rod-like PEs from a separation of  $5\sigma$  to  $d$ , in the presence of monovalent counterions. The averages are taken over a production run of  $10^7$  steps, after the system has been equilibrated over  $10^7$  steps.

chain and the aggregation of rod-like chains are closely related.

### 4.3.3 The effective interaction potential between two rod-like PE chains with monovalent counterions

In this subsection, we measure the effective interaction potential between two similarly charged RLPEs in the presence of monovalent counterions. The effective interaction potential, for a separation  $d$  between the rods, is equal to the reversible work  $W(d)$  done in bringing them from infinite separation to a separation of  $d$ . Since the system is overall charge neutral, we expect the interaction potential to be short-ranged, and hence  $W(d)$  can be approximated by the work done in bringing the rods to a separation  $d$  from a finite separation  $d'$ , where  $d' > d$ .  $W(d)$  is then  $\int_{d'}^d dx f(x)$ , where  $f(x)$  is the normal component of the force required to keep the two rods at a separation  $x$ .

For the evaluation of  $W(d)$ , we consider two parallel RLPEs of 30 monomers each. The system is charge neutralized by monovalent counterions. The density of the system is chosen to be  $4.4 \times 10^{-4}$  monomers/ $\sigma^3$ . Fig. 4.4 shows the variation of  $W(d)$  per monomer

for different values of  $A$ . For low values of  $A$ ,  $W(d)$  is always positive and decreasing with  $d$ , showing repulsion between the rods. At high values of  $A$ ,  $W(d)$  develops a minimum which is the onset of attraction between the rods. When the depth of the potential becomes order  $T$ , the attraction will be strong enough to form stable aggregates.

A similar evaluation of  $W(d)$  for two similarly PEs in the presence of monovalent counterions has been carried out in earlier simulations [30, 32]. These simulations were performed at a range of values of  $A$  which is much less than the values at which we observe the attractive part in  $W(d)$ , and these simulations failed to observe the attractive part in  $W(d)$ . In Ref. [38], solving a simple model of PE system with monovalent counterions, an evaluation of the free energy as a function of the separation between the rods was made. It was found that the free energy has a well of attraction, with the depth of the well being insufficient to bind the two PEs. In this study also, the  $A$  value considered was much smaller (4.10) than the critical value needed to generate a potential well which is deep enough to form bound states.

#### 4.3.4 The angular distribution of the condensed counterions

It has been observed in experiments [107] and simulations [108] that the angular distribution of the condensed multivalent counterions changes as the PEs approach each other. Many theoretical studies [102, 36, 38] also argue that the spatial arrangement of the condensed multivalent counterions around the PEs plays an important role in developing an attractive interaction between the PEs.

We study the relationship between spatial distribution of counterion and the effective interaction between the RLPEs when all counterions are monovalent. For this, we consider the same system specifications as in Sec. 4.3.3. A counterion is said to have condensed on a PE if its separation from any of the monomers of the PE is less than  $1.25\sigma$ . When the PEs come close by, the counterion may be shared by both the PEs, but the qualitative nature of the angular distribution remains the same. In Fig. 4.5, we show the dependence of  $P(\theta)$  on  $\theta$ , where  $P(\theta)d\theta$  is the probability that the condensed counterion is between

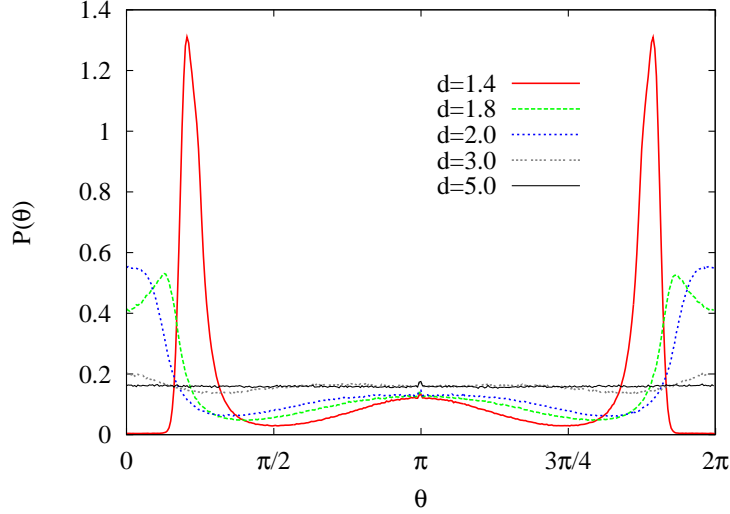


Figure 4.5: The angular distribution  $P(\theta)$  of condensed monovalent counterions around a given PE for  $A = 9.43$ .

angle  $\theta$  and  $\theta + d\theta$ . The data shown are for  $A = 9.43$ . For this value of  $A$ , there is a pronounced minimum in  $W(d)$  (See Fig. 4.4). Here,  $\theta = 0$  or  $2\pi$  corresponds to a location in between the two PEs, and lie in the same plane as that of the PEs, while  $\theta = \pi$  corresponds to the case where the counterion is located away from the second PE, but lie in the same plane as that of the two PEs. When the separation  $d$  between the PEs is much larger than  $1.85\sigma$ , the condensed counterions are distributed uniformly around the PE. As the PEs approach each other, the distribution develops a sharp peak at  $\theta = 0$ , and a broad peak at  $\theta = \pi$ , showing that most condensed counterions are located in the same plane as that of the PEs, and mostly between the PEs. For separations less than  $1.85\sigma$ , the peak at  $\theta = 0$  is shifted to higher values, showing that the condensed counterions are expelled out of the plane of the two PEs, though they remain in the region between the PEs. The exclusion of counterions unscreens the interaction between the similarly charged monomers of the two PEs, causing the repulsion between them. These observations are consistent with the nature of the effective interaction potential between the PEs, i.e., attraction for intermediate separation ( $1.85\sigma \lesssim d \lesssim 4\sigma$ ) and repulsion at very small separation ( $d \lesssim 1.85\sigma$ ).

## 4.4 Conclusions

We studied, using molecular dynamics simulations, the role of the valency of the counterions on the aggregation of similarly charged rod-like polyelectrolyte chains. We showed that monovalent counterions can mediate the aggregation, provided the linear charge density of the polyelectrolyte backbone is larger than a critical value. The absence of aggregation in the presence of monovalent counterions in earlier simulations and experiments is probably due to the linear charge density being smaller than the critical value. The critical linear charge density for aggregation decreases with increasing counterion valency, and is found to be close to the critical value for the extended–collapsed transition of a single flexible polyelectrolyte chain. We also find that, for two parallel rod-like polyelectrolyte chains, the angular distribution of the condensed counterions changes with the separation between the chains. The nature of the angular distribution determines whether the effective interaction between the chains is attractive or repulsive.

It would be interesting to study the aggregation transition in more detail. From our simulations, it appears that the transition is a first order phase transition. However, using molecular dynamics simulations, it is difficult to equilibrate the system in the aggregating regime, especially if the initial density is low. Hybrid simulations using both Monte Carlo and molecular dynamics might be useful to study the transition [98, 101].

Another problem of interest is the kinetics of aggregation. From our simulations, it appears that the density decay is independent of  $A$  and valency of the counterions. This may be due to fact that the attraction is short-ranged for all values of  $A$  and valency. When two aggregates come close by, the probability that they aggregate may depend on  $A$  and valency. This, while affecting the prefactor of the power law decay, does not affect the exponent, suggesting that the kinetics is diffusion limited. Understanding the kinetics better, and also its dependence on hydrodynamic interactions will be part of future study.

# Chapter 5

## Ensemble Equivalence for Counterion Condensation on a Two-Dimensional Charged Disc

### 5.1 Introduction

Statistical mechanics provides a framework to derive the thermodynamic properties of a system with macroscopic number of degrees of freedom. Depending on the nature of the system, suitable statistical ensembles can be used to derive the thermodynamics of the system. The most commonly used statistical ensembles are microcanonical, canonical and grand canonical ensembles. For systems with short range interactions, these ensembles are equivalent in the thermodynamic limit. As a result, the choice of the statistical ensemble becomes only a matter of convenience. In the last two decades, it has been shown, using exactly solvable models, that the thermodynamics derived from microcanonical and canonical ensembles could be different if the interactions in the system are long-ranged. This inequivalence may be manifested as negative specific heat or magnetic susceptibility in the microcanonical ensemble, different order of phase transitions, and different critical points in canonical and microcanonical ensembles. Examples

of long-ranged systems that show ensemble inequivalence include spin systems [109, 110], self-gravitating systems [111, 112, 113], plasma [114, 115], two dimensional hydrodynamic systems [116, 117] and other model systems [118, 119, 120]. The inequivalence of canonical and microcanonical ensemble for these long-range systems results from the lack of additivity of energy. For non-additive long-range systems, the interaction potential at large distances  $r$  decay as  $r^{-d-\sigma}$ , where  $d$  is the dimensionality of the system and  $\sigma \leq 0$ . The electrostatic interactions decay slower than  $r^{-d}$ , and hence charged systems are non-additive systems. It would then be of interest to know if the nature of the counterion condensation transition (CCT) is the same in different ensembles. However, almost all models of CCT are only studied in the canonical ensemble. In this chapter, we solve the model of CCT in Ref. [75] of a system of counterions condensing onto an oppositely charged disc in two dimensions in the microcanonical ensemble to address the question of ensemble equivalence of CCT.

The inequivalence of canonical and microcanonical ensembles, for long-range systems, is related to the concavity properties of the microcanonical entropy. In the next two sections, we briefly review the basic concepts of concavity of a function and then discuss how the non-additivity of energy and non-concavity of microcanonical entropy result in ensemble inequivalence.

### 5.1.1 Concavity of a function and the Legendre transformation

A function  $f(x)$  is said to be concave in the region  $x_1 \leq x \leq x_2$  if for any two points  $z_1$  and  $z_2$  ( $x_1 \leq z_1 < x < z_2 \leq x_2$ )  $f(x) \geq y(x)$ , where  $y(x)$  is the chord joining the points  $(z_1, f(z_1))$  and  $(z_2, f(z_2))$ . A point on the chord can be specified as

$$y(x) = \alpha f(z_1) + (1 - \alpha)f(z_2) , \quad (5.1)$$

where  $\alpha$  take value between zero and one, and is given by

$$\alpha = \frac{x - z_1}{z_2 - z_1} , \quad (5.2)$$

Then the concavity condition reduces to

$$f(x) \geq \alpha f(z_1) + (1 - \alpha)f(z_2) . \quad (5.3)$$

By setting  $z_1 = x - \Delta$  and  $z_2 = x + \Delta$ , one gets

$$2f(x) \geq f(x - \Delta) + f(x + \Delta) . \quad (5.4)$$

Expanding the rhs to the second order, and taking the limit  $\Delta \rightarrow 0$ , one obtains the differential form of the concavity condition

$$\frac{d^2 f}{dx^2} \leq 0 . \quad (5.5)$$

The differential form in Eq. (5.5) defines the local concavity of the function, whereas Eq. (5.3) defines the global concavity. A function may not be globally concave at a point  $x$  even if the local concavity condition is satisfied at that point. For example, the function  $f(x) = ax^2 - bx^4$  is not concave in the region  $-(a/2b)^{1/2} < x < (a/2b)^{1/2}$  even though the condition in Eq. (5.5) is violated only in the region  $-(a/6b)^{1/2} < x < (a/6b)^{1/2}$  (See Fig. (5.1a)).

It is also clear that if a function is locally concave at every point, then it will be globally concave in any interval. Now, we turn to the Legendre transformation of a function. The Legendre transformation  $g(p)$  of a function  $f(x)$  is defined as

$$g(p) = \min_x [px - f(x)] \quad (5.6)$$

$$= px^* - f(x^*) , \quad (5.7)$$

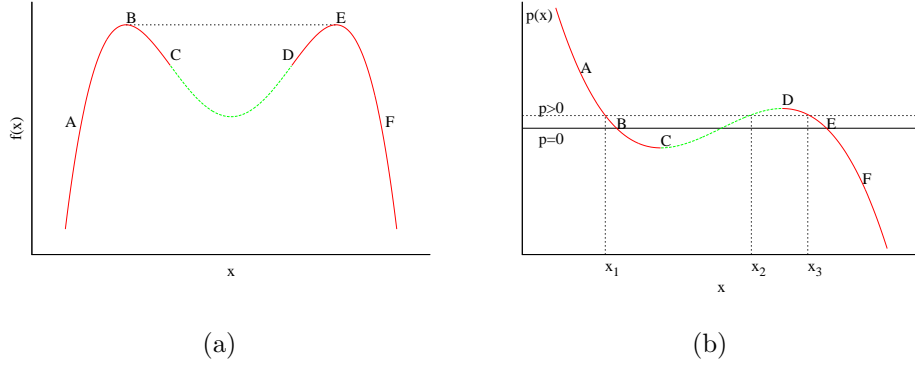


Figure 5.1: (a) Plot of the function  $f(x) = ax^2 - bx^4$ . The local concavity condition in Eq. (5.5) has been violated only in the segment  $CD$ . The segment  $BCDE$  lies below the chord  $BE$ , and hence the global condition in Eq. (5.3) has been violated. In this case, we say that the segment  $BCDE$  is not concave. (b) The derivative of  $f(x)$ ,  $p = 2ax - 4bx^3$ .

where by  $\min_x F(x, p)$  we mean the minimum value of  $F(x, p)$  for a given  $p$ , and  $x^*$  is the value of  $x$  at which  $F(x, p) = px - f(x)$  is minimum. If  $f(x)$  is differentiable, then  $x^*$  is the solution of the equation

$$\frac{\partial F}{\partial x} = 0 , \quad (5.8)$$

or

$$p = \frac{df}{dx} . \quad (5.9)$$

This equation, in general, may have multiple solutions. Some of them may correspond to local minima or maxima of  $F(x, p)$ , and  $x^*$  will be the one which corresponds to the global minimum. From Eq. (5.7) and (5.9), we see

$$\frac{dg}{dp} = x , \quad (5.10)$$

and

$$\frac{d^2g}{dp^2} = 1/\left(\frac{d^2f}{dx^2}\right) . \quad (5.11)$$

Eq. (5.11) says that the concavity of  $f(x)$  is preserved under Legendre transformation. As a result, a concave segment of  $f(x)$  will be mapped to a concave segment of  $g(p)$ . If

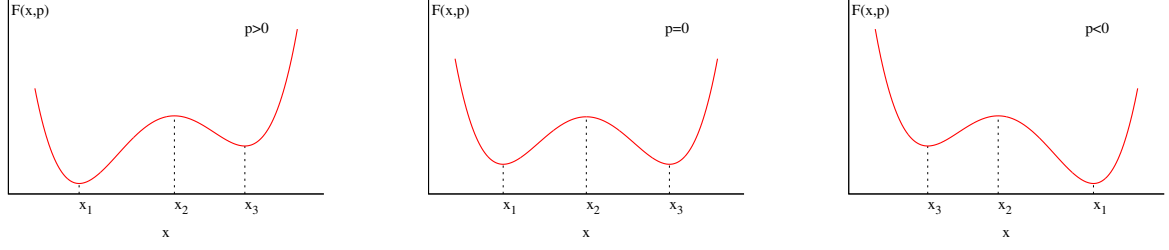


Figure 5.2: Plot of the function  $F(x, p) = px - f(x) = px - ax^2 + bx^4$ . For  $p = 0$ ,  $x_1$  and  $x_3$  are global minima. For  $p > 0$ ,  $x_1$  becomes the global minima and for  $p < 0$   $x_3$  is the global minimum.  $x_2$  is always the local maximum.

$f(x)$  has a non-concave segment, then  $g(p)$  will be the same as the Legendre transform of the concave envelope of  $f(x)$ . We do not give any rigorous proof for this statement, but we illustrate this point graphically using a concrete example. Consider the function  $f(x) = ax^2 - bx^4$ . From Eq. (5.9) and (5.7) we get,

$$p = 2ax - 4bx^3, \quad (5.12)$$

and

$$g(p) = ax^{*2} - 3bx^{*4}. \quad (5.13)$$

where  $x^*$  is the solution of Eq. (5.12) which minimises the function  $F(x, p) = px - f(x)$ . For  $p$  close to zero ( $|p| < f'(-(a/6b)^{1/2})$ ), the cubic equation Eq. (5.12) has three distinct roots (See Fig 5.1b). Let  $x_1, x_2$  and  $x_3$  are the solutions such that  $x_1 < -(a/6b)^{1/2}$ ,  $-(a/6b)^{1/2} \leq x_2 \leq (a/6b)^{1/2}$  and  $(a/6b)^{1/2} < x_3$ . To determine the solution  $x^*$  which minimises  $F(x, p)$ , one need to analyse the stability of these solutions. One can easily see that  $\frac{\partial^2 F}{\partial x^2} = -\frac{\partial^2 f}{\partial x^2}$  is negative for  $|x| < (a/6b)^{1/2}$  and positive for  $|x| > (a/6b)^{1/2}$ . Therefore,  $x_2$  correspond to the local maximum, and  $x_1$  and  $x_3$  correspond to the minima. The stability of  $x_1$  and  $x_3$  depends on the value of  $p$ .

#### Case I : $p = 0$

For  $p = 0$ ,  $F(x, p)$  is symmetric, and both  $x_1$  and  $x_3$  correspond to the global minimum (See Fig. 5.2). It can be easily seen that  $x_1 = -(a/2b)^{1/2}$  and  $x_3 = +(a/2b)^{1/2}$ .

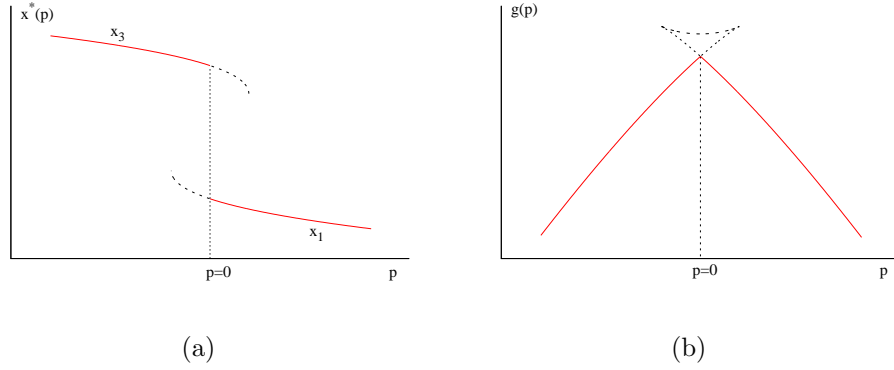


Figure 5.3: (a) Solution of Eq. (5.12) at which  $F(x, p)$  is globally minimum. The stable solution for  $p < 0$  has been extended to the region  $p > 0$  at which it become unstable. Similarly, the stable solution for  $p > 0$  has been extended to the region  $p < 0$  at which it become unstable. (b) The Legendre transformation  $g(p)$  of the function  $f(x) = ax^2 - bx^4$ . It has been plotted parametrically using Eq. (5.12) and (5.13). The extended lines correspond to the unstable solutions and the non-concave curve corresponds to the local maxima of  $F(x, p)$

### Case II : $p < 0$

For  $p < 0$ ,  $x_1$  corresponds to the local minimum and  $x_3$  corresponds to the global minimum. Or,  $x^* = x_3$ .

### Case III : $p > 0$

For  $p > 0$ ,  $x_3$  corresponds to the local minimum and  $x_1$  corresponds to the global minimum. Or,  $x^* = x_1$ .

In summary,  $x^*(p)$  is a smooth function for  $|p| > 0$ , and changes abruptly from  $(a/2b)^{1/2}$  to  $-(a/2b)^{1/2}$  as  $p$  crosses zero from below (See Fig. 5.3a).  $g(p(x^*))$  is symmetric in  $x^*$ , and hence it will be continuous at  $p = 0$  even though  $x^*$  jumps from  $(a/2b)^{1/2}$  to  $-(a/2b)^{1/2}$ . The parametric plot  $(p(x^*), g(p(x^*)))$  is shown in Fig. 5.3b. The extended dashed lines correspond to the local minima and the non-concave dashed curve correspond to the local maximum of  $F(x, p)$ .

Now, we consider the Legendre transformation of the concave envelope of  $f(x)$ . The concave envelope  $\tilde{f}(x)$  of the function  $f(x) = ax^2 - bx^4$  is defined as  $\tilde{f}(x) = f(x)$  for  $|x| \geq (a/2b)^{1/2}$  and  $\tilde{f}(x) = f((a/2a)^{1/2})$  for  $|x| < (a/2b)^{1/2}$ . In Fig. 5.1a, the curve  $ABEF$  is the concave envelope of the curve  $ABCDEF$ . Following the similar arguments as above,

one can easily see that the Legendre transform  $\tilde{g}(p)$  of  $\tilde{f}(x)$  is same as that of  $f(x)$ . As we discussed earlier,  $|p| > 0$  corresponds to  $|x| > (a/2b)^{1/2}$ . Since the functional form of  $\tilde{f}(x)$  is same as that of  $f(x)$  for  $|x| > (a/2b)^{1/2}$ ,  $\tilde{g}(p)$  will be same as  $g(p)$  for  $|p| > 0$ . For the case  $p = 0$ , from Eq. (5.7) we have  $\tilde{g}(0) = \min[-\tilde{f}(x)] = -f(a/2b)$ , which is same as  $g(0)$ .

In summary, we conclude that the Legendre transformation of a concave function with a non-concave region is same as the Legendre transformation of the concave envelope of the function. As a result, the Legendre transformation is not uniquely invertible. It turns out that the double Legendre transformation of a function will indeed give the concave envelope of the original function.

### 5.1.2 The equivalence between canonical and microcanonical ensemble

The canonical free energy  $F$  of a system is defined as

$$e^{-\beta F(\beta)} = \int dE g(E) e^{-\beta E} , \quad (5.14)$$

where  $g(E)$  is the density of states, and  $\beta$  is the inverse temperature (In our calculations, we set  $k_B = 1$ ). Using the definition  $S(E) = \log g(E)$  for the microcanonical entropy, one can write the above equation as

$$e^{-N\phi(\beta)} = N \int du e^{-N[\beta u - s(u)]} , \quad (5.15)$$

where  $N$  is the number of particles in the system,  $\phi = \beta F/N$ ,  $u = E/N$  and  $s(u) = S(E)/N$ . In the limit  $N \rightarrow \infty$ , the integral can be approximated by the maximum value

of the integrand, and one can write

$$\phi(\beta) = \min_u [\beta u - s(u)] \quad (5.16)$$

$$= \beta u^* - s(u^*) , \quad (5.17)$$

where  $u^*$  is the value of  $u$  at which the function  $\beta u - s(u)$  is minimum. Hence, the rescaled canonical free energy  $\phi(\beta)$  is the Legendre transformation of the microcanonical entropy  $s(u)$ . As we discussed in the previous section, Legendre transform of  $s(u)$  is same as the Legendre transform of the concave envelope  $\tilde{s}(u)$  of  $s(u)$ . In that case, one may write

$$\phi(\beta) = \min_u [\beta u - \tilde{s}(u)] \quad (5.18)$$

$$= \beta u^* - \tilde{s}(u^*) , \quad (5.19)$$

where  $u^*$  minimises the function  $\beta u - \tilde{s}(u)$ , and hence satisfies the equation

$$\beta = \frac{\partial \tilde{s}}{\partial u} . \quad (5.20)$$

In the canonical ensemble, the expectation value of energy is given by

$$\langle u \rangle = \frac{d\phi}{d\beta} . \quad (5.21)$$

Using Eq. (5.17), (5.19) and (5.21), we get  $\langle u \rangle = u^*$ , i.e., the value of  $u$  which minimises the restricted free energy  $\beta u - s(u)$  is equal to the canonical expectation value of energy.

In the microcanonical ensemble, the inverse temperature is defined as

$$\beta_{mc} = \frac{\partial s(u)}{\partial u} . \quad (5.22)$$

The equivalence of canonical and microcanonical ensemble can be established by comparing the energy-temperature relations Eq. (5.20) and (5.22). The ensembles may or may not be equivalent, depending on the concavity of the microcanonical entropy.

Consider the case where the  $s$  is strictly concave, i.e.,  $\frac{\partial^2 s}{\partial u^2} < 0$  for all  $u$ . When  $s$  is concave everywhere,  $\tilde{s}$  is same as  $s$ , and we see from Eq. (5.20) and Eq. (5.22) that the energy-temperature relation is the same in both ensembles. In this case we say that the ensembles are equivalent.

Now consider the case where  $s(u)$  is not concave over a region  $u_l \leq u \leq u_h$  (see Fig. (5.4)). Then one may write (see Eq. (5.5))

$$2s(u) < s(u + \Delta) + s(u - \Delta) , \quad (5.23)$$

where  $\Delta$  is small such that  $u + \Delta < u_h$  and  $u - \Delta > u_l$ . Let us assume that the system is divided in to two subsystems of energy  $u - \Delta$  and  $u + \Delta$ . If the system is short-ranged, then  $2u$  will be the total energy of the system. The rhs of Eq. (5.23) is the total entropy of the system with subsystem sharing unequal amount of energy, and the lhs is the total entropy of the system with the subsystem sharing the same amount of energy  $u$ . This equation then says that the entropy of the system increases if the energies are non uniformly distributed among the subsystems, i.e., if the system phase separates. As a result,  $s(u)$  is not the equilibrium microcanonical entropy in the range  $u_l \leq u \leq u_h$ . The entropy of the system will increase spontaneously by phase separation, until the resulting entropy  $s'(u)$  satisfy the equality

$$2s'(u) = s'(u + \Delta) + s'(u - \Delta) . \quad (5.24)$$

Expanding the above equation to the second order in  $\Delta$ , and taking the limit  $\Delta \rightarrow 0$ , one can see that the second derivative of the resulting entropy vanishes, i.e., the phase separated entropy becomes linear.  $s(u)$  remains to be equilibrium entropy for  $u < u_l$  and  $u > u_h$ . Also,  $s'(u_l) = s(u_l)$  and  $s'(u_h) = s(u_h)$ . In other words, the

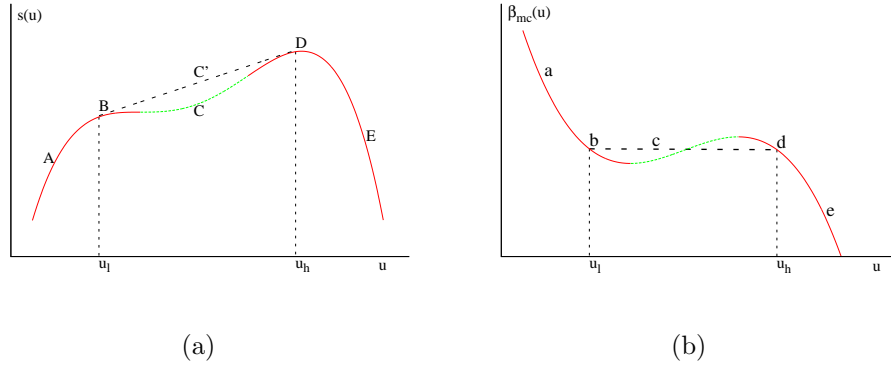


Figure 5.4: (a) Plot of non-concave microcanonical entropy  $s(u)$ . The curve  $ABCDE$  represents  $s(u)$ , and  $ABC'DE$  is the concave envelope  $\tilde{s}(u)$  of  $s(u)$ . (b) The energy-temperature relations. The curve thick curve is obtained from Eq. (5.22) and the curve  $abcde$  corresponds to Eq. (5.20). The specific heat is negative in the green region which corresponds to the green region in (a).

equilibrium microcanonical entropy is given by the concave envelope  $\tilde{s}(u)$  of  $s(u)$ . In this case, one should replace  $s(u)$  by  $\tilde{s}(u)$  in Eq. (5.22), and upon the replacement, Eq. (5.22) becomes identical to Eq. (5.20). In summary, for short-range systems, the canonical and microcanonical ensembles are equivalent even if the microcanonical entropy is not concave for a range of values of energy. The procedure of replacing a non-concave microcanonical entropy by its concave envelope is called the Maxwell construction. The basic assumption behind the Maxwell construction is that the energy in the system is additive. As a result, Maxwell construction may not exist for long-range systems, for which energy is not additive. If energy is not additive, the total energy of a system, which consists of two subsystems of energy  $u - \Delta$  and  $u + \Delta$  is not  $2u$ . In that case, lhs of Eq. (5.23) is not the total entropy of a system with two subsystems of energy  $u$  each. As a result, the system may not gain entropy by distributing energy unequally among the subsystems. In that case, the non-concave entropy  $ABCDE$  in Fig. (5.4.a) may represent the equilibrium microcanonical entropy. Then we see from Eq. (5.20) and (5.22) that the energy-temperature relation in the microcanonical ensemble is different from that in canonical ensemble. In Fig. (5.4.b), the thick curve is the energy-temperature in the microcanonical ensemble and the curve  $abcde$  correspond to the canonical ensemble. The

most striking difference is that the specific heat can be negative in the microcanonical ensemble, which is always positive in the canonical ensemble. In Fig. (5.4.b), in the green region,  $\beta$  increases with  $u$ , and hence the specific heat  $C_v = \left(-\beta^2 \frac{\partial \beta}{\partial u}\right)^{-1}$  is negative.

## 5.2 Ensemble equivalence for counterion condensation transition on a charged disk

Polyelectrolytes are long-range systems, and hence the thermodynamics derived from different statistical ensemble may not be identical. Unfortunately, the number of exactly solvable models of polyelectrolyte systems where one can pinpoint the ensemble equivalence is very much limited. In 2006, Burak et. al. solved an exactly solvable model of counterion condensation on a two dimensional charge disc in the canonical ensemble [75]. The canonical partition was evaluated exactly, and it was shown that the counterion condensation is a series of transitions at a number of critical points. We solve this model in the microcanonical ensemble by calculating the microcanonical entropy exactly. We first derive the canonical partition function closely following the steps in Ref. [75]. We then calculate the microcanonical entropy from the density of states which can be calculated by taking the inverse Laplace transform of the canonical partition function. Finally, we compare the thermodynamic properties derived from the canonical partition function and microcanonical ensemble.

### 5.2.1 Model and canonical partition function

Consider a uniformly charged disc of charge  $q$  and radius  $a$ .  $N$  counterions, each carrying a charge  $-q'$ , are distributed in the annular region between the charged disc and a circular boundary of radius  $R$ . Overall charge neutrality is achieved by choosing  $q = Nq'$ . Let  $\mathbf{r}_i$  be the position of counterion  $i$  in a coordinate system with origin at the center of the disc. The Hamiltonian of the system is given by [75]

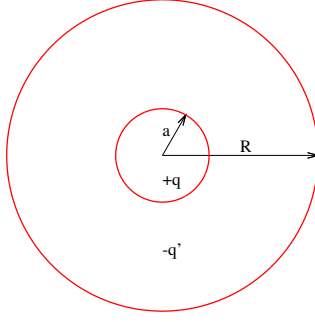


Figure 5.5: A charged disc of charge  $+q$  and radius  $a$  is placed at the center of a circular container of radius  $R$ . The counterions are distributed in the annular region between the disc and the circular boundary, and each counterion carries a charge  $-q'$ .

$$H = 2\chi \sum_{i=1}^N \ln \left( \frac{r_i}{a} \right) - \frac{\chi}{N} \sum_{i \neq j} \ln \left( \frac{r_{ij}}{a} \right), \quad (5.25)$$

where  $r_i = |\mathbf{r}_i|$ ,  $r_{ij} = |\mathbf{r}_i - \mathbf{r}_j|$  and  $\chi = qq' = Nq'^2$ . The permittivity  $\epsilon$  has been set equal to  $1/(4\pi)$ . The first term in Eq. (5.25) corresponds to the interaction between the disc and the counterions, and the second term to that between the counterions. The origin of the electrostatic potential is chosen such that the potential vanishes when the separation between two particles is  $a$ . We now obtain the expression for the partition function following closely the steps in Ref. [75].

The Hamiltonian can be rewritten in terms of  $u_i = \ln(r_i/a)$  as

$$H = \chi \left( 1 + \frac{1}{N} \right) \sum_{i=1}^N u_i - \frac{\chi}{2N} \sum_{i \neq j} \ln [2 \cosh(u_i - u_j) - 2 \cos \theta_{ij}], \quad (5.26)$$

where  $\cos \theta_{ij} = \mathbf{r}_i \cdot \mathbf{r}_j / (r_i r_j)$ . This Hamiltonian is analytically intractable. However, some simplifications occur when the limit of infinite dilution,  $N/R^2 \rightarrow 0$ , is considered. This corresponds to the limit of finite number of counterions in infinite volume, similar to the limit considered in Manning condensation [15]. In this limit, counterions are far away from each other. Thus,  $|u_i - u_j| \gg 1$ , and the summand in the second term of Eq. (5.26)

may be approximated by  $|u_i - u_j|$ , since  $2 \cosh(u_i - u_j) \approx \exp(|u_i - u_j|)$ . In this limit, the partition function

$$Z = \frac{1}{N!} \int \prod_{i=1}^N dr_i r_i d\theta_i \exp(-\beta H) \quad (5.27)$$

can be written as

$$Z = \frac{(2\pi a^2)^N}{N!} \int_0^L du_1 \dots \int_0^L du_N \exp \left[ \left( \chi + \frac{\chi}{N} - \frac{2}{\beta} \right) \sum_{i=1}^N u_i - \frac{\chi}{2N} \sum_{i \neq j} |u_i - u_j| \right], \quad (5.28)$$

where  $L = \log(R/a)$ . If we order the particles such that  $u_1 \leq u_2 \leq \dots \leq u_N$ , then  $Z$  can be rewritten as,

$$Z = (2\pi a^2)^N \int_0^L du_1 \int_{u_1}^L du_2 \dots \int_{u_{N-1}}^L du_N \exp \left( -\beta \sum_{m=1}^N A_m u_m \right), \quad (5.29)$$

where

$$A_m = \frac{2\chi}{N} (N - m + 1) - \frac{2}{\beta}, \quad (5.30)$$

By introducing a new set of  $N + 1$  variables  $\alpha_m$ 's such that,

$$\alpha_m = \alpha_0 - \sum_{l=1}^m A_l, \quad (5.31)$$

the partition function can be written as,

$$Z = \exp(\beta \alpha_N L) \int_0^L du_1 \int_{u_1}^L \dots \int_{u_{N-1}}^L du_N \exp \left( -\beta \sum_{m=0}^N \alpha_m (u_{m+1} - u_m) \right), \quad (5.32)$$

In writing Eq. (5.32), we have used,  $u_0 = 0$  and  $u_{N+1} = L$ , and the constant factor  $(2\pi a^2)^N$  is dropped. The integral on the right hand side of Eq. (5.32) is a convolution of exponential functions. Making use of the fact that the Laplace transform of a convolution is the product of Laplace transforms of the convoluted functions, the Laplace transform

of the integral  $I(L)$  on the right hand side can be written in the form,

$$\begin{aligned}\tilde{I}(s) &= \int_0^\infty dL I(L) \exp(-sL) \\ &= \prod_{m=0}^N \frac{1}{s + \beta\alpha_m},\end{aligned}\tag{5.33}$$

Performing the inverse Laplace transform of  $\tilde{I}(s)$ , and substituting back  $I(L)$  in Eq. (5.32)

we get,

$$Z = \sum_{k=0}^N \prod_{\substack{m=0 \\ m \neq k}}^N \frac{1}{\beta(\alpha_m - \alpha_k)} \exp[-\beta(\alpha_k - \alpha_N)L],\tag{5.34}$$

From Eq. (5.30) and Eq. (5.31),  $\alpha_m - \alpha_k$  is given by,

$$\alpha_m - \alpha_k = \frac{2(k-m)\chi}{\beta\xi(k,m)} \left[ \beta - \frac{\xi(k,m)}{\chi} \right],\tag{5.35}$$

where,  $\xi(k,m)$  is given by,

$$\xi(k,m) = \frac{2N}{2N - k - m + 1},\tag{5.36}$$

Using Eq. (5.34) and Eq. (5.35), we get,

$$Z = \sum_{k=0}^N \prod_{\substack{m=0 \\ m \neq k}}^N \left[ \frac{\xi(k,m)}{2(k-m)\chi \left[ \beta - \frac{\xi(k,m)}{\chi} \right]} \right] \times \exp \left[ \frac{-2(N-k)\chi L}{\xi(N,k)} \left( \beta - \frac{\xi(N,k)}{\chi} \right) \right],\tag{5.37}$$

In the limit  $L \rightarrow \infty$  keeping  $N$  fixed, the sum in Eq. (5.37) is dominated by the largest summand. Given a value of  $\beta\chi$ , the  $k$  corresponding to the largest summand is obtained by solving  $\beta\chi = N/(N-k+1)$  for  $k$  and taking the integer part [75]. As  $\beta\chi$  is increased,  $k$  changes by unity, resulting in non-analytic behaviour of the free energy. These critical

points occur at

$$(\beta\chi)_c = \frac{N}{N-k+1} = \xi(k-1, k), \quad k = 1, 2, \dots, N. \quad (5.38)$$

The first transition is at  $\beta\chi = 1$  ( $k = 1$ ), corresponding to the Manning condensation temperature on cylinders [15].

### 5.2.2 The microcanonical ensemble

To show the ensemble equivalence, we now compute the entropy in the microcanonical ensemble from the canonical partition function in Eq. (5.37). We then show that the entropy is concave everywhere and the CCT temperatures coincide in both the ensembles.

The density of states  $g(E)$  is defined as

$$g(E) = \frac{1}{N!} \int \prod_{i=1}^N dr_i r_i d\theta_i \delta(E - H). \quad (5.39)$$

$g(E)$  is obtained from the partition function  $Z$  by performing an inverse Laplace transform, i.e.,

$$g(E) = \frac{1}{2\pi i} \int_{-i\infty+c}^{+i\infty+c} d\beta Z(\beta) \exp(\beta E), \quad (5.40)$$

where the constant  $c$  is to be chosen such that the path of integration lies to the right of all the poles of  $Z(\beta)$ . This corresponds to  $\xi(k, m)/\chi < c$  for all  $k$  and  $m$ . We evaluate the above integral by the method of residues, by closing the contour of integration with a semi-circle that is either to the left or right such that the contribution to the integral from the semi-circle is zero. If  $E$  and  $k$  do not satisfy the condition,

$$E - \frac{2(N-k)\chi L}{\xi(k, N)} > 0, \quad (5.41)$$

then the contour of integration is closed to the right in the complex plane. The closed contour does not enclose any of the poles of the partition function, and, hence, the

contribution to  $g(E)$  from such  $k$  is zero. On the other hand, if  $E$  and  $k$  satisfy the condition in Eq (5.41), the contour is closed to the left, and  $g(E)$  is the sum of the residues of the partition function, and is given by

$$g(E) = \sum_{k=k^*}^N \sum_{\substack{l=0 \\ l \neq k}}^{k^*-1} \frac{\xi(k, l)}{2(k-l)\chi} \exp \left[ \frac{(N-k)(N-l)\xi(k, l)L}{N} + \frac{\xi(k, l)E}{\chi} \right] \\ \times \prod_{\substack{m=0 \\ m \neq k \\ m \neq l}}^N \left[ \frac{N}{(k-m)(l-m)\xi(k, l)} \right], \quad (5.42)$$

where  $k^*$  is the smallest value of  $k$ , given  $E$ , that satisfies Eq. (5.41). In writing Eq. (5.42), we have used the relation

$$\xi(l, k) - \xi(m, k) = \frac{(l-m)\xi(l, k)\xi(m, k)}{2N}, \quad (5.43)$$

derived from Eq. (5.36). The terms in the summation with  $l \geq k^*$  do not contribute to  $g(E)$  because the summand is antisymmetric in  $k$  and  $l$ . This leads to an upper bound  $k^* - 1$  for  $l$ . Also, the maximum possible value of the energy of the system is  $(N+1)\chi L$ , corresponding to  $u_i = L$  for all  $i$ . It then follows from Eq. (5.41) that the lowest value of  $k^*$  is 1.

The density of states  $g(E)$  in Eq (5.42) is a sum of exponentials of the form  $\exp[f(k, l, E/L)L]$ , where the function  $f$  is derivable from Eq (5.42). In the limit  $L \rightarrow \infty$ , keeping  $N$  fixed, the sum is dominated by that  $k, l$  which maximise the function  $f$ .  $E$  is implicitly dependent on  $L$  and we make this dependence explicit by converting the inequality in Eq. (5.41) into an equality by replacing  $k$  by  $k^* - \delta$ , where  $0 < \delta < 1$ . Thus, eliminating  $E$ ,  $f$  becomes a function of  $k, l$  and  $k^*$ . It is then easy to show (See appendix 5.A) that  $f$  increases with

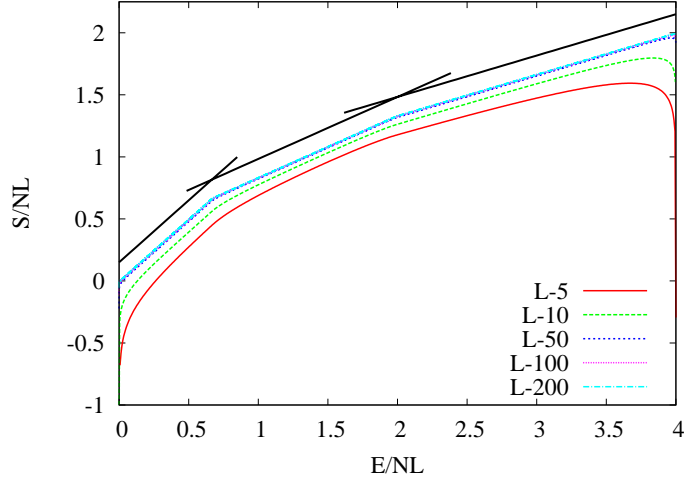


Figure 5.6: The variation of microcanonical entropy  $S$  with energy  $E$  is shown for different  $L$ . The data are for  $N = 3$  and  $\chi = 3$ . The solid black lines correspond to the limiting curve obtained from Eq. (5.44). They have been shifted upwards and extended to the left and right for clarity since the unshifted lines are indistinguishable from the curve for  $L = 200$ .

$l$  for  $k \geq k^*$ , and decreases with  $k$  for  $l \leq k^*$ . As a result, the dominant contribution to  $g(E)$  comes from the term with  $k = k^*$  and  $l = k^* - 1$ .

By considering only the largest term, we obtain the entropy  $S = \ln[g(E)]$  to be

$$\lim_{L \rightarrow \infty} \frac{S}{NL} = 1 - \frac{k^*}{N} + \frac{\xi(k^*, k^* - 1)}{\chi} \frac{E}{NL}, \quad (5.44)$$

where  $\xi(k^*, k^* - 1) = N/(N - k^* + 1)$ . In Fig. 5.6, we show the dependence of entropy on energy, obtained by considering all the terms in  $g(E)$  [see Eq. (5.42)], and compare it with the entropy in Eq. (5.44). On increasing  $L$ ,  $S/(NL)$  approaches the limiting curve with  $N$  linear portions, determined by Eq. (5.44).

### 5.2.3 The ensemble equivalence

We now show that the entropy is concave in energy  $E$ . In Eq. (5.44),  $k^*$ , though a function of  $E$ , takes on integer values and is a constant over a range of  $E$ . As  $E$  increases from 0 to its maximum value,  $k^*$  decreases from  $N$  to 1, in steps of unity. Thus, the entropy curve

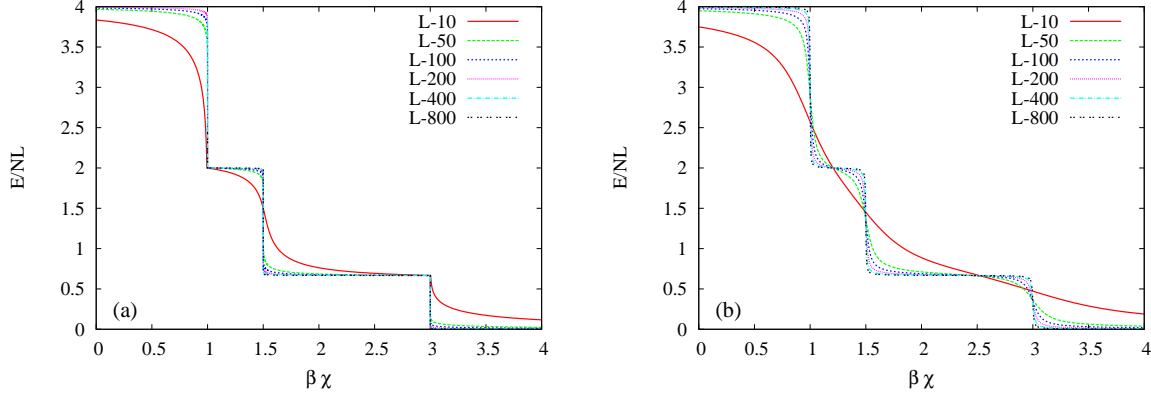


Figure 5.7: The energy–temperature relation for  $N = 3$ ,  $\chi = 3$  for different  $L$  in the (a) microcanonical ensemble and (b) canonical ensemble. For large values of  $L$ , the transition points are given by  $(\beta\chi)_c = \xi(k^*, k^* - 1)$ .

consists of  $N$  linear segments of slope  $\xi(k^*, k^* - 1)/\chi$ ,  $k^* = 1, \dots, N$ , where the segment with larger energy has smaller slope, thereby implying that the curve is concave. The piecewise linear character of microcanonical entropy has its origin in the first order poles of the canonical partition function, with the slopes being equal to the strength of the poles [121]. The energy–temperature relation in the microcanonical ensemble is obtained from the thermodynamic relation  $\beta = \frac{\partial S}{\partial E}$ . This gives  $\beta\chi = \xi(k^*, k^* - 1)$ , implying that  $\beta\chi$  takes on  $N$  distinct values, corresponding to the  $N$  transition points, which coincide with those obtained from the canonical partition function [see Eq. (5.38)]. In Fig. 5.7(a), we show the energy–temperature relation in the microcanonical ensemble for finite  $L$  by considering all the terms in  $g(E)$ . As  $L$  is increased we obtain the limiting step function determined by the relation  $\beta\chi = \xi(k^*, k^* - 1)$ . The corresponding data for the canonical partition function from Eq. (5.37) is shown in Fig. 5.7(b). Thus, in the thermodynamic limit ( $L \rightarrow \infty$ ), we obtain the same limiting curve in both the ensembles.

We can further quantify the energy–temperature relation shown in Fig. 5.7. The energies of the plateaus are obtained by solving Eq. (5.41) as an equality, and are given by  $E_{\text{plateau}} = \chi N^{-1}(N - k)(N - k + 1)L$ ,  $k = 0, \dots, N$ . A simple physical interpretation can be ascribed to these plateaus, as explained below. Consider a scenario when  $m$  counterions have condensed onto the disc, while the remaining  $N - m$  counterions are at

the boundary  $R$ . The energy of this configuration, in the limit of large  $L$  has contribution from two parts: (1)  $q'^2 L(N-m)^2$  corresponding to interaction between a disc of charge  $(N-m)q'$  and  $N-m$  counterions and (2)  $q'^2 L(N-m)(N-m-1)/2$  corresponding to interaction between counterion pairs. The total energy of this geometry is thus  $\chi N^{-1}(N-m)(N-m+1)$ . Comparing this energy with the energy of a plateau, it is clear that the plateau corresponding to a certain value of  $k$  corresponds to a case where  $k$  counterions have condensed and the remaining ones are at the boundary.

We stress that we have not used the Legendre transformation to evaluate the microcanonical entropy from the canonical free energy. The entropy obtained by the Legendre transformation will always give the concave envelope of the microcanonical entropy [110, 122]. Since the entropy that we have calculated directly from the density of states is concave, we should be able to obtain the same by a Legendre transform of the free energy,  $S(E) = \beta E - \beta F(\beta)$ , where  $\beta$  is to be eliminated using the energy-temperature relation  $E = \frac{\partial}{\partial \beta}(\beta F)$ . In the thermodynamic limit, it is straightforward to do so for this model.

### 5.3 Summary

To summarise, we studied counterion condensation transition on a two dimensional charged disc in the microcanonical ensemble. In the limit of infinite dilution, we obtained an expression for the microcanonical entropy, and showed that the entropy-energy curve consisted of linear segments with decreasing slope, and hence that the entropy is concave with respect to energy. This implies the equivalence of the microcanonical and canonical ensembles. In particular, the energy-temperature relation and the transition points of CCT obtained from the microcanonical entropy are shown to be identical with those obtained from the canonical partition function.

## 5.A The leading term in $g(E)$

The exponential term in summation in Eq. (5.42) can be written as  $\exp[f(k, l, E/L)L]$ , where  $f$  is given by

$$f = \frac{(N-k)(N-l)\xi(k, l)}{N} + \frac{\xi(k, l)E}{\chi L} . \quad (5.45)$$

The expression for  $E/L$  can be obtained by converting the inequality in Eq. (5.41) into an equality by replacing  $k$  with  $k^* - \delta$ , and is given by

$$\frac{E}{N} = (N - k^* + \delta)(N - k^* + \delta + 1)\chi . \quad (5.46)$$

Substituting Eq. (5.46) in Eq. (5.45), we get

$$f(k^*, k, l) = \xi(k, l) [(N - k)(N - l) + (N - k^* + \delta)(N - k^* + 1 + \delta)] / N . \quad (5.47)$$

By using the expression

$$\frac{\partial \xi(k, l)}{\partial l} = \frac{\xi(k, l)^2}{2N} , \quad (5.48)$$

we get

$$\frac{\partial f}{\partial l} = \frac{\xi(k, l)^2}{2N^2} [-(N - k)(N - k + 1) + (N - k^* + \delta)(N - k^* + 1 + \delta)] . \quad (5.49)$$

Since  $k \geq k^*$ , one may write  $k = k^* + m$ . Then the above equation can be written as

$$\frac{\partial f}{\partial l} = \frac{\xi(k, l)^2}{2N^2} [2(N - k^*) + 1 - m] [m + \delta] . \quad (5.50)$$

Since  $0 \leq m \leq N - k^*$ , the above expression is always positive, and hence  $f(k^*, k, l)$  is an increasing function in  $l$ . The maximum possible value of  $l$  is  $k^* - 1$ , and as a result,  $l = k^* - 1$  corresponds to the maximum value of  $f(k^*, k, l)$ . A similar condition for the

variable  $l$  can be obtained by interchanging  $l$  and  $k$  in Eq. (5.49).

$$\frac{\partial f}{\partial k} = \frac{\xi(k, l)^2}{2N^2} [-(N - l)(N - l + 1) + (N - k^* + \delta)(N - k^* + 1 + \delta)] . \quad (5.51)$$

Since  $l < k^*$ , one may write  $l = k^* - m$ . Substituting for  $l$  in Eq. (5.51), we get

$$\frac{\partial f}{\partial k} = \frac{\xi(k, l)^2}{2N^2} [2(N - k^*) + 1 + m] [-m + \delta] . \quad (5.52)$$

Since  $1 < m \leq k^*$ ,  $\frac{\partial f}{\partial k}$  is always negative, and hence  $f(k^*, k, l)$  decreases with increasing  $k$ . The lowest possible value of  $k$  is  $k^*$ , and as a result,  $k = k^*$  corresponds to the maximum of  $f(k^*, k, l)$ . In summary,  $k = k^*$  and  $l = k^* - 1$  correspond to the leading term in the summation in Eq. (5.42).

# Chapter 6

## Conclusion and Future Directions

### 6.1 Conclusions

In this dissertation, we presented our results of the study of three different polyelectrolyte systems. In our simulations, we used the bead-spring model to study the behaviour of these systems.

The first system is a single flexible polyelectrolyte chain in the presence of explicit counterions. Our main results are

- The counterion condensation is a second-order phase transition, and the critical value of the linear charge density of the transition decreases with increase in valency of the counterions.
- Collapse of the polyelectrolyte chain induced by condensed counterions is a first-order phase transition, and the critical value of the linear charge density of the transition decreases with increase in valency of the counterions.
- The recently proposed intermediate phase between the extended and collapsed phase is an artefact of small systems, and such phase does not exist in the thermodynamic limit.

The second system that we studied is a collection of rod-like polyelectrolyte chains in the presence of neutralising counterions. Our main results are

- Monovalent counterions can induce aggregation of rod-like polyelectrolyte chains when the linear charge density of the chain exceeds a critical value.
- The potential of mean force between two parallel, similarly charged rod-like polyelectrolyte chains develops a well of attraction at high enough values of linear charge density of the chains. The linear charge density at which the depth of the well is of the order of the thermal fluctuations roughly coincides with the onset of aggregation.
- The absence of the aggregation, and that of attraction in the potential of mean force, in the presence of monovalent counterions, in earlier simulations can be attributed to the low range of the linear charge density values used in these simulations.
- The dynamics of aggregation is independent of the valency of counterions and linear charge density. The number of aggregates decays as a power law, and the exponent is independent of the valency of counterions and the linear charge density of the polyelectrolyte backbone.
- The critical value of the linear charge density for aggregation decreases with increase in valency of counterions, and is close to the critical value of the extended-collapsed transition of a single polyelectrolyte chain for all valencies of counterions. We therefore suggest that the mechanism of both aggregation of similarly charged rod-like polyelectrolytes and the extended-collapsed transition of a single flexible polyelectrolyte chain are closely related.
- The distribution of condensed counterions plays an important role in developing attraction between two similarly charged polyelectrolytes. For two parallel rod-like polyelectrolyte chains, the distribution of counterions around the rods changes with the separation between them. For intermediate separations, for which there is an

attraction between the rods, the counterions prefer to lie in the plane of the rods, and mostly in between the rods. At very small separations, for which the interaction is repulsive, the counterions are expelled out of the plane of the two rods.

The third system that we studied is a two-dimensional charged disc, surrounded by oppositely charged freely moving counterions. This system was recently studied by Burak et. al. in the canonical ensemble. We derived a slightly different form of the canonical partition function, following closely the steps of Burak et. al., and then derived an exact expression for the microcanonical entropy. Our main results are

- The microcanonical entropy is piecewise linear and concave in energy.
- The linear portions of the microcanonical entropy correspond to the first-order poles of the canonical partition function.
- Since the microcanonical entropy is concave in energy, the canonical and microcanonical ensembles are equivalent for the system that we have considered.
- As an illustration of the equivalence, we showed that the energy–temperature relation in the microcanonical ensemble is identical to that of the canonical ensemble.

## 6.2 Future Directions

Polyelectrolytes remains an active area of research, and based on our studies on different polyelectrolyte systems, we propose a few research problems.

- The extended-collapsed transition of a single flexible polyelectrolyte chain is a first-order transition in the absence of added salts. The presence of salts would screen the electrostatic interactions among the monomers, and the extended-collapsed transition of the polyelectrolyte chain may become identical to that of a neutral polymer with short-ranged interactions. It would be interesting to verify this.

- In our simulations, we have not taken into account the effects of hydrodynamic interactions on the phase transitions. It would be interesting to study the effects of such interactions on the counterion condensation transition, extended-collapsed transition, and aggregation of similarly charged polyelectrolyte chains.
- In the last decade, single molecule stretching experiments and simulations have drawn increased attention, due to the invention of new thermodynamic equalities and fluctuation theorems. A recently proposed equality, namely the Jarzynski equality [123], provides a way to measure the free energy difference between configurations of complex molecules [124], described by reaction coordinates such as end to end distance, from the non-equilibrium work performed on the molecule to change its configuration. It would be interesting to measure the free energy difference along the end to end distance reaction coordinate of a condensed-collapsed phase of a polyelectrolyte chain. Since the extended-collapsed transition is first-order, the free energy as a function of end to end distance is expected to have two minima; corresponding to the extended and collapsed phase. The linear charge density of the polyelectrolyte chain for which the depths of the two minima are equal will determine a critical point. It would be interesting to see if this critical point coincides with the critical point of the extended-collapsed transition, since the free energy measured as a function of the end to end distance is only a projection of the complete free energy along that reaction coordinate.
- In a recent simulation [125] which studied the unwrapping of a single macromolecule, a new transient fluctuation relation for the stretching force was proposed. To our knowledge, the validity of this fluctuation relation has not been studied using any other model systems or realistic systems of macromolecules. We believe that polyelectrolyte system would be one of the nontrivial systems for which the validity of this fluctuation theorem can immediately be checked. The unwrapping of a condensed-collapsed phase of a flexible or semi-flexible polyelectrolyte chain can be

used for this purpose. The force-time profile can be obtained by anchoring one of the ends of the collapsed chain and then stretching the other end at a constant velocity. The probability distribution of the stretching force can then be measured to verify the transient fluctuation relation.

- The field of aggregation of similarly charged polyelectrolytes is still its nascent stage. Though simulations exist for rod-like polyelectrolytes, very few simulations exist for flexible chains. The dynamics of aggregation of flexible chains can have more interesting features, and the degree of flexibility itself can be a parameter in exploring the aggregation phase space. Preliminary investigations of such systems are under way.

# Bibliography

- [1] A. V. Dobrynin and M. Rubinstein *Prog. Polym. Sci.*, vol. 30, p. 1049, 2005.
- [2] R. R. Netz and D. Andelman, *Encyclopedia of Electrochemistry*, vol. 1, p. 282. Weinheim: Wiley-VCH, 2002.
- [3] Y. Levin *Rep. Prog. Phys.*, vol. 65, p. 1577, 2002.
- [4] J. M. Berg, J. L. Tymoczko, and L. Stryer, *Biochemistry*. New York: W. H. Freeman and Company, 2007.
- [5] M. Rubinstein and R. Colby, *Polymer Physics*. USA: Oxford University Press, 2003.
- [6] M. Doi and S. F. Edwards, *The Theory of Polymer Dynamics*. New York: Oxford University Press, 1988.
- [7] N. G. V. Kampen, *Stochastic Processes in Physics and Chemistry*. Oxford: Elsevier, 2007.
- [8] P. G. de Gennes, *Scaling Concepts in Polymer Physics*. Ithaca: Cornell University Press, 1991.
- [9] D. A. McQuarrie, *Statistical Mechanics*. USA: University Science Books, 2003.
- [10] P. J. Flory, *Principles of Polymer Chemistry*. Ithaca: Cornell University Press, 1953.

- [11] I. M. Lifshitz, A. Y. Grosberg, and A. R. Khokhlov *Rev. Mod. Phys.*, vol. 50, p. 683, 1978.
- [12] W. B. Russel, D. A. Saville, and W. R. Schowalter, *Colloidal Dispersions*. Cambridge: Cambridge University Press, 1989.
- [13] Q. Liao, A. V. Dobrynin, and M. Rubinstein *Macromolecules*, vol. 39, p. 1920, 2006.
- [14] J. Jeon and A. V. Dobrynin *Macromolecules*, vol. 40, p. 7695, 2007.
- [15] G. S. Manning *J. Chem. Phys.*, vol. 51, p. 924, 1969.
- [16] G. S. Manning *Q. Rev. Biophys.*, vol. 11, p. 179, 1978.
- [17] R. M. Fuoss, A. Katchalsky, and S. Lifson *Proc. Natl. Acad. Sci. USA*, vol. 37, p. 579, 1951.
- [18] C. F. Anderson and M. T. Record *Ann. Rev. Phys. Chem.*, vol. 33, p. 191, 1982.
- [19] K. Jayasree, P. Ranjith, M. Rao, and P. B. S. Kumar *J. Chem. Phys.*, vol. 130, p. 094901, 2009.
- [20] L. C. Gousule and J. A. Shellman *Nature*, vol. 259, p. 333, 1976.
- [21] V. A. Bloomfield *Biopolymers*, vol. 31, p. 1471, 1991.
- [22] J. X. Tang, S. Wong, P. T. Tran, and P. A. Janmey *Ber. Bunsenges. Phys. Chem.*, vol. 100, p. 796, 1996.
- [23] M. Sedláč and E. J. Amis *J. Chem. Phys.*, vol. 96, p. 817, 1992.
- [24] J. J. Tanahatoc and M. E. Kuil *J. Phys. Chem. B*, vol. 101, p. 5905, 1997.
- [25] R. Borsali, H. Nguyen, and R. Pecora *Macromolecules*, vol. 31, p. 1548, 1998.
- [26] B. D. Ermi and E. J. Amis *Macromolecules*, vol. 31, p. 7378, 1998.

- [27] Y. Zhang, J. F. Douglas, B. D. Ermi, and E. J. Amis *J. Chem. Phys.*, vol. 114, p. 3299, 2001.
- [28] N. G. Jensen, R. J. Mashl, R. F. Bruinsma, and W. M. Gelbart *Phys. Rev. Lett.*, vol. 78, p. 2477, 1997.
- [29] M. J. Stevens *Phys. Rev. Lett.*, vol. 82, p. 101, 1999.
- [30] K. C. Lee, I. Borukhov, W. M. Gelbart, A. J. Liu, and M. J. Stevens *Phys. Rev. Lett.*, vol. 93, p. 128101, 2004.
- [31] A. Diehl, H. A. Carmona, and Y. Levin *Phys. Rev. E*, vol. 64, p. 011804, 2001.
- [32] E. Allahyarov, G. Gompfer, and H. Löwen *Phys. Rev. E*, vol. 69, p. 041904, 2004.
- [33] A. Savelyev and G. A. Papoian *J. Am. Chem. Soc.*, vol. 129, p. 660, 2007.
- [34] J. O. Ray and G. S. Manning *Macromolecules*, vol. 33, p. 2901, 2000.
- [35] A. Perico and A. Rapallo *J. Chem. Phys.*, vol. 134, p. 055108, 2011.
- [36] J. J. Arenzon, J. F. Stilck, and Y. Levin *Eur. Phys. J. B*, vol. 12, p. 79, 1999.
- [37] J. J. Arenzon, Y. Levin, and J. F. Stilck *Physica A*, vol. 283, p. 1, 2000.
- [38] F. J. Solis and M. O. de la Cruz *Phys. Rev. E*, vol. 60, p. 4496, 1999.
- [39] T. Dauxois, S. Ruffo, E. Arimondo, and M. Wilkens, *Dynamics and Thermodynamics of Systems with Long-Range Interactions*. Berlin: Springer, 2002.
- [40] A. Campa, T. Dauxois, and S. Ruffo *Phys. Rep.*, vol. 480, p. 57, 2009.
- [41] L. Verlet *Phys. Rev.*, vol. 159, p. 98, 1967.
- [42] W. C. Swope, H. C. Andersen, P. H. Berens, and K. R. Wilson *J. Chem. Phys.*, vol. 76, p. 637, 1982.

- [43] D. Frenkel and B. Smit, *Understanding Molecular Dynamics Simulation*. New York: Academic Press, 2002.
- [44] H. C. Andersen *J. Chem. Phys.*, vol. 72, p. 2384, 1980.
- [45] S. Nosé *J. Chem. Phys.*, vol. 81, p. 511, 1984.
- [46] W. G. Hoover *Phys. Rev. A*, vol. 31, p. 1695, 1985.
- [47] T. Schneider and E. Stoll *Phys. Rev. B*, vol. 17, p. 1302, 1978.
- [48] P. Ewald *Ann. Phys.*, vol. 64, p. 253, 1921.
- [49] R. W. Hockney and J. W. Eastwood, *Computer Simulations Using Particles*. New York: McGraw-Hill, 1975.
- [50] B. Y. Ha and D. Thirumalai *Phys. Rev. A*, vol. 46, p. R3012, 1992.
- [51] Y. Kantor and M. Kardar *Europhys. Lett.*, vol. 27, p. 643, 1994.
- [52] P. R. E *Europhys. Lett.*, vol. 51, p. 1299, 1995.
- [53] A. V. Dobrynin, M. Rubinstein, and S. P. Obukhov *Macromolecules*, vol. 29, p. 2974, 1996.
- [54] A. V. Lyulin, B. Dunweg, O. V. Borisov, and A. A. Darinskii *Macromolecules*, vol. 32, p. 3264, 1999.
- [55] M. Muthukumar *J. Chem. Phys.*, vol. 120, p. 9343, 2004.
- [56] H. Schiessel and P. Pincus *Macromolecules*, vol. 31, p. 7953, 1998.
- [57] J. Jeon and A. V. Dobrynin *J. Phys. Chem. B*, vol. 110, p. 24652, 2006.
- [58] R. G. Winkler, M. Gold, and P. Reineker *Phys. Rev. Lett.*, vol. 80, p. 3731, 1998.
- [59] U. Micka, C. Holm, and K. Kremer *Langmuir*, vol. 15, p. 4033, 1999.

- [60] H. J. Limbach and C. Holm *J. Phys. Chem. B*, vol. 107, p. 8041, 2003.
- [61] V. O. Aseyev, S. I. Klenin, H. Tenhu, I. Grillo, and E. Geissler *Macromolecule*, vol. 34, p. 3706, 2001.
- [62] C. E. Williams and M. D. C. Tinoco *Europhys. Lett.*, vol. 52, p. 284, 2000.
- [63] M. D. C. Tinoco, R. Ober, I. Dolbnya, W. Bras, and C. E. Williams *J. Phys. Chem. B*, vol. 106, p. 12165, 2002.
- [64] M. N. Spiteri, C. E. Williams, and F. Boue *Macromolecules*, vol. 40, p. 6679, 2007.
- [65] V. O. Aseyev, H. Tenhu, and S. I. Klenin *Macromolecules*, vol. 32, p. 1838, 1999.
- [66] F. Bordini, C. Cametti, T. Gili, S. Sennato, S. Zuzzi, S. Dou, and R. H. Colby *Phys. Rev. E*, vol. 72, p. 031806, 2005.
- [67] P. Loh, G. R. Deen, D. Vollmer, K. Fischer, M. Schmidt, A. Kundagrami, and M. Muthukumar *Macromolecules*, vol. 41, p. 9352, 2008.
- [68] L. Rayleigh *Philos. Mag.*, vol. 14, p. 184, 1882.
- [69] M. Deserno *Eur. Phys. J. E*, vol. 6, p. 163, 2001.
- [70] R. Chang and A. Yethiraj *J. Chem. Phys.*, vol. 118, p. 6634, 2003.
- [71] R. Golestanian, M. Kardar, and T. B. Liverpool *Phys. Rev. Lett.*, vol. 82, p. 4456, 1999.
- [72] N. V. Brilliantov, D. V. Kuznetsov, and R. Klein *Phys. Rev. Lett.*, vol. 81, p. 1433, 1998.
- [73] A. Naji and R. R. Netz *Phys. Rev. Lett.*, vol. 95, p. 185703, 2005.
- [74] A. Naji and R. R. Netz *Phys. Rev. E*, vol. 73, p. 056105, 2006.
- [75] Y. Burak and H. Orland *Phys. Rev. E*, vol. 73, p. 010501(R), 2006.

- [76] J. W. Klein and B. R. Ware *J. Chem. Phys.*, vol. 80, p. 1334, 1984.
- [77] L. M. Panafiel and T. A. Litovitz *J. Chem. Phys.*, vol. 96, p. 3033, 1991.
- [78] L. S. Lerman *Proc. Natl. Acad. Sci. USA*, vol. 68, p. 1886, 1971.
- [79] R. W. Wilson and V. A. Bloomfield *Biochemistry*, vol. 18, p. 2192, 1979.
- [80] R. Marquet and C. Houssier *J. Biomol. Struct. Dyn.*, vol. 9, p. 159, 1991.
- [81] N. V. Brilliantov, D. V. Kuznetsov, and R. Klein *Phys. Rev. Lett.*, vol. 81, p. 1433, 1998.
- [82] F. J. Solis and M. O. de la Cruz *J. Chem. Phys.*, vol. 112, p. 2030, 2000.
- [83] <http://lammps.sandia.gov>.
- [84] S. J. Plimpton *J. Comp. Phys.*, vol. 117, p. 1, 1995.
- [85] H. Gould, J. Tobochnik, and W. Christian, *An Introduction to Computer Simulation Methods: Applications to Physical Systems*. San Fransisco: Addison Wesley, 2007.
- [86] S. Liu and M. Muthukumar *J. Chem. Phys.*, vol. 116, p. 9975, 2002.
- [87] C. Vanderzande, *Lattice Models of Polymers*. Cambridge: Cambridge University Press, 1999.
- [88] O. V. Zribi, H. Kyung, R. Golestanian, T. B. Liverpool, and G. C. L. Wong *Phys. Rev. E*, vol. 73, p. 031911, 2006.
- [89] J. C. Butler, T. Angelini, J. X. Tang, and G. C. L. Wong *Phys. Rev. Lett.*, vol. 91, p. 028301, 2003.
- [90] B. Y. Ha and A. J. Liu *Phys. Rev. E*, vol. 60, p. 803, 1999.
- [91] B. Y. Ha and A. J. Liu *Physica A*, vol. 259, p. 235, 1998.
- [92] B. Y. Ha and A. J. Liu *Phys. Rev. Lett.*, vol. 79, p. 1289, 1997.

- [93] B. I. Skhlovskii *Phys. Rev. Lett.*, vol. 82, p. 3268, 1999.
- [94] I. I. Potemkin, R. E. Limberger, A. N. Kudlay, and A. R. Khokhlov *Phys. Rev. E*, vol. 66, p. 011802, 2002.
- [95] R. Bruinsma *Phys. Rev. E*, vol. 63, p. 061705, 2001.
- [96] A. V. Ermoshkin and M. O. de la Cruz *Phys. Rev. Lett.*, vol. 90, p. 125504, 2003.
- [97] S. Pietronave, L. Arcesi, C. D’Arrigo, and A. Perico *J. Phys. Chem. B*, vol. 112, p. 15991, 2008.
- [98] M. Sayar and C. Holm *Euro. Phys. Lett.*, vol. 77, p. 10601, 2007.
- [99] H. Fazli and R. Golestanian *Phys. Rev. E*, vol. 76, p. 041801, 2007.
- [100] B. Luan and A. Aksimentiev *J. Am. Chem. Soc.*, vol. 130, p. 15754, 2008.
- [101] M. Sayar and C. Holm *Phys. Rev. E*, vol. 82, p. 031901, 2010.
- [102] Y. Levin, J. J. Arenzon, and J. F. Stilck *Phys. Rev. Lett.*, vol. 83, p. 2680, 1999.
- [103] J. M. Shurr and B. S. Fujimoto *J. Phys. Chem. B*, vol. 107, p. 4451, 2003.
- [104] A. Varghese, S. Vemparala, and R. Rajesh *J. Chem. Phys.*, vol. 135, p. 154902, 2011.
- [105] F. Leyvraz, “Scaling theory and exactly solved models in the kinetics of irreversible aggregation,” *Physics Reports*, vol. 383, pp. 95 – 212, 2003.
- [106] C. Connaughton, R. Rajesh, and O. Zaboronski, “Kinetics of cluster-cluster aggregation,” in *Handbook of Nanophysics: Clusters and Fullerenes* (K. D. Sattler, ed.), Taylor and Francis, 2010.
- [107] T. E. Angelini, H. Liang, W. Wriggers, and G. C. L. Wong *Eur. Phys. J. E*, vol. 16, p. 389, 2005.

- [108] M. Deserno, A. Arnold, and C. Holm *Macromolecules*, vol. 36, p. 249, 2003.
- [109] J. Barré, D. Mukamel, and S. Ruffo *Phys. Rev. Lett.*, vol. 87, p. 030601, 2001.
- [110] R. S. Ellis, H. Touchette, and B. Turkington *Physica A*, vol. 335, p. 518, 2004.
- [111] T. Padmanabhan *Phys. Rep.*, vol. 188, p. 285, 1990.
- [112] B. N. Miller and P. Youngkins *Phys. Rev. Lett.*, vol. 81, p. 4794, 1998.
- [113] B. Stahl, M. K. H. Kiessling, and K. Schindler *Planet. Space Sci.*, vol. 43, p. 1995, 271.
- [114] M. K. H. Kiessling and T. Neukirch *Proc. Natl. Acad. Sci.*, vol. 100, p. 1510, 2003.
- [115] R. A. Smith and T. M. O’Neil *Phys. Fluids B*, vol. 2, p. 2961, 1990.
- [116] R. S. Ellis, K. Haven, and B. Turkington *J. Stat. Phys.*, vol. 101, p. 999, 2000.
- [117] R. S. Ellis, K. Haven, and B. Turkington *Nonlinearity*, vol. 15, p. 239, 2002.
- [118] P. Hartel and W. Thirring *Ann. Phys. (NY)*, vol. 63, p. 520, 1971.
- [119] M. Antoni, S. Ruffo, and A. Torcini *Phys. Rev. E*, vol. 66, p. 025103(R), 2002.
- [120] A. Lederhendler and D. Mukamel *Phys. Rev. Lett.*, vol. 105, p. 150602, 2010.
- [121] H. Touchette, R. J. Harris, and J. Tailleur *Phys. Rev. E*, vol. 81, p. 030101(R), 2010.
- [122] H. Touchette *Phys. Rep.*, vol. 478, p. 1, 2009.
- [123] C. Jarzynski *Phys. Rev. Lett.*, vol. 78, p. 2690, 1997.
- [124] S. Park, F. K. Araghi, E. Tajkhorshid, and K. Schulten *J. Chem. Phys.*, vol. 119, p. 3559, 2003.
- [125] M. Ponmurugan and S. Vemparala *Phys. Rev. E*, vol. 84, p. 060101(R), 2011.